NASA CONTRACTOR REPORT

NASA CR-1618

ACOUSTIC TESTS OF A FLEXIBLE SPACECRAFT MODEL

by W. E. Noonan and J. R. Daiber

Prepared by
MCDONNELL DOUGLAS ASTRONAUTICS COMPANY
St. Louis, Mo.
for Langley Research Center

NATIONAL AERONAUTICS AND SPACE ADMINISTRATION • WASHINGTON, D. C. • JUNE 1970

NASA CR-1618

ACOUSTIC TESTS OF A FLEXIBLE SPACECRAFT MODEL

By W. E. Noonan and J. R. Daiber

1. Vibration Testing
2. Space Vehicles
3. Acoustics

Prepared under Contract No. NAS 1-8838 by
MCDONNELL DOUGLAS ASTRONAUTICS COMPANY
St. Louis, Mo.

for Langley Research Center

NATIONAL AERONAUTICS AND SPACE ADMINISTRATION

For sale by the Clearinghouse for Federal Scientific and Technical Information
Springfield, Virginia 22151 – CFSTI price $3.00

TABLE OF CONTENTS

SUMMARY

An acoustic test program has been conducted with a 1/10 scale dynamic model of a representative spacecraft structure to investigate the effectiveness of producing vibration response over a wide frequency range. The model which included a spacecraft and shroud assembly was supplied by NASA Langley Research Center. The acoustic test facility utilized four airstream modulators and a laminated fiberglass progressive wave tube. Model configuration and position were varied during testing. Accelerometers, strain gages and displacement probes were used to determine the response of the vehicle while microphones were used to measure the acoustic field external and internal to the model. Acoustic noise levels of 140 to 146 dB were produced in the progressive wave tube.

Results of the program have shown that wide band vibration was produced with little dependence on model configuration and position within the progressive wave tube.

1. INTRODUCTION

Among the many factors that affect mission success of aerospace vehicles are the closely related acoustic and vibration environments. The simulation of these environments for tests to demonstrate the adequacy of vehicle design and to provide assurance of reliable performance has been the subject of numerous investigations. Approaches to the simulation for recent programs has included high-level vibration testing of complete spacecraft (References 1 through 5) and acoustic tests to excite vibration of complete spacecraft (References 4 through 6). Acoustic testing is preferred because: (1) it is difficult to provide adequate vibration excitation over a wide frequency range with electromechanical exciters, and (2) the dynamic environment produced in flight results from fluctuating pressure excitation which is distributed over the surface of the vehicle. The Apollo program has included investigation of many facets of the simulation problems and included the fabrication of a large facility tailored for the vehicle (Reference 7). To provide information on facilities which can be expanded to produce dynamic environments for many space vehicles, acoustic tests were made with a dynamically scaled spacecraft model. No attempt was made during this test program to simulate the actual flight environments. Specific objectives of the program were to determine: (1) the capability to produce dynamic response over a wide frequency range using a progressive wave tube, (2) the linearity of the response with changes in the acoustic field, (3) the sensitivity of the test article to unsymmetrical positioning in the acoustic field, and (4) the effects on the dynamic response resulting from variations in the structural configuration.

Information contained in this report summarizes the results obtained from specific transducers to satisfy these limited objectives.

2. TEST FACILITY

The basic components of the test facility are the four airstream modulators used as acoustic sources and a fiberglass acoustic enclosure. These components are shown schematically in Figure 1. Descriptions of these components and their functions are given in the following paragraphs.

2.1 AIRSTREAM MODULATORS. The airstream modulator shown in cross-section in Figure 2 is an electro-pneumatic device that converts pneumatic energy into acoustic energy. As shown in the drawing, compressed air enters through a straight pipe, and impinges on a pointed surface which directs the air into a narrow annulus. One end of a thin cylindrical segment, the modulating element, protrudes into the air path. A coil of wire on the other end of this element is in a magnetic field, and provides an oscillatory driving force on the element, causing it to move in and out of the air gap and changing the area through which the air flows. The motion of the cylindrical element appears to the moving stream of air as a variable area orifice, and a pressure is generated that is approximately proportional to the deflection of the cylindrical modulating element. This type of acoustic source has the advantage of being able to reproduce any electrical signal applied to the modulator, within the amplitude and frequency response limits of the system. Sinusoidal or wideband random acoustic signals can therefore be generated. Four airstream modulators are utilized in the acoustic test facility, with the modulator feeding each quadrant of the cylindrical enclosure. The modulators can be driven by common or separate power amplifiers, with either a common electrical signal or by four independent electrical signals. The resultant sound fields generated by the airstream modulators are identified as correlated (for the common source case) or uncorrelated.

2.2 ACOUSTIC ENCLOSURE. The airstream modulators were mounted to a fiberglass enclosure. The enclosure, which consisted basically of exponential horns, and the progressive wave section were constructed from a fiberglass laminate material. The facility was originally designed for tests which were conducted to define the acoustic field on a McDonnell rigid model. The facility was not changed for the NASA flexible model tests because the flexible model closely conformed to the size and shape of the rigid model. The segments of the enclosure were fabricated by preparing templates that defined the desired inner surface of the section and by using a smooth wooden or plaster mold. Complex angles, flanges or other critically dimensioned areas are incorporated by including closely machined members as part of the mold. The fiberglass part is then laid-up on the mold. First, a smooth epoxy surface coat is applied followed by a 3/8-inch layer of 14-mil glass cloth, all bonded together with an epoxy laminate material. Bonded to this layer is a 1/4-inch foam blanket, which is backed up by another 3/8-inch layer of laminated glass cloth. The result is a one-inch thick section that has several desirable properties for use as an acoustic enclosure for this application. First, the smooth inner surface of each fiberglass segment is dense and nonporous, resulting in extremely low absorption of acoustic energy into the fiberglass segments. In addition, the one-inch thick segments are very stiff and have high internal damping, with correspondingly low vibration response to the high intensity fields in the enclosure. The enclosure is

sufficiently massive to provide good attenuation of sound. Because the material and fabrication costs are low as compared to other designs, the enclosure may easily be changed to permit testing of models with major differences in size or shape.

3. TEST ARTICLE AND INSTRUMENTATION

The test article consisted of a dynamically scaled model of the Voyager spacecraft. The model was supplied by NASA Langley Research Center and was considered to be a representative spacecraft assembly. Scaling factors were: length, 1/10; mass, 1/1000; and acceleration, 10. The model included a spacecraft within a shroud closed at each end with bulkheads. A nose fairing was attached to the forward end of the shroud, and a spacer section was attached to the aft end. Weight of the major components are presented in Table 1. An illustration indicating the overall dimensions and showing the model fully assembled is presented in Figure 3. Photographs of the various components of the test article are shown in Figures 4 through 8.

Variations in the structural configuration of the model were obtained by changing the model elements. These included removal of the aft bulkhead, replacement of the spacer section with a rigid wooden element, and replacement of the total spacecraft with a wooden cylinder of equal mass and inertia. Included in the aforementioned photographs (Figure 7) is the aft bulkhead which failed during an early part of the testing. This bulkhead was replaced for later testing.

The spacecraft assembly was cantilevered from a wooden termination section. The wooden section provided a means of model support in the progressive wave tube and a termination for the acoustic field. The termination was designed to have a decreasing area which allowed the cross sectional area of the progressive wave tube to expand exponentially. The exponential area expansion corresponds to a horn having an exponential flare constant of .024 and a cutoff frequency of 25 Hz. The wooden section was suspended in the test facility with soft springs to provide suspension frequencies below the frequencies of acoustic excitation. Figure 9 shows the model installed in the progressive wave section. A muffler section with acoustic absorbtion material was installed at the aft end of the progressive wave tube to provide additional dissipation of the sound field.

Test data for the spacecraft model was measured with fifteen accelerometers, nine strain gage circuits, two microphones, and two displacement probes. The acoustic field in the progressive wave section was surveyed with fifteen microphones. Table 2 defines the location of the transducers and specifies the corresponding illustration which shows the specific locations. Also, the primary transducers from which data will be presented in this report are noted in Table 2. Figures 10 through 18 define the accelerometer locations. Figure 19 shows the microphone locations and Figure 20 presents the locations of the strain gages and probes on the aft bulkhead. The orientations of the transducers are referenced to the axes of the test article defined in Figure 19.

The orientation of the axes corresponded to the "right hand rule" notation. The +Z axis was horizontal and in the forward direction. The radial axes were oriented with the +X axis directed downward. Station zero for the Z axis corresponded to the aft suspension point for the assembly, and the spacecraft was oriented in the shroud with the spacecraft disk antenna downward or along the +X axis.

4. TEST PROCEDURE

There were two basic types of tests conducted, sinusoidal and random. Sinusoidal tests were conducted to determine the model response and to define the acoustic field. Random tests were conducted to obtain specific results to meet the following test objectives:

a. Investigation of the acoustic field and model response

b. Effects of modulator configuration

c. Linearity of the model response with changes in the acoustic field

d. Effects of model translation and rotation on the model response

e. Effects of model boundary condition, spacecraft flexibility and aft bulkhead removal

Table 3 defines the various tests conducted on the model. Translation of the model was accomplished by moving the model downward 1.75 inches in the +X direction. Rotation was accomplished by pitching the nose of the model upward approximately five degrees. This corresponded to a rotation in the X-Z plane.

The four airstream modulators were driven by electronic power amplifiers. The type of excitation (sinusoidal or random) was produced by using a sinusoidal sweep oscillator or a random octave band equalizer as an excitation source. Correlated modulator configurations were produced by connecting the coils of the airstream modulators in series. Uncorrelated modulator configurations were produced by connecting the coils of the airstream modulators to individual power amplifiers and driving each amplifier with an independent random source. The outputs of the transducer signal conditioners were recorded on FM magnetic tape. Figure 21 presents the data acquisition system which was used for the sinusoidal and random tests. The results of the sinusoidal tests are presented in the form of frequency response data. The frequency response was obtained by measuring the ratio of the absolute values of the data from the response transducer with respect to the absolute value of the pressure at station 64 (microphone 9) in the progressive wave tube. Before obtaining the ratio the data was filtered with 10 Hz bandwidth tracking filters. The random data was analyzed on a 1/3 octave band analyzer. A digital computer was used to convert the units of decibels into engineering units and compute the ratios of the 1/3 octave data for comparing results.

5. TEST RESULTS

5.1 DISCUSSION OF ACOUSTIC FIELD. The acoustic field in the progressive wave tube was evaluated to determine the magnitude of standing waves. The response of the progressive wave tube was determined by conducting a sinusoidal survey. The response pressures at various stations along the tube length were determined by measuring the pressure at the station of interest while maintaining a constant pressure at station 64 (microphone 9) with a servo control system. Figures 22 and 23 present the response amplitudes for the pressures at stations 52 and 103 referenced to station 64. The peak and null amplitudes in the response curves represent frequencies where standing waves may be present. For example, the null response at 120 Hz and the peak response at 175 Hz in Figures 22 and 23, correspond to standing waves of 1 1/4 and 1 3/4 wavelengths. The fundamental standing wave frequency was 25 Hz and is indicated as a peak in the response curve at station 103, Figure 23. The length of the progressive wave tube was one-fourth of the wavelength of the standing wave at 25 Hz. The higher order standing waves that were easily excited were odd multiples of the fundamental.

The circumferential pressure variation is presented in Figure 24. The curve presents the response amplitude at station 69, 112 1/2 degrees referenced to the pressure at station 69, 292 1/2 degrees. The circumferential pressure variation was much less than the longitudinal variation for frequencies below 1500 Hz.

Examples of standing waves at 125 Hz and 575 Hz are presented in Figures 25 and 26. The standing wave at 125 Hz represents 1 1/4 wavelengths as stated previously while the standing wave at 575 Hz corresponds to 5 3/4 wavelengths. These curves indicate the amplitude and phase variation of the pressure with respect to the model length. The amplitude represents the absolute value of the pressure and the phase was referenced to the modulator displacement. The standing waves were measured by slowly moving a microphone along a track in the progressive wave tube from station 0 to station 70. This allowed the amplitude and the phase to be displayed continuously between these two stations. The data points forward of station 70 represent the response of microphones 14, 15, and 16. The effects of the acoustic termination are shown by the relatively low standing wave ratio (ratio maximum to minimum pressure) and the nearly linear phase change. The standing wave ratio was 1.4 at 125 Hz and 1.22 at 575 Hz. These characteristics result from low reflection of the acoustic pressure in the progressive wave tube. A comparison of Figures 25 and 26 indicate that absorption increases with increasing frequency.

5.2 RESPONSE OF SPACECRAFT TO ACOUSTIC FIELD. The response of the spacecraft for the 146 dB test is presented in Figures 27 through 33. These tests were conducted with correlated sources, rigid spacer section, and the model centered in the plane wave tube. The overall acceleration on the shroud was approximately 17.4 g_{rms} at accelerometer location 11. The accelerations on the spacecraft payload were 5.4 g_{rms} in the radial direction (accelerometer 3) and 7.3 g_{rms} in the longitudinal direction (accelerometer 1). The acceleration of the retromotor support structure was 2.8 g_{rms} in

the radial direction (accelerometer 9). These values correspond to a decrease in acceleration of 8 to 16 dB from the shroud to the spacecraft. The maximum response of the shroud and spacecraft payload occurred above 1500 Hz which is the region of maximum variation in circumferential pressure. The overall acoustic pressures inside the shroud were .016 psi_{rms} at the spacecraft payload immediately below the aeroshell (microphone 1) and .011 psi_{rms} between the spacecraft and shroud near the shroud payload attach points (microphone 2). When compared to the acoustic pressure in the progressive wave tube (.058 psi_{rms}, at microphone 9) the pressure decrease is 11 to 14 dB, which is the same order as the acceleration change. The maximum pressure response inside the shroud cavity occurred at 630 Hz and 1600 Hz. The pressure response at 1600 Hz corresponds to the maximum response of the spacecraft and shroud. This result could indicate that the source of the vibration energy for the spacecraft is the acoustic pressure in the shroud. To verify this result a more detailed analysis, including narrow band power and cross power spectral density, would be required. The results of these tests showed that considerable vibration response can be produced with acoustic excitation, and there appears to be a correlation between the vibration response of the spacecraft and the acoustic pressure inside the shroud.

5.3 EFFECT OF MODULATOR CONFIGURATION ON SPACECRAFT RESPONSE. The change in response of the spacecraft for various modulator configurations is shown in Figures 34 through 43. These curves present the spacecraft and shroud response for 4 correlated, 2 correlated, and 4 uncorrelated random sources. These tests were conducted with a rigid spacer section and with the model centered in the progressive wave tube. The curves were obtained by normalizing the 1/3 octave analysis of the acceleration to the 1/3 octave analysis of the acoustic pressure. The normalization was necessary to eliminate the effects of the differences in sound pressure between the comparative tests. These tests indicate a slight increase in response for 4 uncorrelated sources. But in general, the modulator configuration for this facility had little effect on the overall model vibration response.

5.4 LINEARITY OF RESPONSE. Acoustic tests were conducted at sound pressure levels of 140 dB and 146 dB. These tests were conducted with a flexible spacecraft, including bulkheads, centered in the progressive wave tube and with a rigid spacer. The purpose of these tests was to determine the linearity of model vibration response to changes in the acoustic pressure. Figures 44 through 53 present the response (g/psi) of the spacecraft and shroud for the 140 dB and 146 dB test conditions. A review of these curves indicates insignificant changes in response ratios for the two test conditions. The results of these tests demonstrate that the vibration response of the model is linear with changes in the acoustic pressure for the limited range that was investigated.

5.5 EFFECT OF MODEL POSITION ON VIBRATION RESPONSE. Acoustic tests were conducted with the model centered, translated, and rotated in the progressive wave tube. These tests were conducted with the flexible spacecraft and rigid spacer section. Figures 54 through 63 present the spacecraft and shroud response (g/psi) and response pressures at station 52, referenced to

microphone 9 for the various test conditions. The results indicate that the model position did not have a major effect on the acoustic field or spacecraft response. The effect should be small, since translating or rotating the model does not change the geometric characteristics of the progressive wave tube. It is these geometric characteristics which are major factors in determining the acoustic pressure distribution.

5.6 EFFECT OF CONFIGURATION CHANGE ON MODEL RESPONSE

5.6.1 BOUNDARY CONDITION EFFECTS. Tests were conducted to determine the effects of model boundary conditions on the response of the spacecraft and shroud. This was accomplished by comparing the results of tests which altered the characteristics of the 6-inch spacer section. A rigid spacer section fabricated from mahogany with a 2-inch wall thickness and a flexible spacer section fabricated in a similar manner as the shroud were used. Figures 64 through 73 compare the response of the spacecraft, shroud and acoustic field for the two spacer configurations. These tests were conducted at 146 dB. The spacecraft and shroud were not significantly affected by the boundary condition change. The shroud was affected only at the lower end of the spectrum which is the frequency region where the additional section would have the primary effect on the structural modes of the shroud.

5.6.2 EFFECT OF AFT BULKHEAD ON MODEL RESPONSE. An investigation was conducted to determine the effects of the aft bulkhead on the response of the model. The aft bulkhead failed during the early phases of the test program as shown in Figure 7. Strain gages were installed on the new bulkhead and noncontacting displacement transducers were installed in the wooden termination to detect bulkhead displacement. Responses of the spacecraft, shroud and acoustic field with and without the bulkhead, were obtained and the information is presented in Figures 74 through 83. Only minor changes in the response of the spacecraft or shroud could be detected for this variation in configuration. The removal of the bulkhead increased the length of the cavity in which the spacecraft was mounted. This increase in cavity length would lower the internal standing wave frequencies and would not be expected to affect the primary model response above 1500 Hz. The acoustic pressure response in the shroud (Figure 78) indicated little change except for an increase in response at 165 Hz. This frequency corresponds to a standing wave which has a wavelength of 84 inches. This is approximately the length of the cavity formed by the shroud, spacer section, and wooden termination.

The displacement transducers and the strain gages did not reveal any significant magnitudes which could induce bulkhead failure. The maximum bulkhead displacement was .0017 inch and the maximum strain was 125 μ in./in. These levels were measured during a 146 dB test with the flexible spacecraft and flexible spacer. Possible explanation for the failure of the original bulkhead may be a manufacturing defect or buckling of the dome due to combined static and dynamic loads. Buckling would induce local yielding and accelerate sonic fatigue.

5.6.3 EFFECT OF THE SPACECRAFT ON MODEL RESPONSE. Tests were conducted to determine the effects of the dynamically similar spacecraft on the response of the shroud. The dynamically similar spacecraft was replaced with a mass and inertia simulator as shown in Figures 10 and 11. Responses of the shroud and spacecraft were measured for a 146 dB broadband random acoustic test. Comparative data resulting from the rigid and flexible spacecraft tests are presented in Figures 84 through 92. Very little change in shroud response was indicated while the response of the rigid spacecraft in the Z-axis decreased appreciably.

6. CONCLUSIONS

In the tests conducted for this program, it was shown that significant dynamic response of the model could be obtained using a simple fiberglass enclosure and acoustic sources. The magnitudes of these responses are representative of those that would be expected in an actual flight environment. However, no attempt was made to simulate the actual acoustic environment to which an aerospace vehicle is exposed in terms of the spatial amplitude and phase relationships of the acoustic pressure. Only minor variations in the dynamic response were observed for variations in the rotational or translational position of the model within the test enclosure. Therefore, for this type of testing, it should be possible to use relatively simple and inexpensive support systems that do not require precise positioning devices.

The testing to evaluate the effects of variations in the structural configuration produced some significant results. The use of a rigid or flexible spacer section between the shroud and the termination section affected the response only in the low frequency range of the shroud where the spacer could have affected structural modes. The inclusion or removal of the aft bulkhead enclosing the spacecraft within the shroud had an insignificant effect on the model response.

The use of a rigid model with the same mass and center of gravity to replace the spacecraft affected the shroud response only in a small frequency range. The response of the flexible spacecraft model as compared to the rigid model indicates a significant change in response associated with the elastic modes of the model and its components.

These results indicate that the changes in the dynamic response of the model due to variations in the structural configuration are primarily restricted to the local areas where the structural changes are made except in the frequency range where there is a significant dynamic interaction between the components. However, it should be noted that the negligible effect of removing the aft bulkhead probably results from the high acoustic attenuation of the nose fairing and shroud.

Finally, the results of this program indicate that acoustic testing using a simple fiberglass enclosure is an effective means of producing broadband dynamic response of flexible vehicles. In addition, minor variations in structural configuration and variations of model position in the test facility indicated minor effects on the test results.

7. REFERENCES

1. Daiber, J. R.; and Noonan, V. S.: The Vibration Design Approval and Acceptance Test Program for the Gemini Spacecraft - Component, Module and Whole Vehicle Testing. The Shock and Vibration Bulletin, Bulletin 35, Part 2, U.S. Naval Research Laboratory, Washington, D.C., January 1966.

2. Cooper, J. L.: Advantages of Multipoint Control for Vibration Testing of Complete Ranger Flight Spacecraft. The Shock and Vibration Bulletin, Bulletin 35, Part 2, U.S. Naval Research Laboratory, Washington, D.C., January 1966.

3. Baruch, J.J.; and Davis, S.: Implications of Spacecraft Vibration Qualification Testing Requirements on Structural Design. The Shock and Vibration Bulletin, Bulletin 35, Part 2, U.S. Naval Research Laboratory, Washington, D.C., January 1966.

4. Chirley, A. E.; Stevens, R. A.; and Wood, W. R. Jr.: Apollo CSM Dynamic Test Program. The Shock and Vibration Bulletin, Bulletin 39, Part 2, U.S. Naval Research Laboratory, Washington, D.C., February 1969.

5. Jacobs, D. B.: Summary of Vibration and Acoustic Tests on Four Spacecraft Programs. Document No. D2-120001-2 (NASw-1650), The Boeing Company, 28 June 1968.

6. Trummel, M. C.: Ground Test Simulation of Lift-off and Transonic Vibration Excitation Mechanisms on the Ranger Spacecraft. The Shock and Vibration Bulletin, Bulletin 35, Part 2, U.S. Naval Research Laboratory, Washington, D. C., January 1966.

7. Wren, R. J.; Dorland, W. D.; Johnston, J. D. Jr.; and Eldred, K. McK.: Concept, Design, and Performance of the MSC Spacecraft Acoustic Laboratory. The Shock and Vibration Bulletin, Bulletin 37, Part 5, U.S. Naval Research Laboratory, Washington, D.C., January 1968. (Available as NASA TMX-58017, March 1968.

TABLE 1

WEIGHTS OF MAJOR COMPONENTS OF TEST VEHICLE

Nose Cone	2.74 lbs.
Shroud Section	4.39 lbs.
Flexible Spacer Section	1.05 lbs.
Surface Mass Density of Cylinder Sections	2.44×10^{-6} to 2.70×10^{-6} $\frac{lb\text{-}sec^2}{in^3}$
Total Spacecraft (including support legs)	19-20 lbs.
Simulated Surface Lab System	1.31 lbs.

TABLE 2

TRANSDUCER LOCATIONS

TRANSDUCER	LOCATION	MODEL CONFIGURATION	AXIS OF SENSITIVITY	ILLUSTRATION
Accel. 1*	Surface laboratory system	Flexible model, flexible and rigid spacers	Z-axis	Fig. 12, Pg. 30
Accel. 1a*	Upper surface of rigid model	Rigid model, rigid spacer	Z-axis	Fig. 11, Pg. 29
Accel. 2	Surface laboratory system	Flexible model, flexible and rigid spacers	45° off X-axis	Fig. 12, Pg. 30
Accel. 2a	Next to upper surface of rigid model	Rigid model, rigid spacer	45° off X-axis	Fig. 11, Pg. 29
Accel. 3*	Surface laboratory system	Flexible model, flexible and rigid spacers	45° off Y-axis	Fig. 12, Pg. 30
Accel. 3a*	Next to upper surface of rigid model	Rigid model, rigid spacer	45° off Y-axis	Fig. 11, Pg. 29
Accel. 4	Fuel cell surface	Flexible model, rigid and flexible spacers	X-axis	Fig. 13, Pg. 30
Accel. 4a	Next to bottom surface of rigid model	Rigid model, rigid spacer	X-axis	Fig. 10, Pg. 29

* Selected transducers used in discussion of this report.

TABLE 2 (Cont.)

TRANSDUCER LOCATIONS

TRANSDUCER	LOCATION	MODEL CONFIGURATION	AXIS OF SENSITIVITY	ILLUSTRATION
Accel. 5	Fuel cell surface	Flexible model, flexible and rigid spacers	Z-axis	Fig. 13, Pg. 30
Accel. 5a	On bottom surface of rigid model	Rigid model, rigid spacer	Z-axis	Fig. 10, Pg. 29
Accel. 6	Fuel cell surface	Flexible model, flexible and rigid spacers	Y-axis	Fig. 13, Pg. 30
Accel. 6a	Next to bottom surface of rigid model	Rigid model, rigid spacer	Y-axis	Fig. 10, Pg. 29
Accel. 7	Retrorocket nozzle	Flexible model, flexible and rigid spacers	Z-axis	Fig. 14, Pg. 31
Accel. 8	Retrosupport structure	Flexible model, flexible and rigid spacers	X-axis	Fig. 15, Pg. 31
Accel. 9*	Retrosupport structure	Flexible model, flexible and rigid spacers	Y-axis	Fig. 15, Pg. 31
Accel. 10	Fuel cell support structure	Flexible model, flexible and rigid spacers	Z-axis	Fig. 15, Pg. 31

* Selected transducers used in discussion of this report.

TABLE 2 (Cont.)

TRANSDUCER LOCATIONS

TRANSDUCER	LOCATION	MODEL CONFIGURATION	AXIS OF SENSITIVITY	ILLUSTRATION
Accel. 11*	Vehicle attach ring	Flexible model, flexible and rigid spacers; runs 1-16	X (radial)	Fig. 16, Pg. 32
Accel. 11a*	Vehicle attach ring	Flexible model, flexible and rigid spacers; runs 17-34	X (radial)	Fig. 18, Pg. 33
Accel. 12	Vehicle attach ring	Flexible model, flexible and rigid spacers; runs 1-16	Between supports (radial)	Fig. 16, Pg. 32
Accel. 12a	Aft bulkhead attach ring	Flexible model, flexible and rigid spacers; runs 17-34	15° off X-axis (radial)	Fig. 18, Pg. 33
Accel. 13	Planetary vehicle support	Flexible model, flexible and rigid spacers; runs 1-16	Y-axis	Fig. 17, Pg. 32
Accel. 13a	Aft bulkhead attach ring	Flexible model, flexible and rigid spacers; runs 17-34	45° off X-axis (radial)	Fig. 18, Pg. 33
Accel. 14	Planetary vehicle support	Flexible model, flexible and rigid spacers; runs 1-16	Z-axis	Fig. 17, Pg. 32

* Selected transducers used in discussion of this report.

TABLE 2 (Cont.)

TRANSDUCER LOCATIONS

TRANSDUCER	LOCATION	MODEL CONFIGURATION	AXIS OF SENSITIVITY	ILLUSTRATION
Accel. 15	Planetary vehicle support inside spacecraft bus	Flexible model, flexible and rigid spacers; runs 1-16	X-axis (radial)	Fig. 13, Pg. 30
Accel. 15a	Flexible spacer aft	Flexible model, flexible spacer; runs 17-31	X-axis (radial)	Fig. 18, Pg. 33
Accel. 15b	Saturn V shroud aft	Flexible model, rigid and flexible spacers; runs 17-31	X-axis (radial)	Fig. 18, Pg. 33
Micr. 1*	Surface laboratory system	Flexible model, flexible and rigid spacers	Z-axis	Fig. 12, Pg. 30
Micr. 1a*	Center of rigid model forward	Rigid model, rigid spacer	Z-axis	Fig. 11, Pg. 29
Micr. 2*	Planetary vehicle support	Flexible model, flexible and rigid spacers	15° off X-axis (radial)	Fig. 10, Pg, 29
Micr. 2a*	Planetary vehicle support	Rigid model, rigid spacer	15° off X-axis	Fig. 10, Pg. 29
Micr. 3	Plane wave tube Sta. 3-22.5°	All configurations	-	Fig. 19, Pg. 34

* Selected transducers used in discussion of this report.

TABLE 2 (Cont.)

TRANSDUCER LOCATIONS

TRANSDUCER	LOCATION	MODEL CONFIGURATION	AXIS OF SENSITIVITY	ILLUSTRATION
Micr. 4*	Plane wave tube Sta. 52-22.5°	All configurations	-	Fig. 19, Pg. 34
Micr. 5*	Plane wave tube Sta. 52-112.5°	All configurations	-	Fig. 19, Pg. 34
Micr. 6*	Plane wave tube Sta. 52-202.5°	All configurations	-	Fig. 19, Pg. 34
Micr. 7*	Plane wave tube Sta. 52-292.5°	All configurations	-	Fig. 19, Pg. 34
Micr. 8	Plane wave tube Sta. 58-22.5°	All configurations	-	Fig. 19, Pg. 34
Micr. 9*	Plane wave tube Sta. 64-22.5°	All configurations	-	Fig. 19, Pg. 34
Micr. 10	Plane wave tube Sta. 69-22.5°	All configurations	-	Fig. 19, Pg. 34
Micr. 11	Plane wave tube Sta. 69-112.5°	All configurations	-	Fig. 19, Pg. 34
Micr. 12	Plane wave tube Sta. 69-202.5°	All configurations	-	Fig. 19, Pg. 34
Micr. 13	Plane wave tube Sta. 69-292.5°	All configurations	-	Fig. 19, Pg. 34
Micr. 14	Plane wave tube Sta. 80-22.5°	All configurations	-	Fig. 19, Pg. 34

* Selected transducers used in discussion of this report.

TABLE 2 (Cont.)

TRANSDUCER LOCATIONS

TRANSDUCER	LOCATION	MODEL CONFIGURATION	AXIS OF SENSITIVITY	ILLUSTRATION
Micr. 15	Plane wave tube Sta. 91-22.5°	All configurations	-	Fig. 19, Pg. 34
Micr. 16	Plane wave tube Sta. 103-22.5°	All configurations	-	Fig. 19, Pg. 34
Micr. 17	Plane wave tube Sta. 115.5-22.5°	All configurations	-	Fig. 19, Pg. 34
Str. Gage 1	Planetary vehicle support	All configurations	-	Fig. 13, Pg. 30
Str. Gage 2	Planetary vehicle support	All configurations	-	Fig. 13, Pg. 30
Str. Gage 3	Planetary vehicle support	All configurations	-	Fig. 13, Pg. 30
Str. Gage 4	Forward bulkhead X-axis	Flexible model, runs 17-20 runs 29-31	-	Fig. 20, Pg. 35
Str. Gage 5	Forward bulkhead 120° off X-axis	Flexible model, runs 17-20 runs 29-31	-	Fig. 20, Pg. 35
Str. Gage 6	Forward bulkhead 240° off X-axis	Flexible model, runs 17-20 runs 29-31	-	Fig. 20, Pg. 35

TABLE 2 (Concluded)

TRANSDUCER LOCATIONS

TRANSDUCER	LOCATION	MODEL CONFIGURATION	AXIS OF SENSITIVITY	ILLUSTRATION
Str. Gage 7	Aft bulkhead X-axis	Flexible model, runs 17-20 runs 29-31	-	Fig. 20, Pg. 35
Str. Gage 8	Aft bulkhead 120° off X-axis	Flexible model, runs 17-20 runs 29-31	-	Fig. 20, Pg. 35
Str. Gage 9	Aft bulkhead 240° off X-axis	Flexible model, runs 17-20 runs 29-31	-	Fig. 20, Pg. 35
S.G. Mod. 1	Modulator 1	-	-	N/A
S.G. Mod. 2	Modulator 2	-	-	N/A
S.G. Mod. 3	Modulator 3	-	-	N/A
S.G. Mod. 4	Modulator 4	-	-	N/A
Disp. Probe 1	Aft bulkhead bottom, X-axis	Flexible model, runs 17-20 runs 29-31	-	Fig. 20, Pg. 35
Disp. Probe 2	Aft bulkhead at failure	Flexible model, runs 17-20 runs 29-31	-	Fig. 20, Pg. 35

TABLE 3

TEST PLAN

RUN NO.	NO. OF SOURCES	SIGNAL	COMMENT
	MODEL CENTERED, RIGID SPACER, FLEXIBLE MODEL		
1	1	Sine	
2	2	Sine, In-phase	
3	4	Sine, In-phase	
4	4	Sine, In-phase	Standing Wave Survey
5	4	Random, Correlated	146 dB
6	4	Random, Correlated	143 dB
7	4	Random, Correlated	140 dB
8	4	Random, Uncorrelated	140 dB
9	2	Random, Correlated	146 dB
	MODEL TRANSLATED, RIGID SPACER, FLEXIBLE MODEL		
10	4	Sine, In-phase	
11	4	Random, Correlated	146 dB
12	2	Random, Correlated	146 dB
13	4	Random, Uncorrelated	140 dB
	MODEL ROTATED, RIGID SPACER, FLEXIBLE MODEL		
14	4	Sine, In-phase	
15	4	Random, Correlated	146 dB
16	2	Random, Correlated	146 dB

TABLE 3 (Concluded)

RUN NO.	NO. OF SOURCES	SIGNAL	COMMENT
		MODEL CENTERED, FLEXIBLE SPACER WITH BULKHEAD	
17	4	Sine, In-phase	
18	4	Random, Correlated	146 dB
19	4	Random, Correlated	140 dB
20	4	Random, Uncorrelated	140 dB
		MODEL CENTERED, RIGID SPACER, RIGID MODEL	
21	4	Sine, In-phase	146 dB
22	4	Random, Correlated	140 dB
23	4	Random, Correlated	140 dB
24	4	Random, Uncorrelated	140 dB
		MODEL CENTERED, RIGID SPACER, FLEXIBLE MODEL, NO BULKHEAD	
25	4	Sine, In-phase	
26	4	Random, Correlated	140 dB
27	4	Random, Correlated	146 dB
28	4	Random, Uncorrelated	146 dB
		MODEL CENTERED, RIGID SPACER, FLEXIBLE MODEL, WITH BULKHEAD	
29	4	Random, Correlated	140 dB
30	4	Random, Correlated	146 dB
31	4	Random, Uncorrelated	140 dB
		MODEL CENTERED, FLEXIBLE SPACER, FLEXIBLE MODEL, NO BULKHEAD	
32	4	Sine, In-phase	
33	4	Random, Correlated	146 dB
34	4	Random, Correlated	140 dB

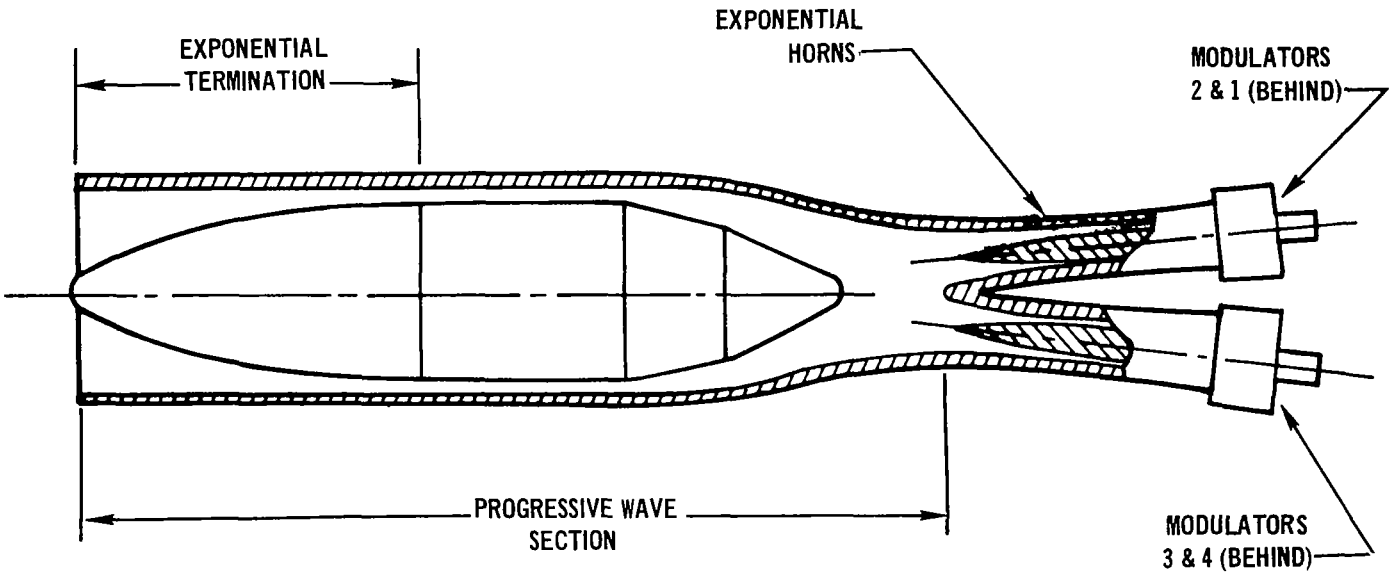

FIGURE 1

TEST FACILITY

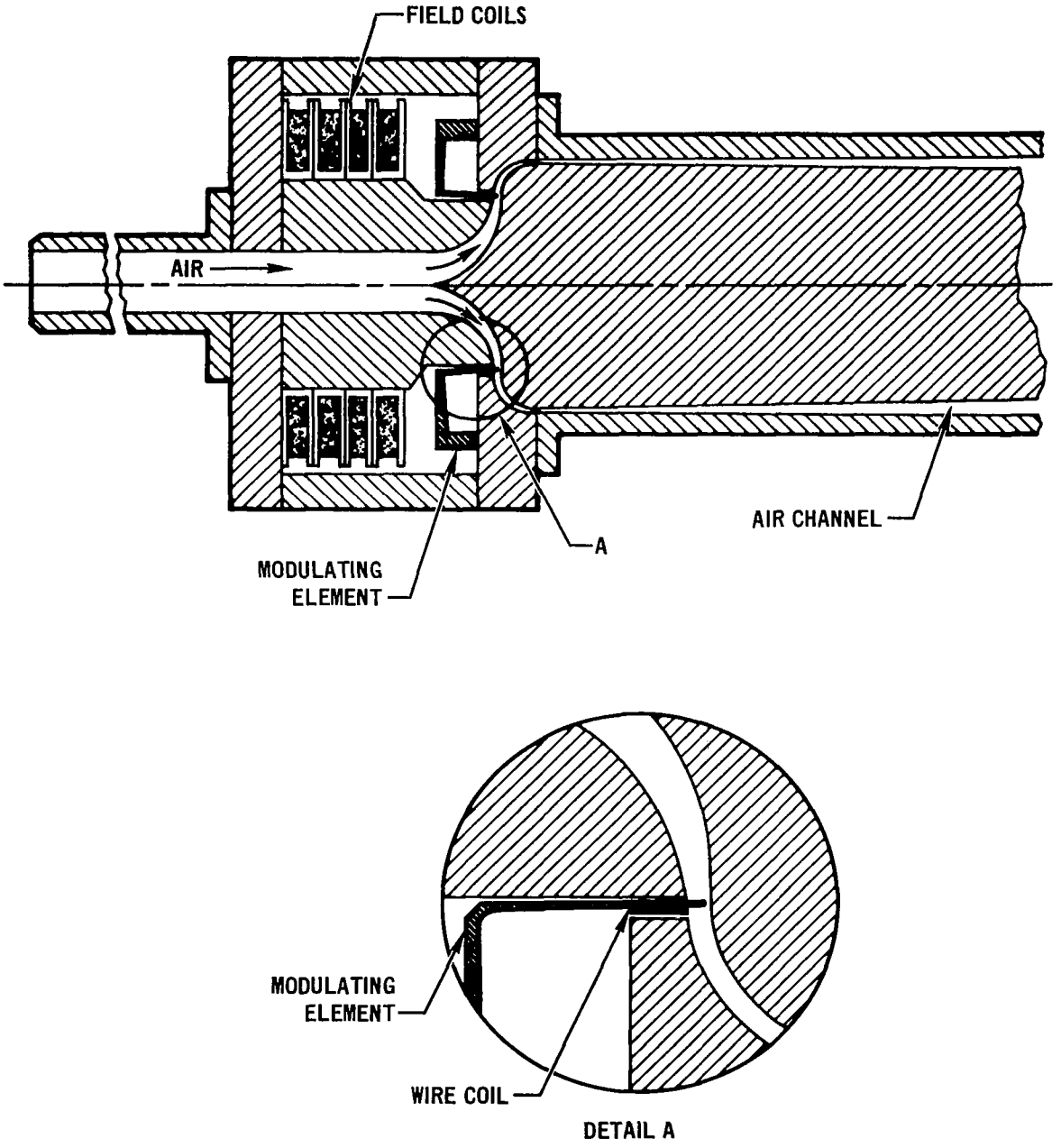

CROSS–SECTIONAL VIEW OF AIR STREAM MODULATOR
FIGURE 2

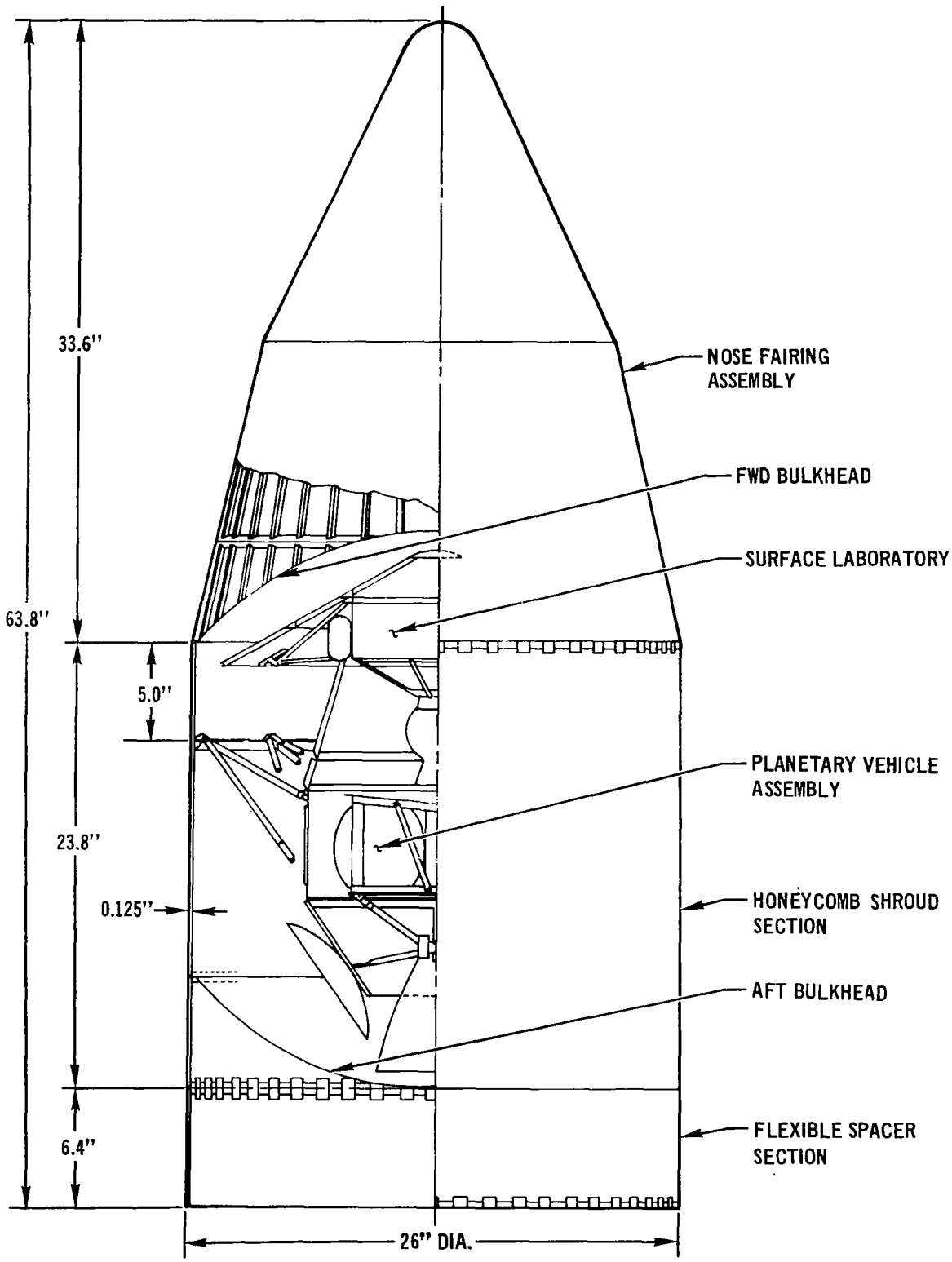

TEST MODEL
FIGURE 3

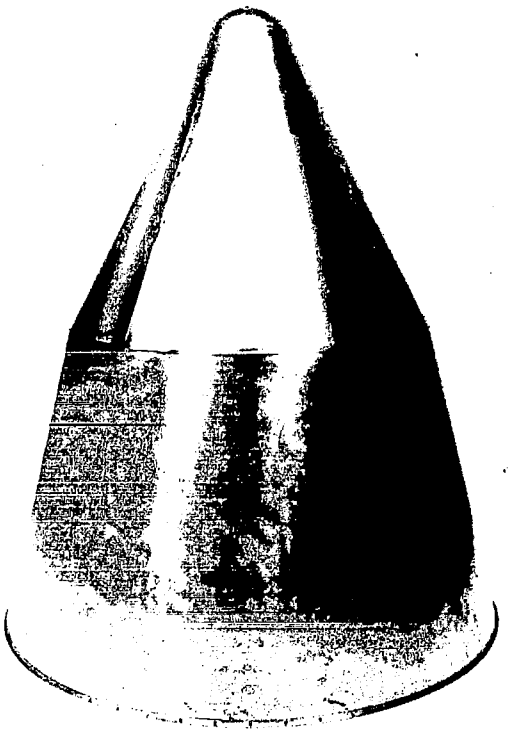

SPACECRAFT NOSE FAIRING
FIGURE 4

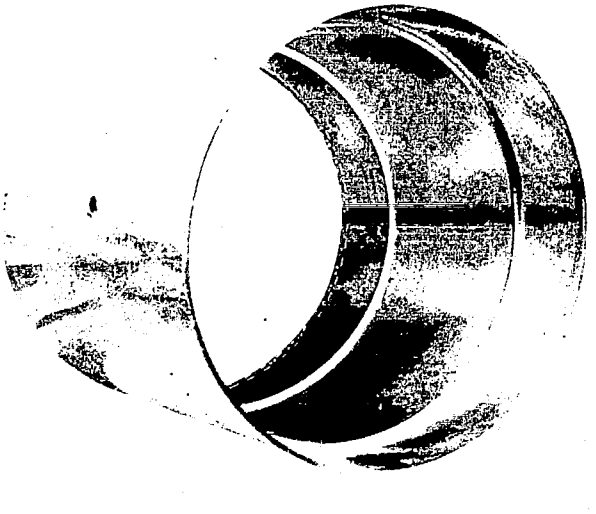

SATURN V SHROUD
FIGURE 5

SPACECRAFT PRESSURE BULKHEAD
Viewing Inner Surface

FIGURE 6

AFT PRESSURE BULKHEAD FAILURE
Viewing Vehicle from Rear in +Z Direction

FIGURE 7

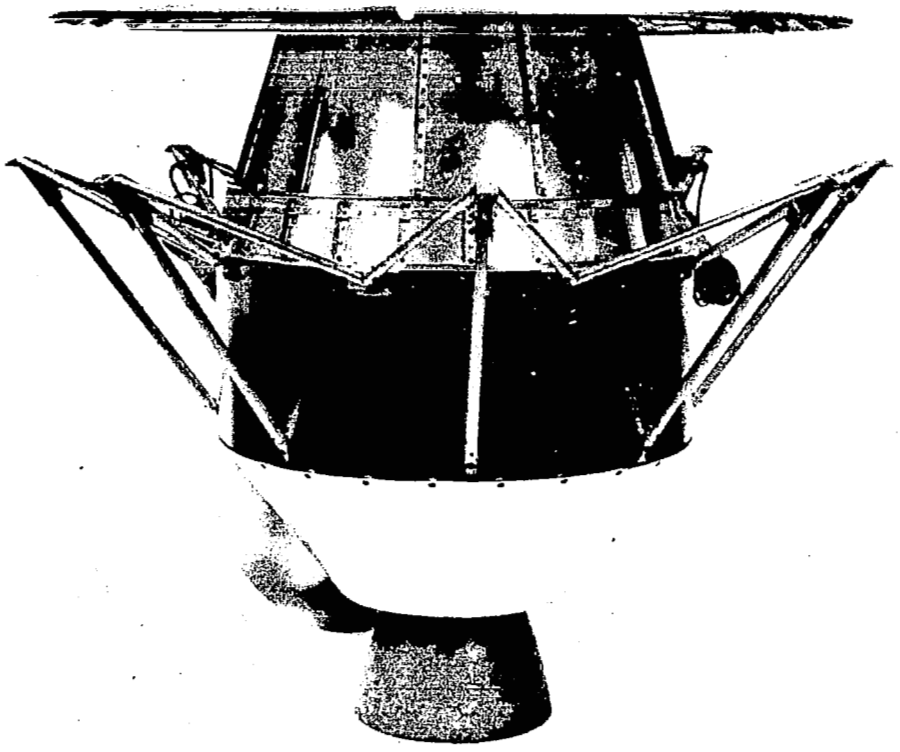

1/10 SCALED MODEL OF REPRESENTATIVE SPACECRAFT ASSEMBLY

FIGURE 8

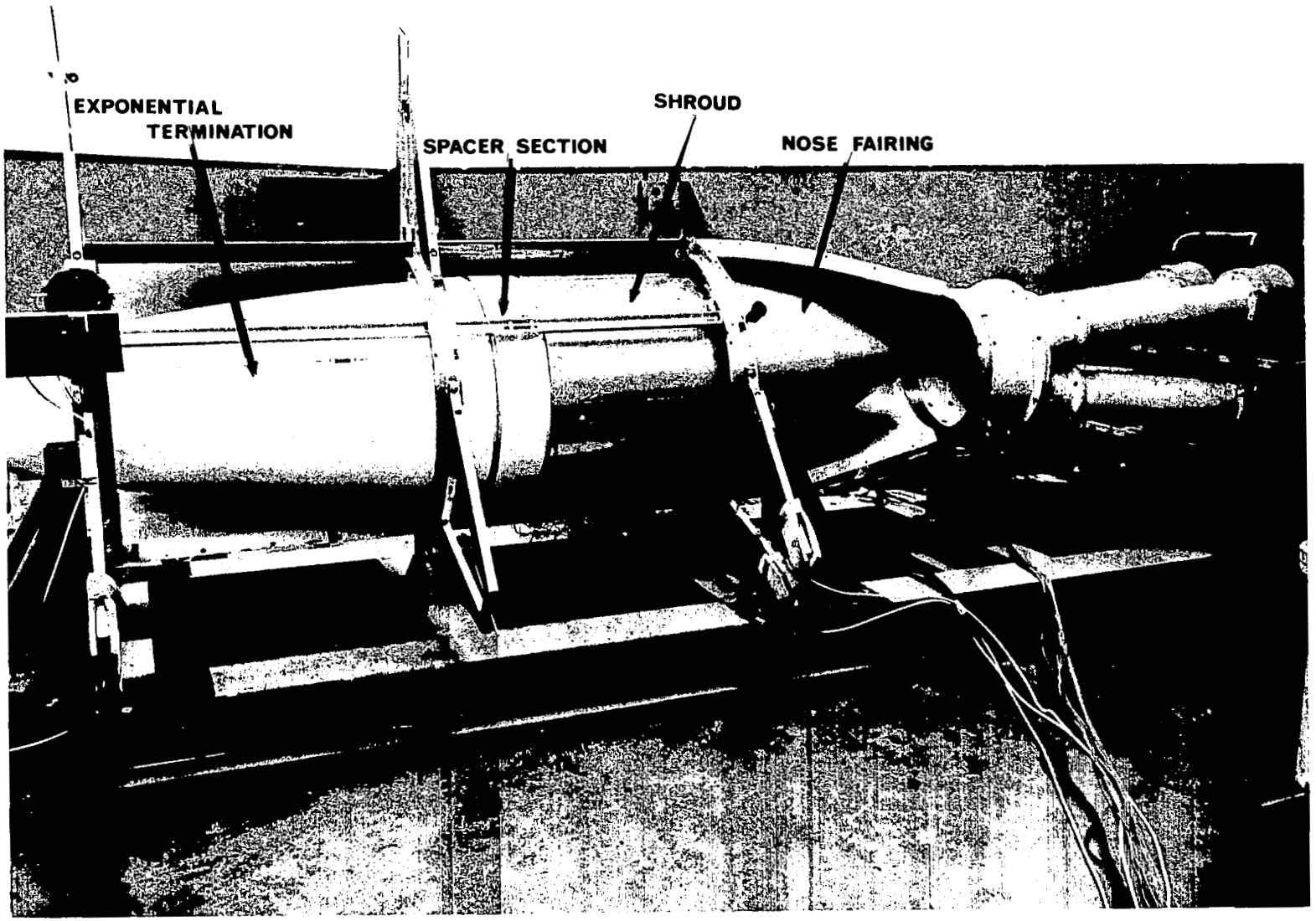

FIGURE 9

MODEL INSTALLATION IN ACOUSTIC FACILITY

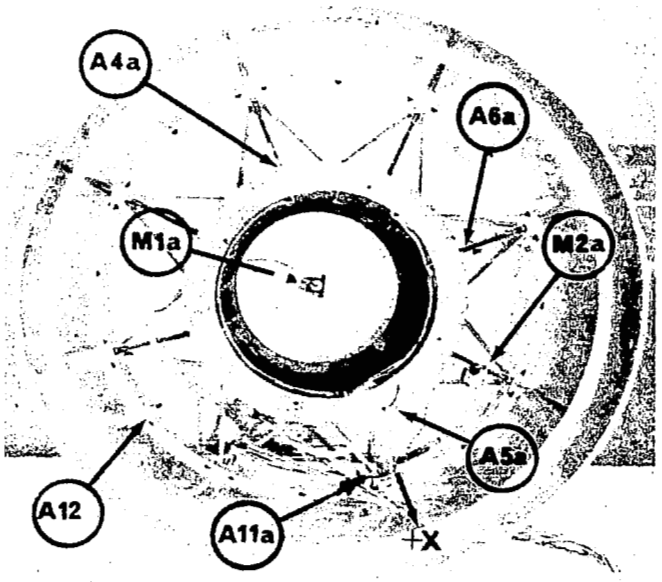

RIGID MODEL TRANSDUCER LOCATIONS
Viewing Model in +Z Direction

FIGURE 10

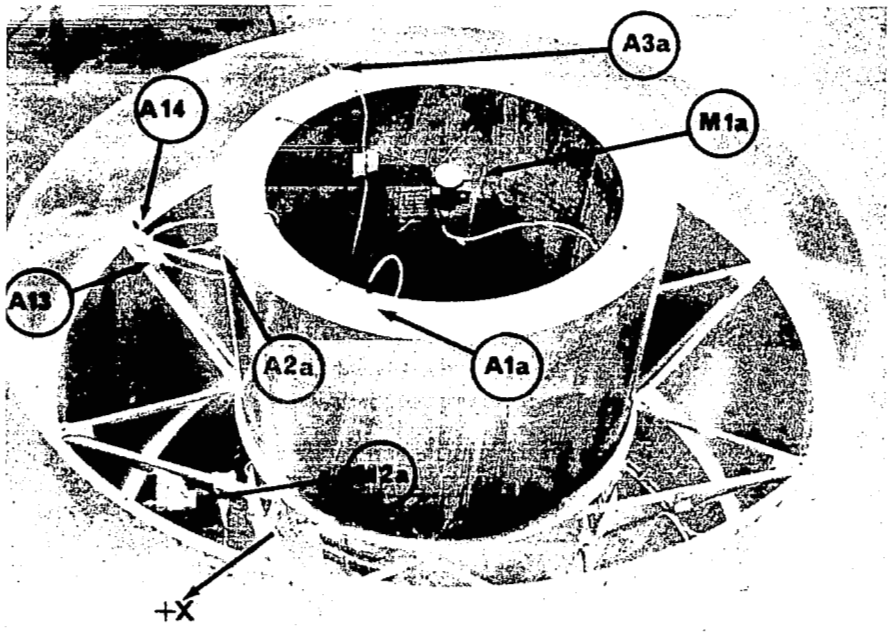

RIGID MODEL TRANSDUCER LOCATIONS
Viewing Model from Top

FIGURE 11

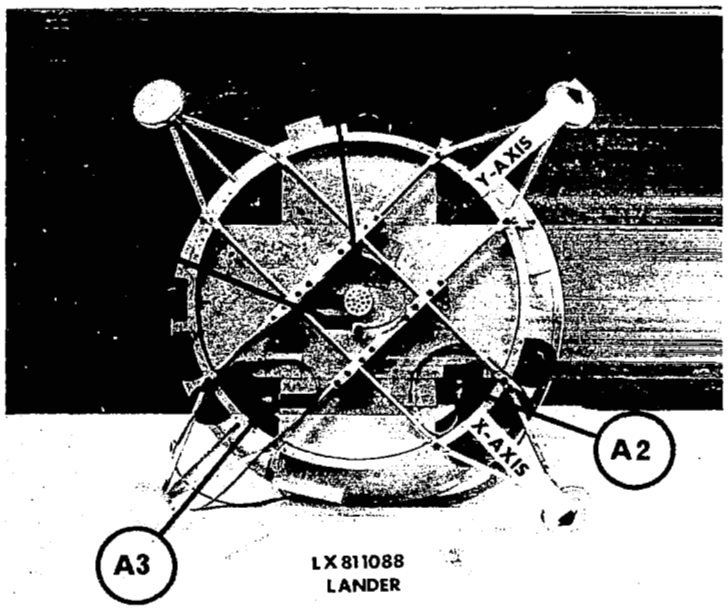

FLEXIBLE MODEL TRANSDUCER LOCATIONS
Viewing Lander (LX811088) from Top in -Z Direction

FIGURE 12

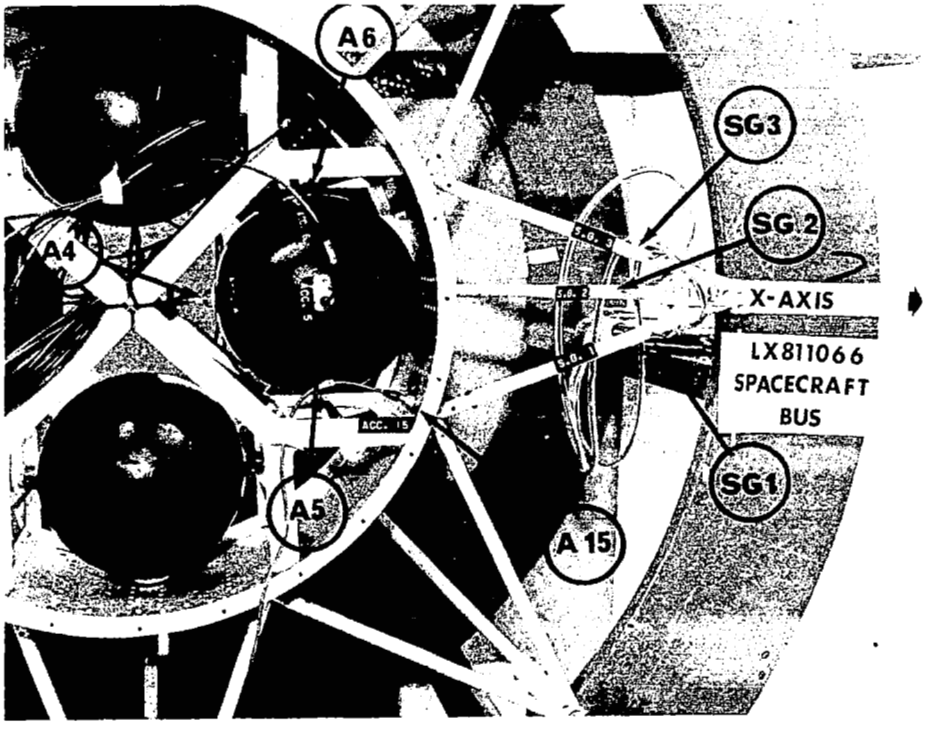

FLEXIBLE MODEL TRANSDUCER LOCATIONS
Viewing Spacecraft Bus (LX811066) from Top in -Z Direction

FIGURE 13

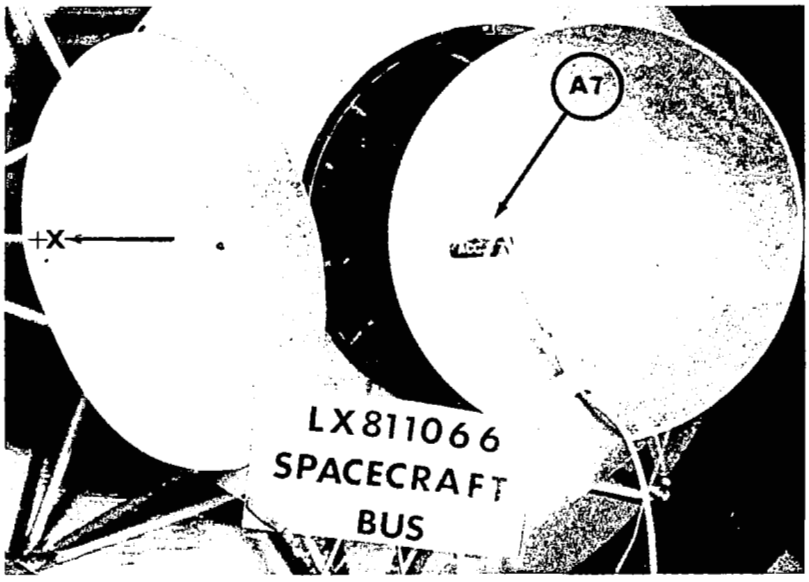

FLEXIBLE MODEL ACCELEROMETER LOCATIONS
Viewing Spacecraft Bus (LX811066) from Bottom in +Z Direction

FIGURE 14

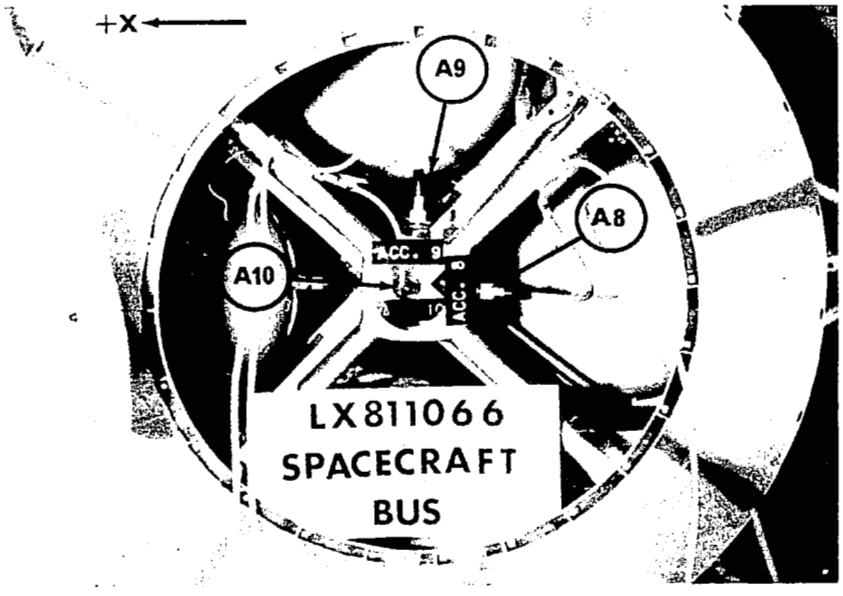

FLEXIBLE MODEL ACCELEROMETER LOCATIONS
Viewing Spacecraft Bus (LX811066) from Bottom in +Z Direction
with Retrorocket Nozzle Removed

FIGURE 15

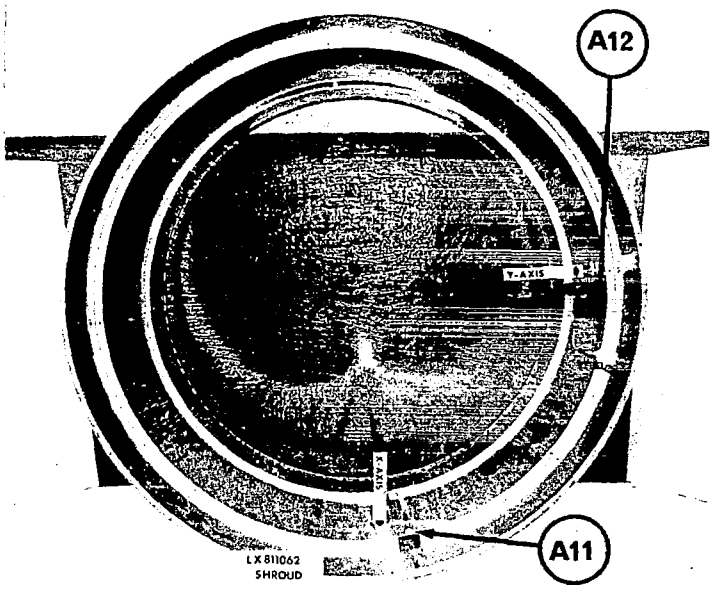

SATURN V SHROUD (LX811062) ACCELEROMETER LOCATIONS
Viewing Shroud from Top in -Z Direction

FIGURE 16

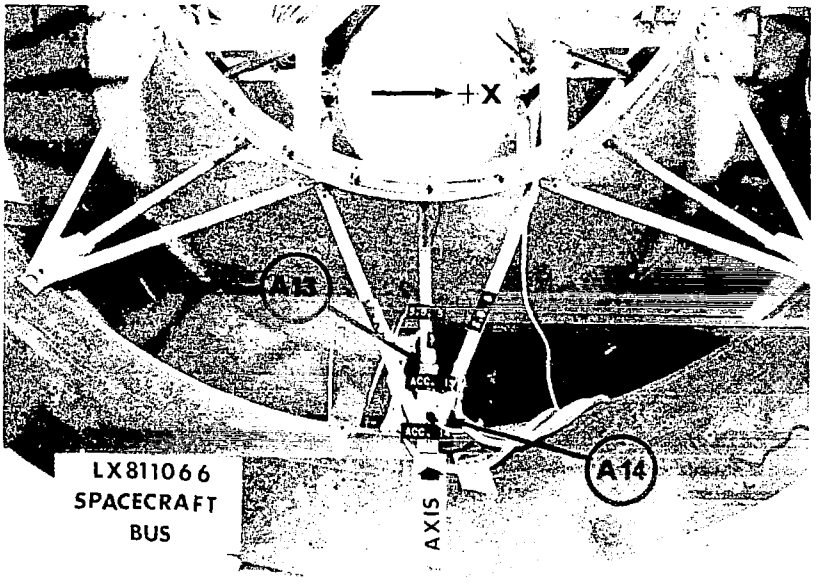

FLEXIBLE MODEL ACCELEROMETER LOCATIONS
Viewing Section of Spacecraft Bus (LX811066) in -Z Direction

FIGURE 17

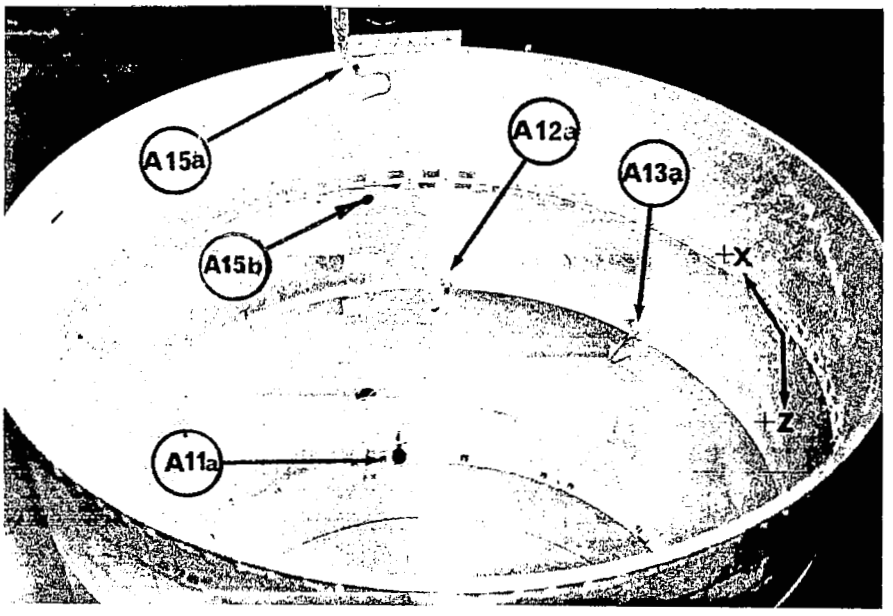

SATURN V SHROUD AND FLEXIBLE ACCELEROMETER LOCATIONS
Viewing Assembly from Bottom in +Z Direction

FIGURE 18

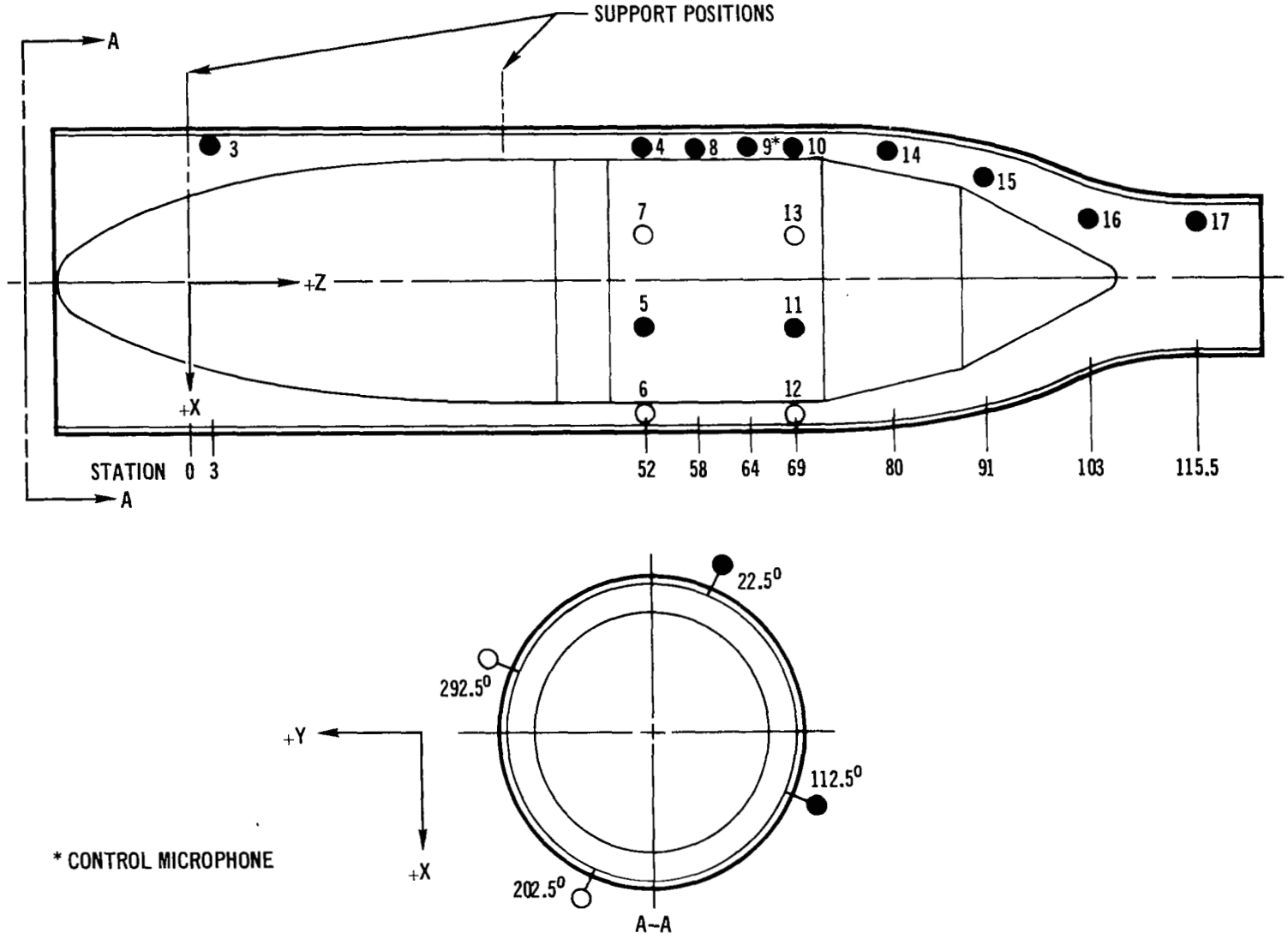

FIGURE 19

MICROPHONE LOCATIONS

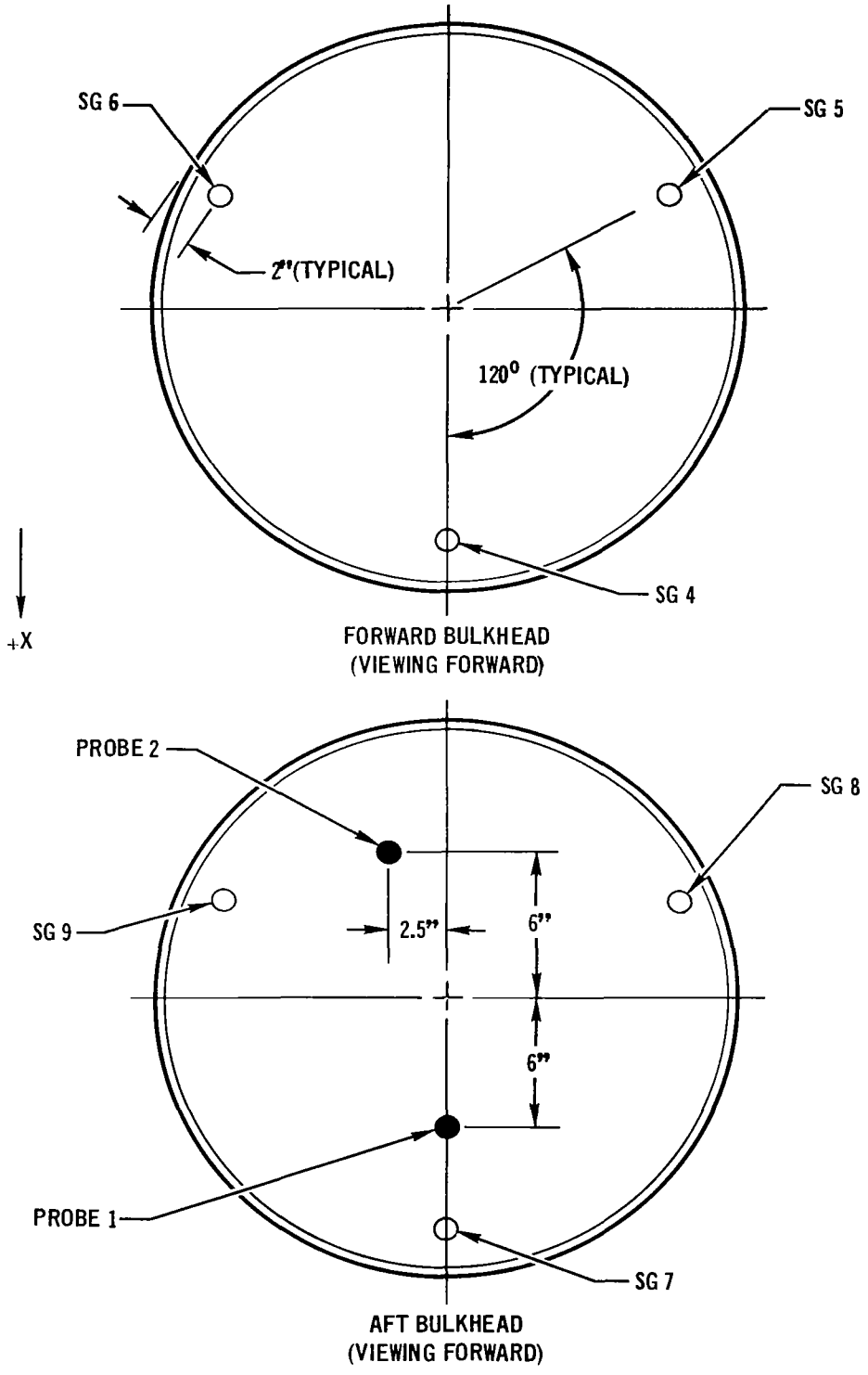

BULKHEAD INSTRUMENTATION

FIGURE 20

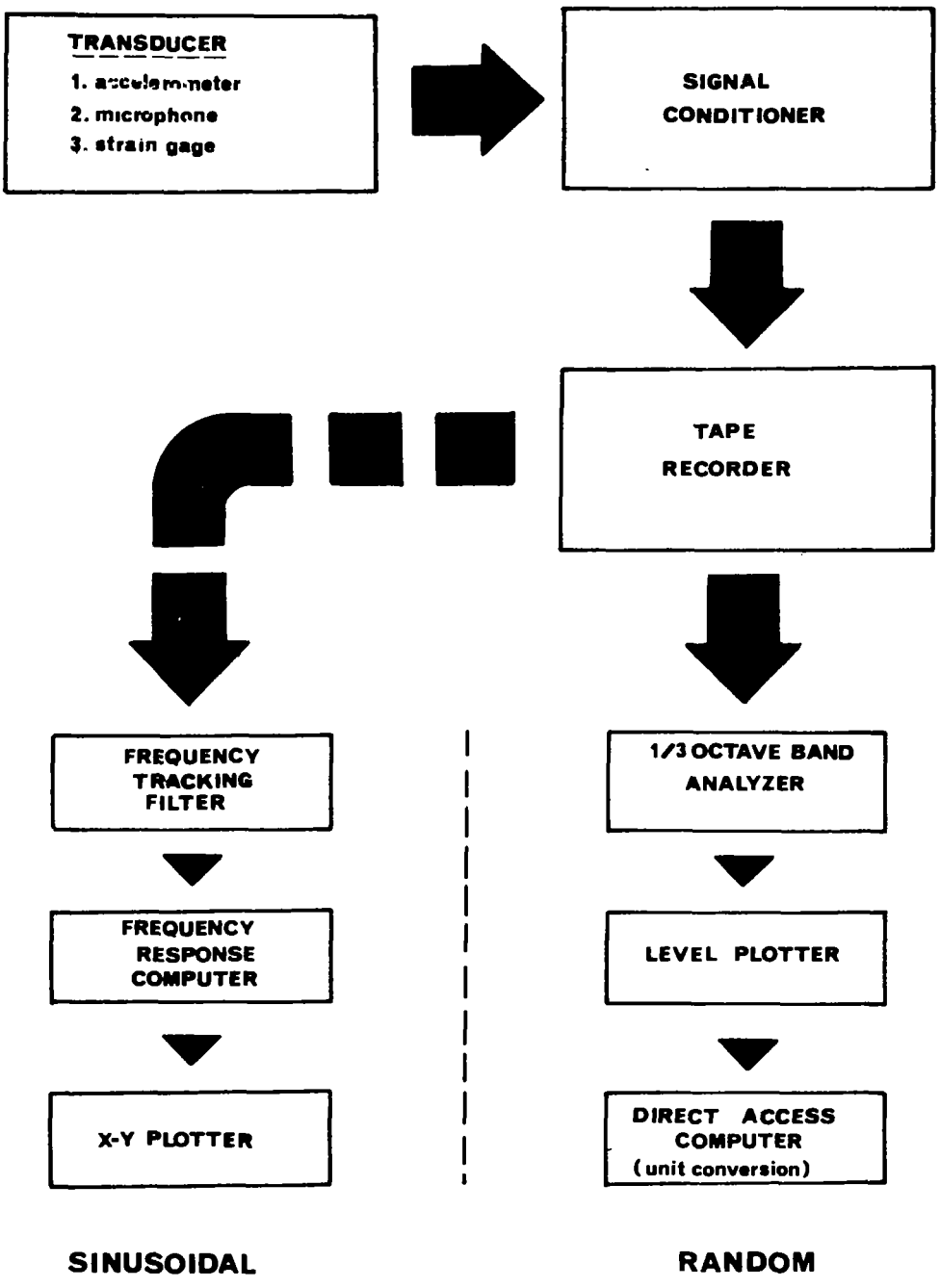

DATA ACQUISITION

FIGURE 21

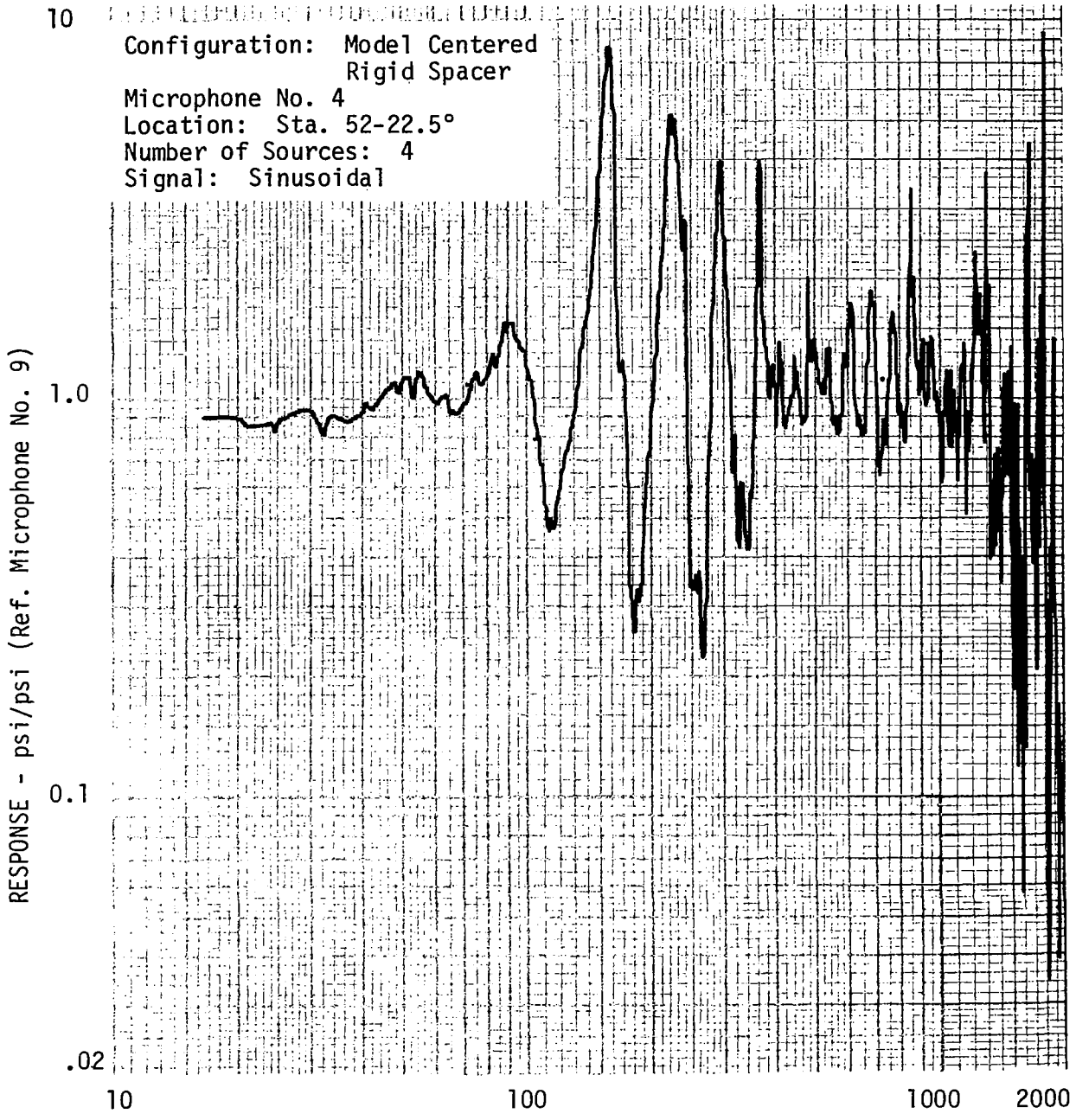

SOUND PRESSURE RESPONSE

FIGURE 22

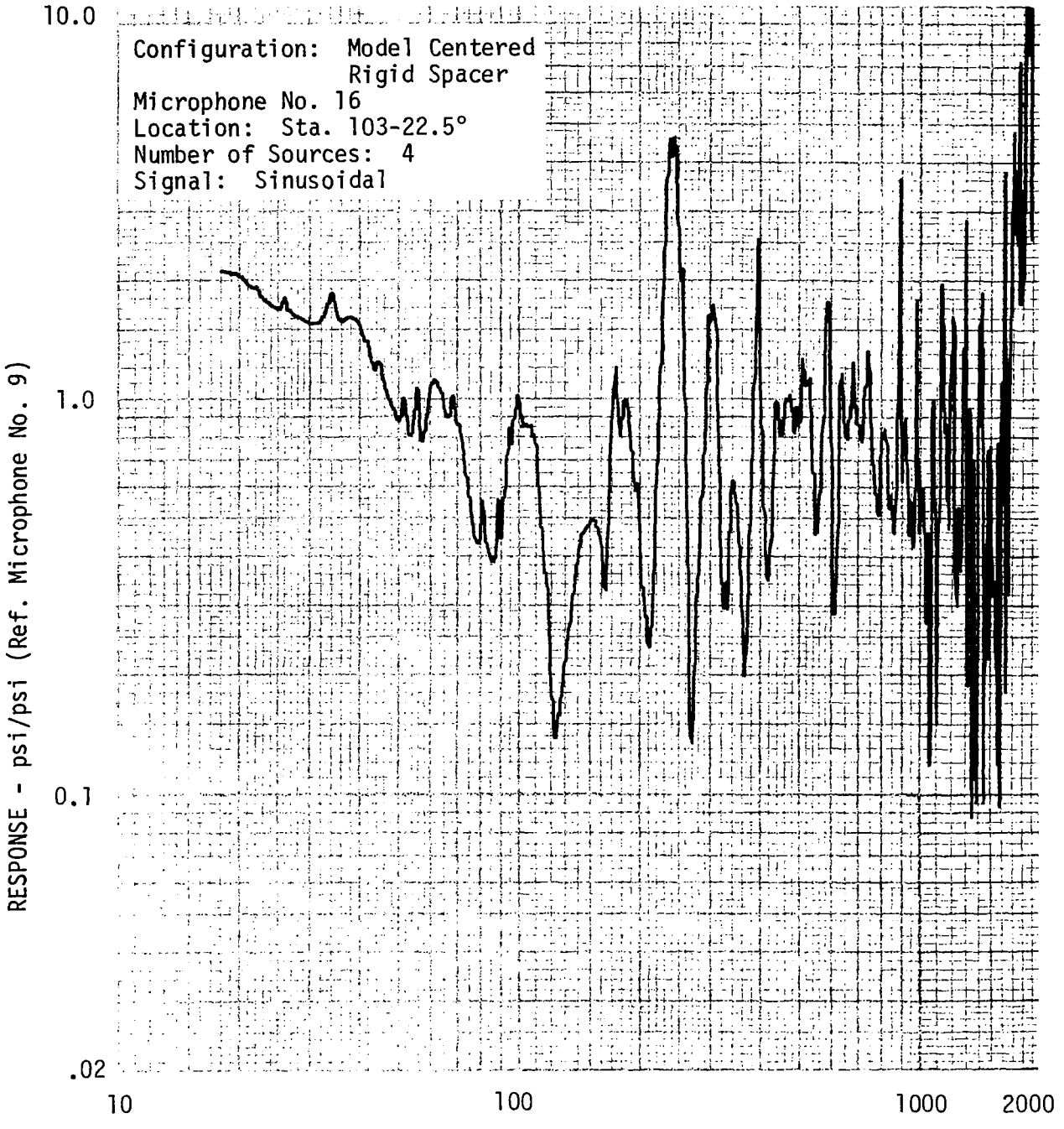

SOUND PRESSURE RESPONSE

FIGURE 23

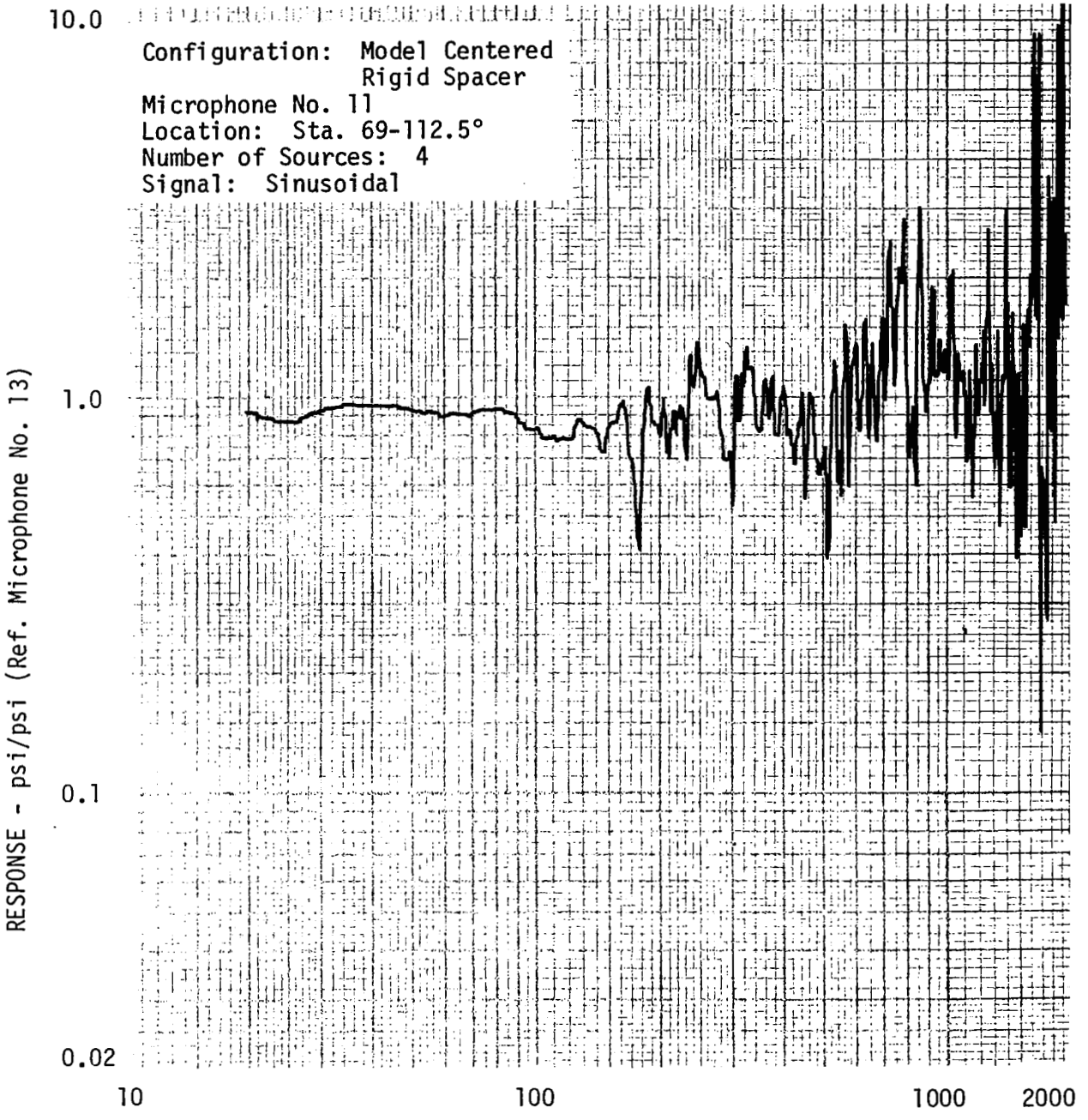

SOUND PRESSURE RESPONSE

FIGURE 24

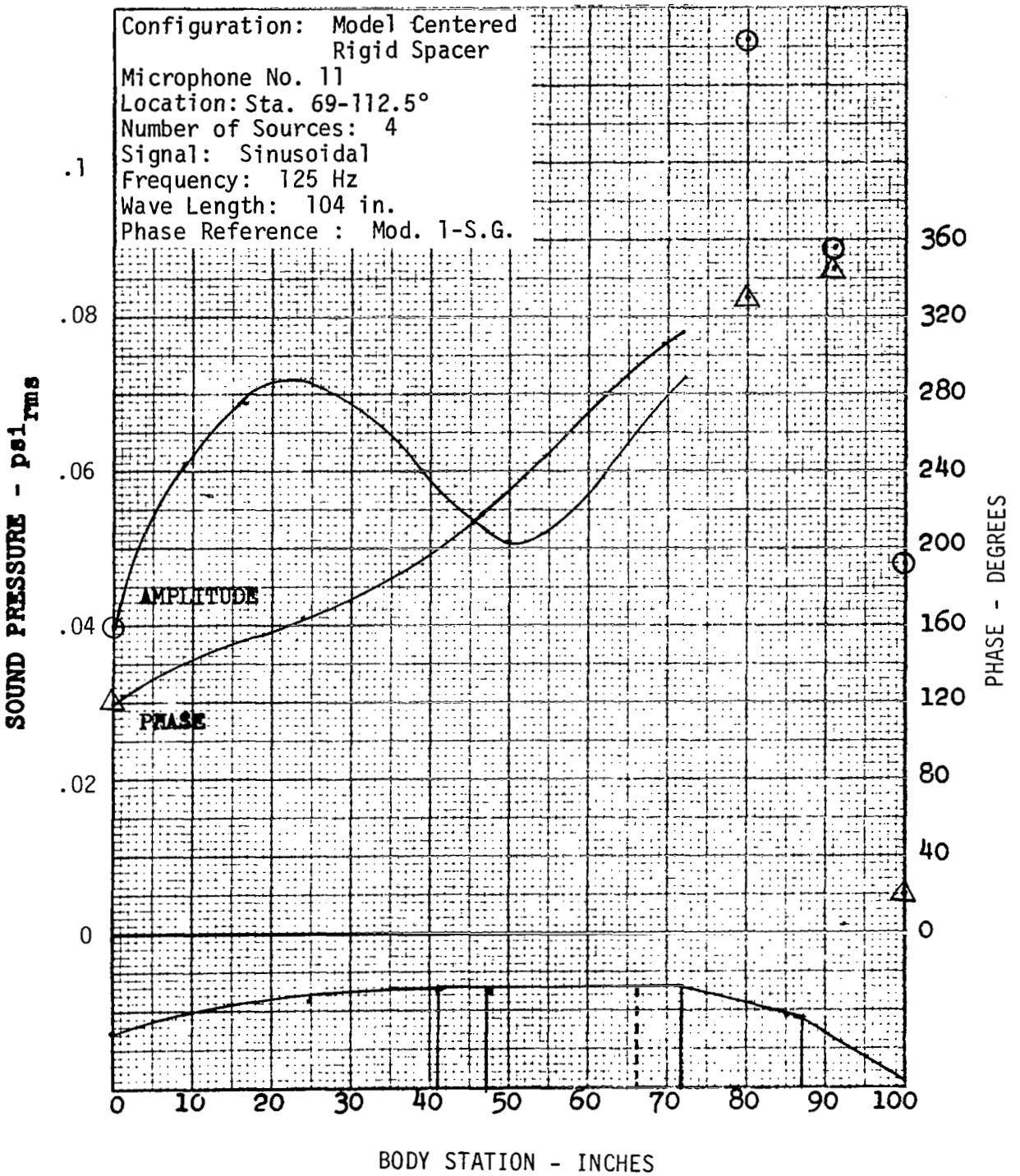

SOUND PRESSURE - LONGITUDINAL DISTRIBUTION

FIGURE 25

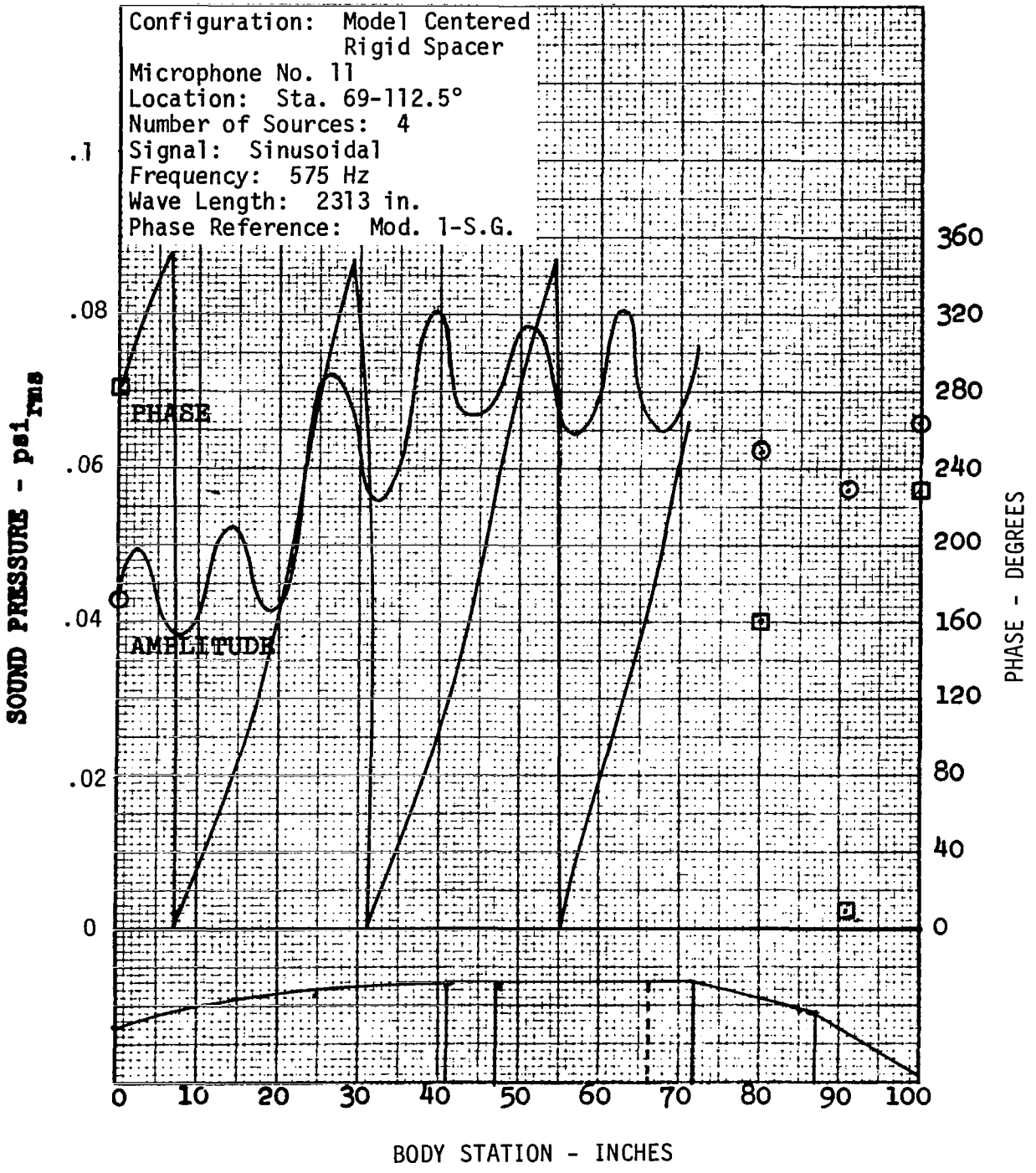

SOUND PRESSURE - LONGITUDINAL DISTRIBUTION

FIGURE 26

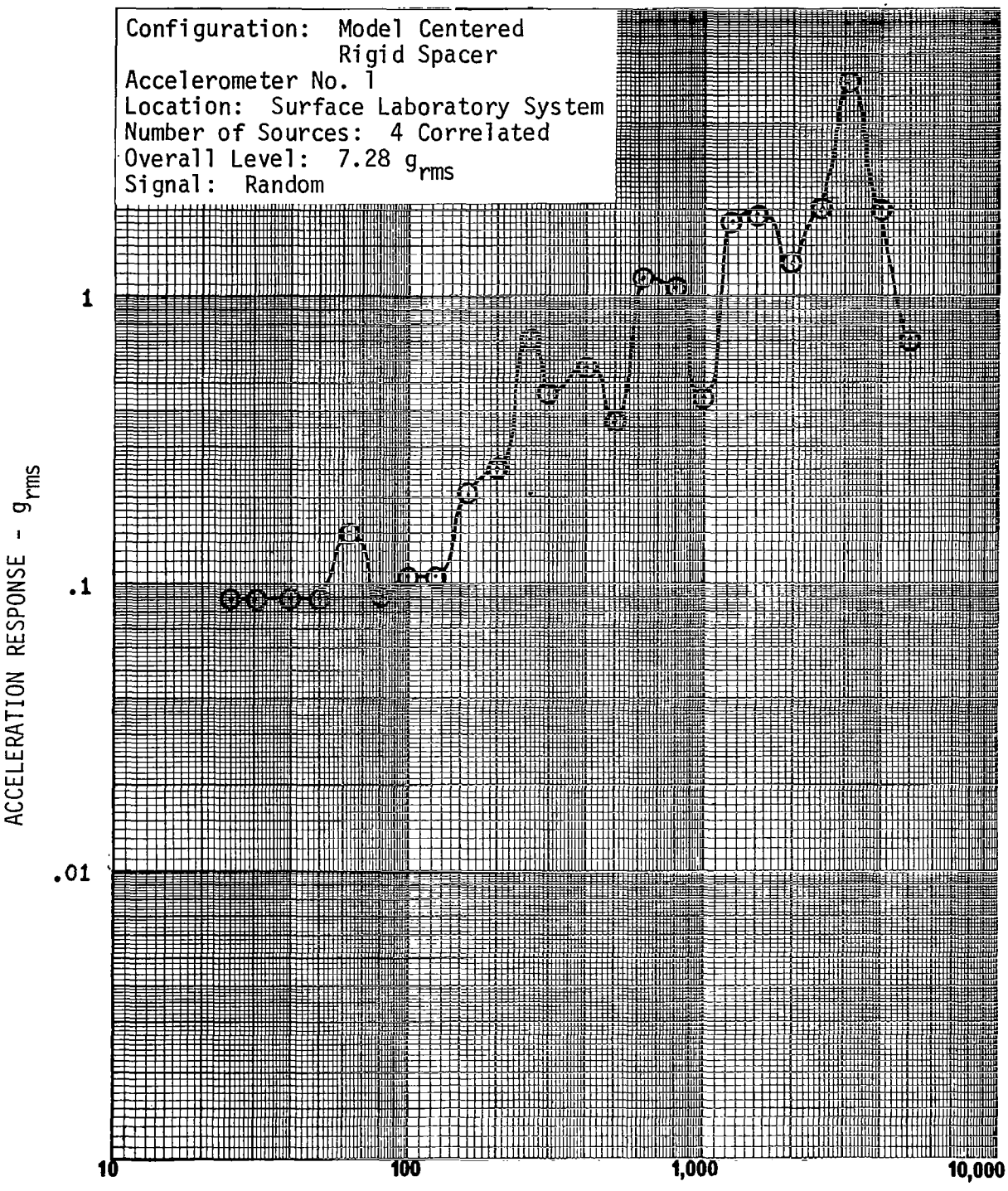

ACCELERATION RESPONSE

FIGURE 27

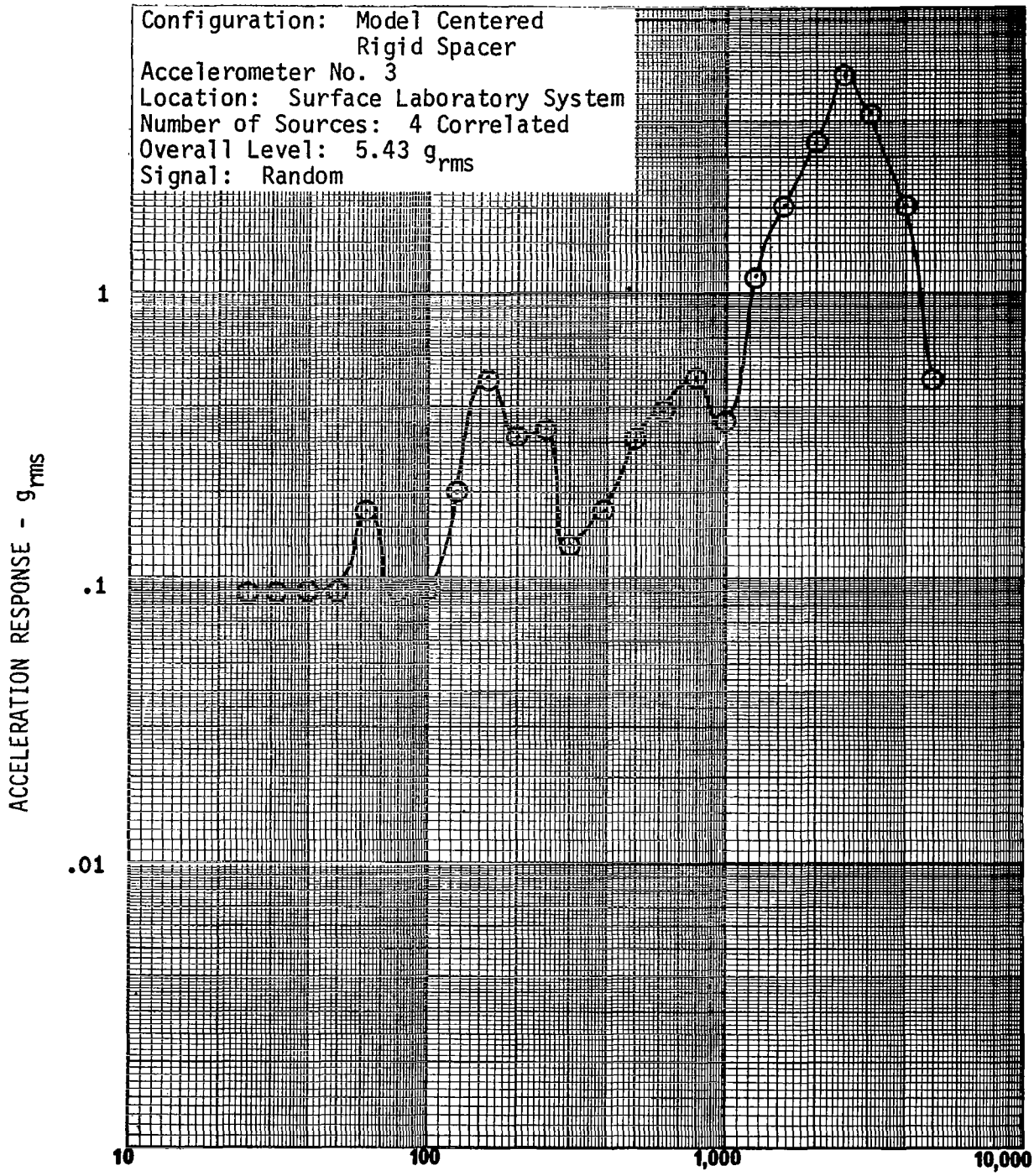

ACCELERATION RESPONSE

FIGURE 28

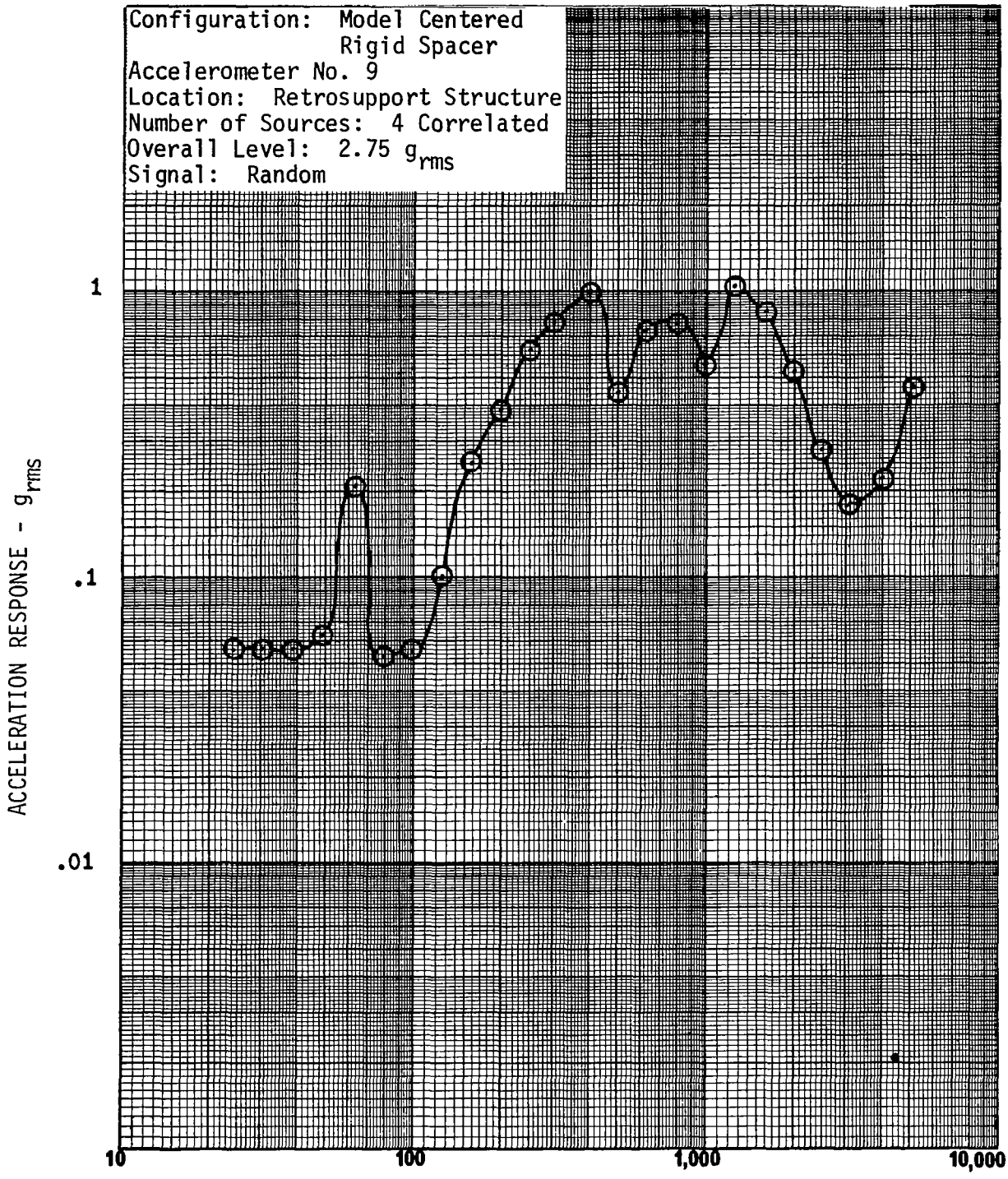

ACCELERATION RESPONSE

FIGURE 29

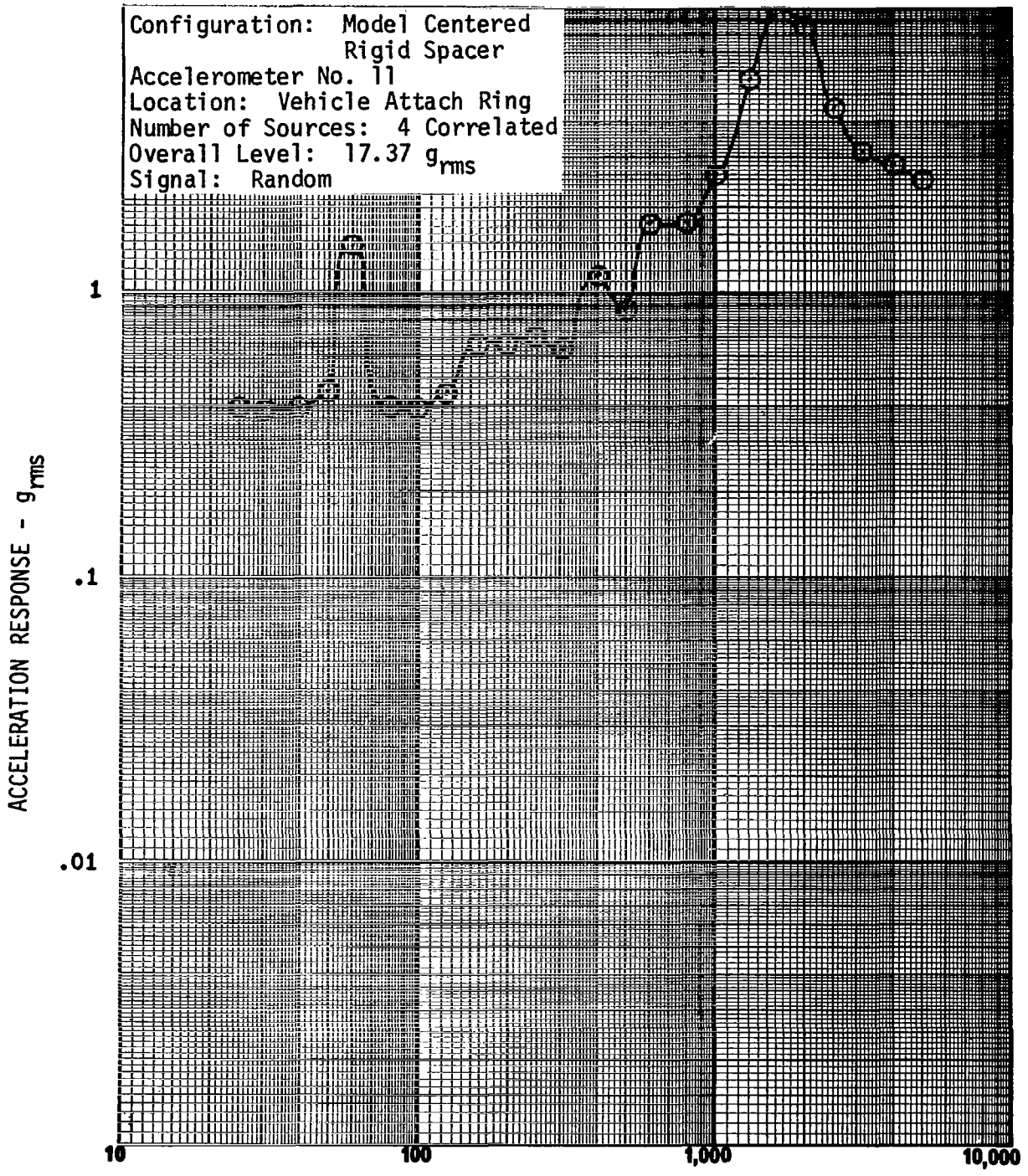

ACCELERATION RESPONSE

FIGURE 30

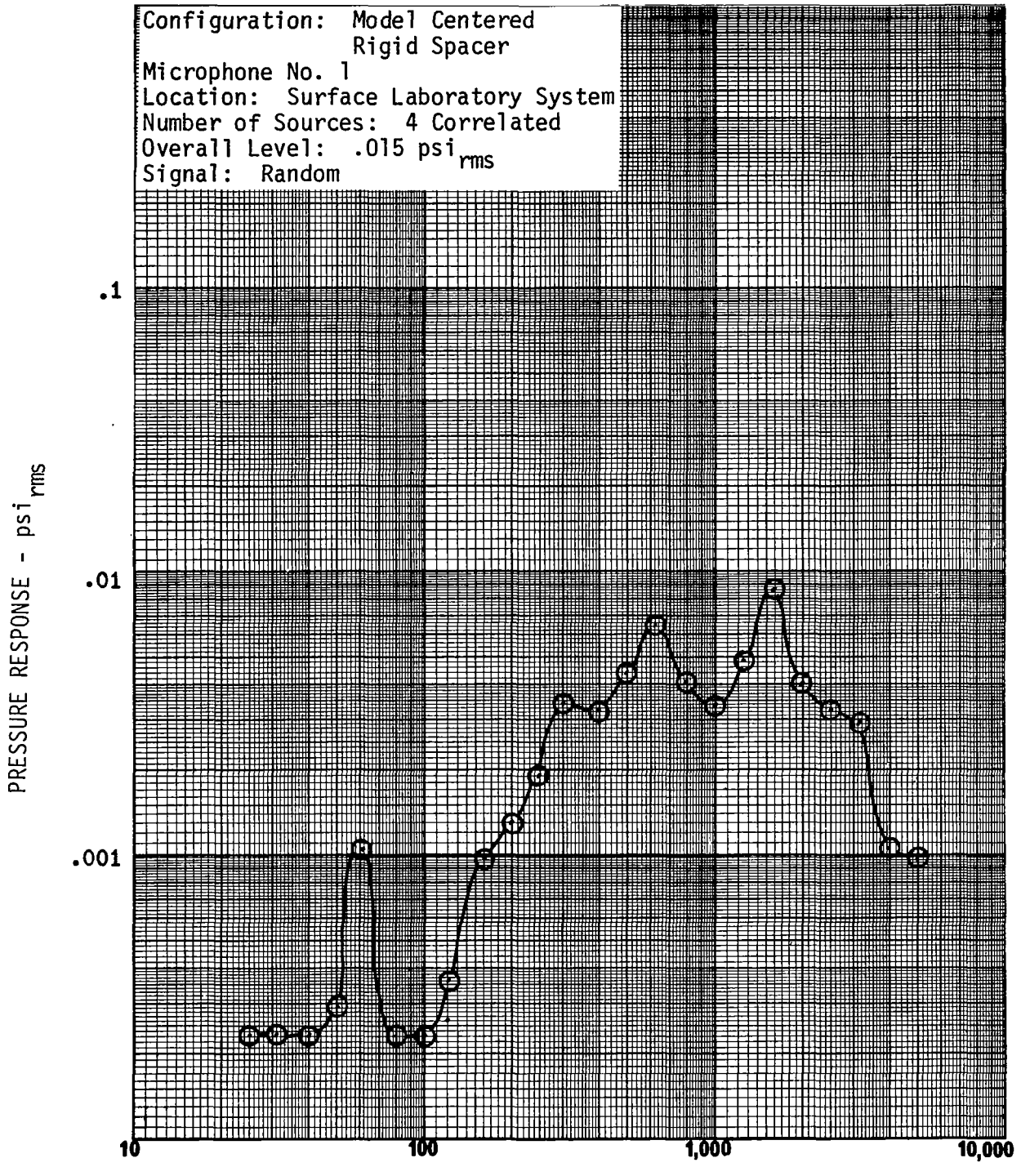

PRESSURE RESPONSE

FIGURE 31

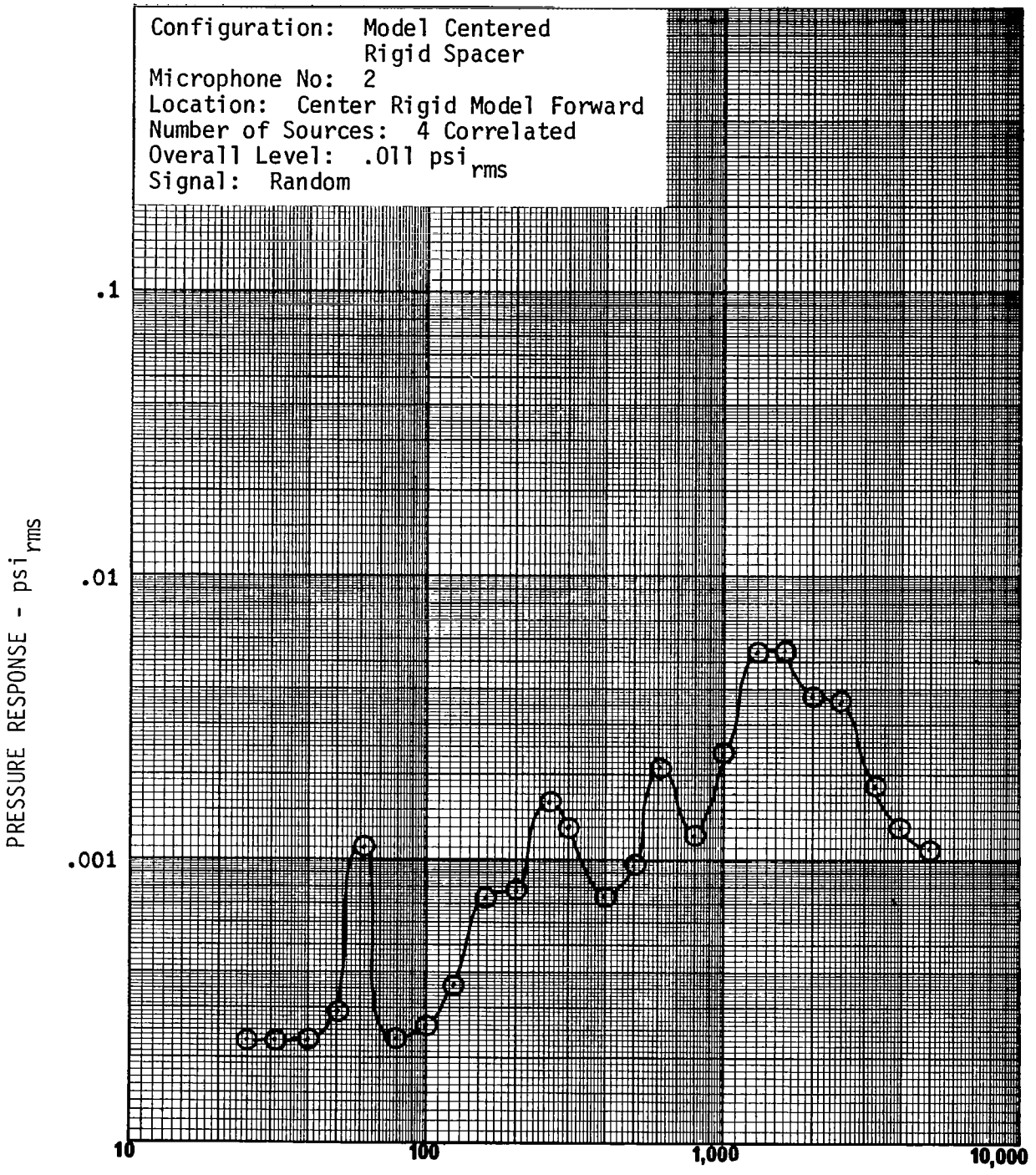

PRESSURE RESPONSE

FIGURE 32

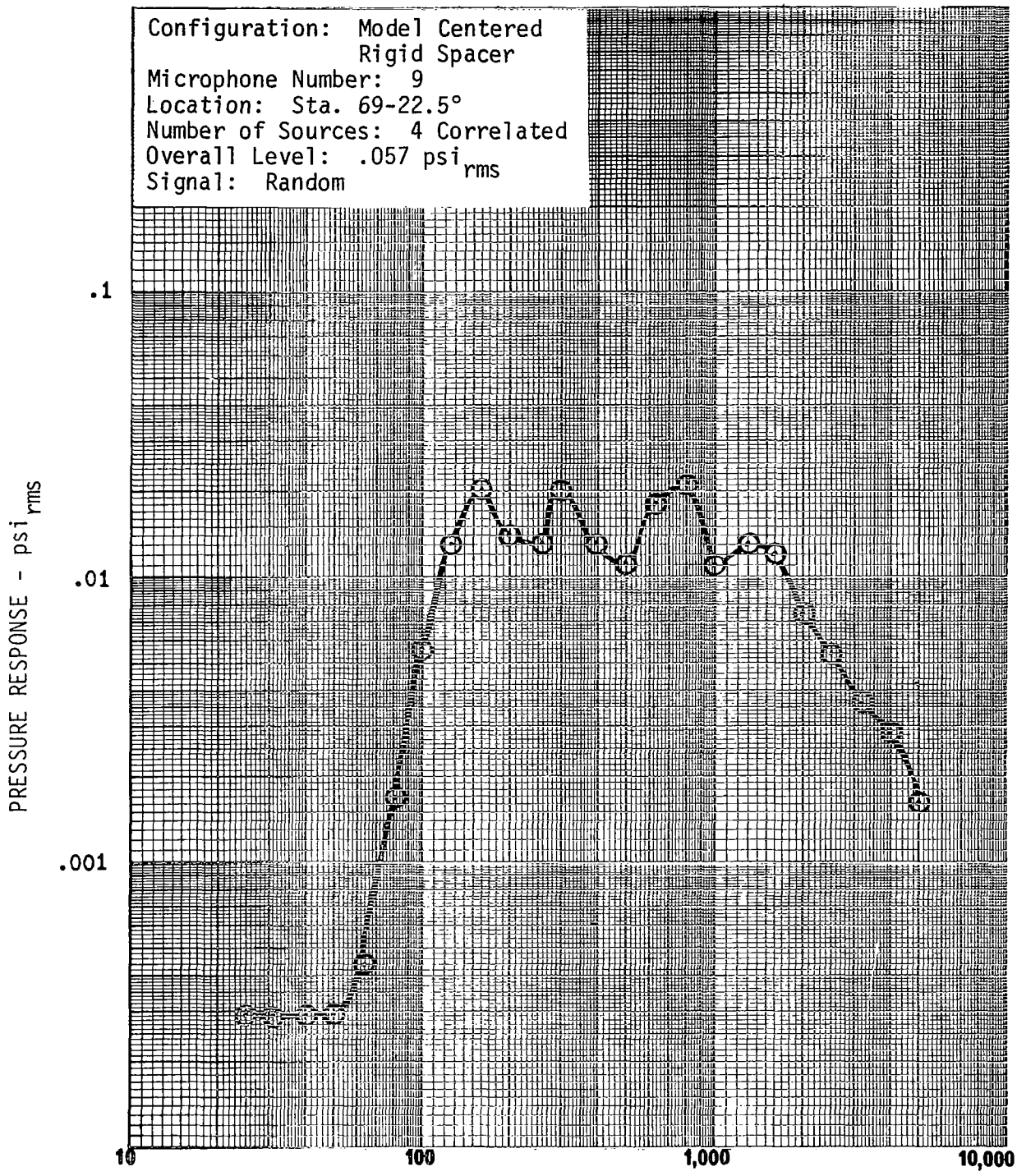

PRESSURE RESPONSE

FIGURE 33

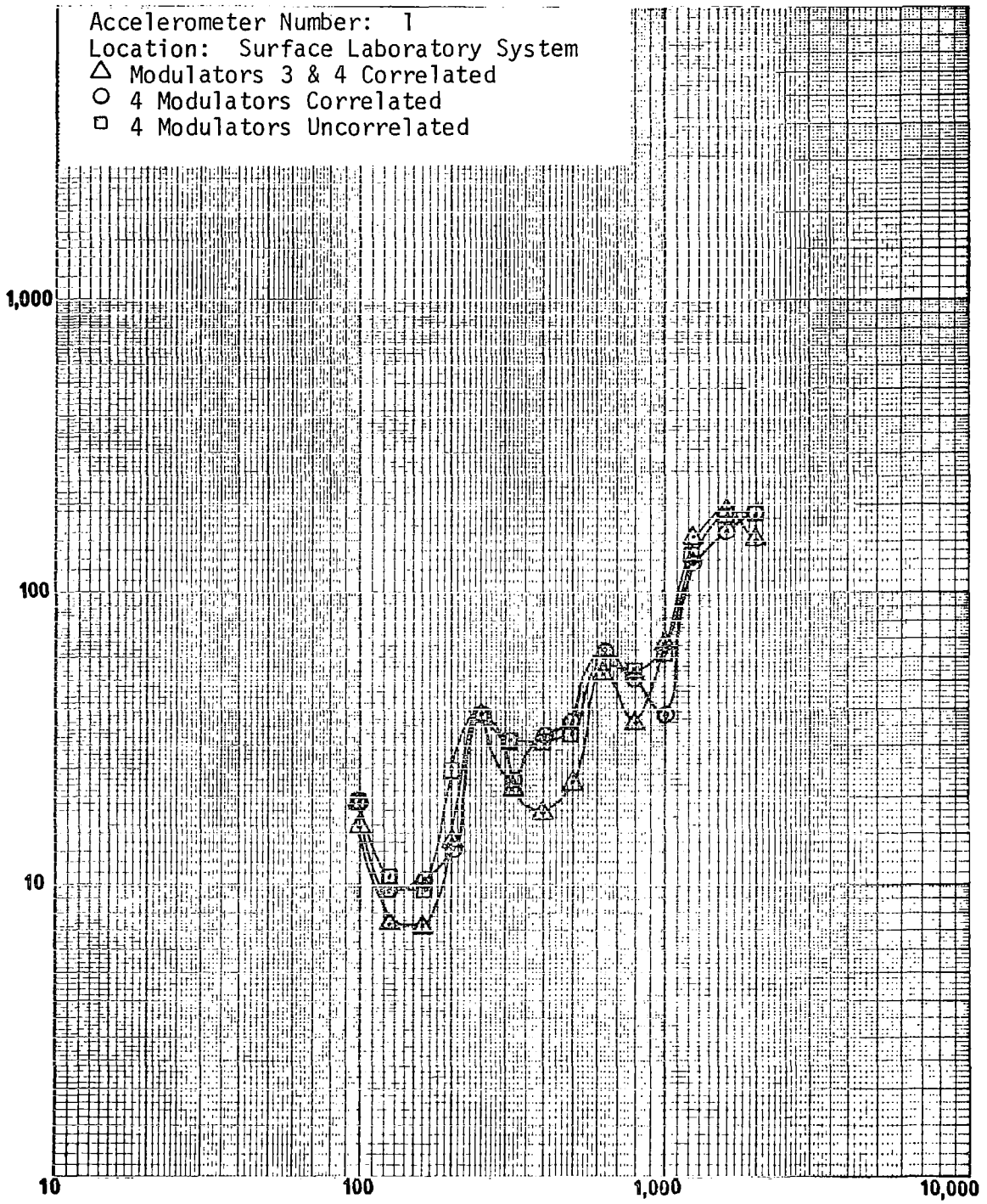

FREQUENCY RESPONSE - EFFECT OF MODULATOR CONFIGURATION

FIGURE 34

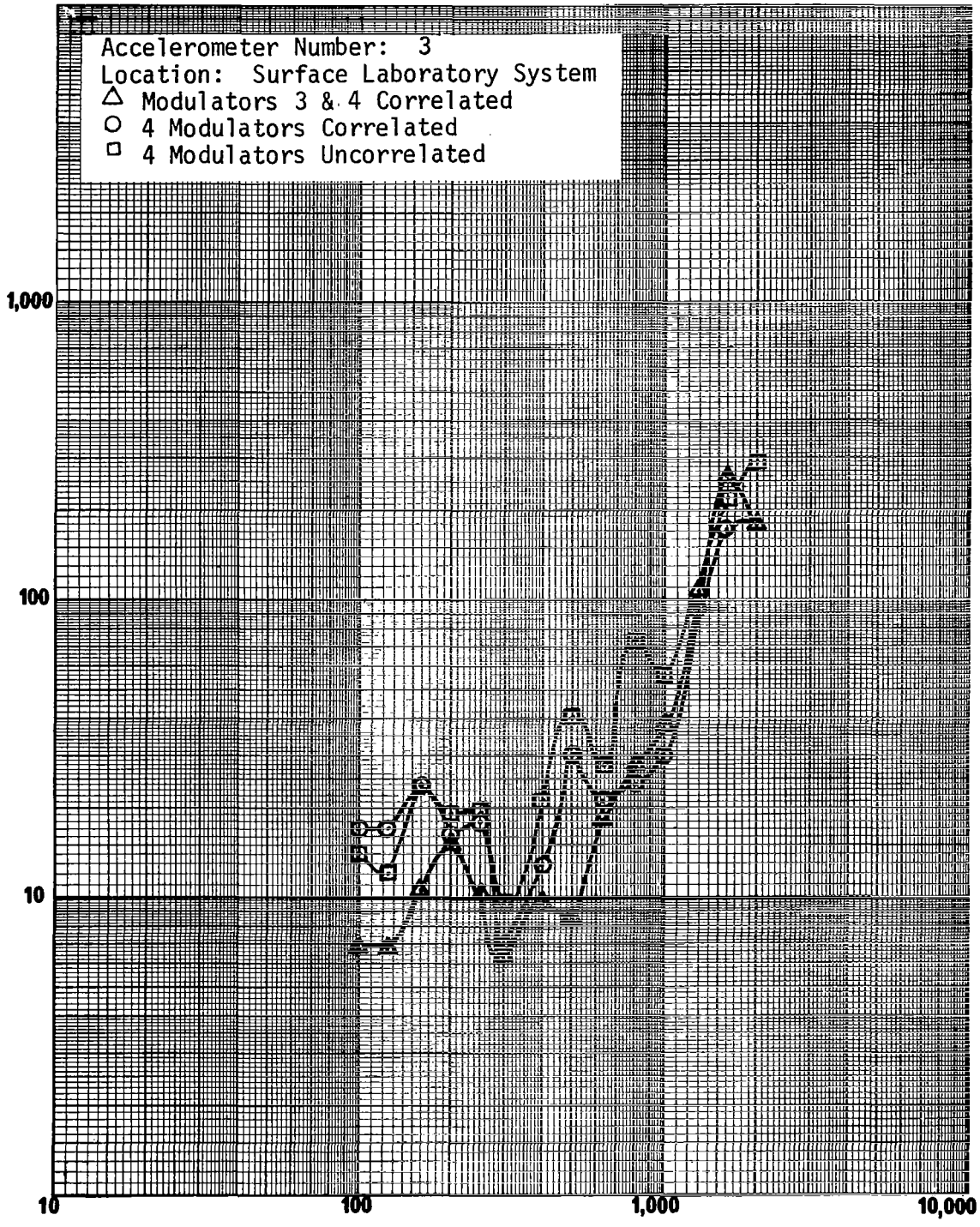

FREQUENCY RESPONSE - EFFECT OF MODULATOR CONFIGURATION

FIGURE 35

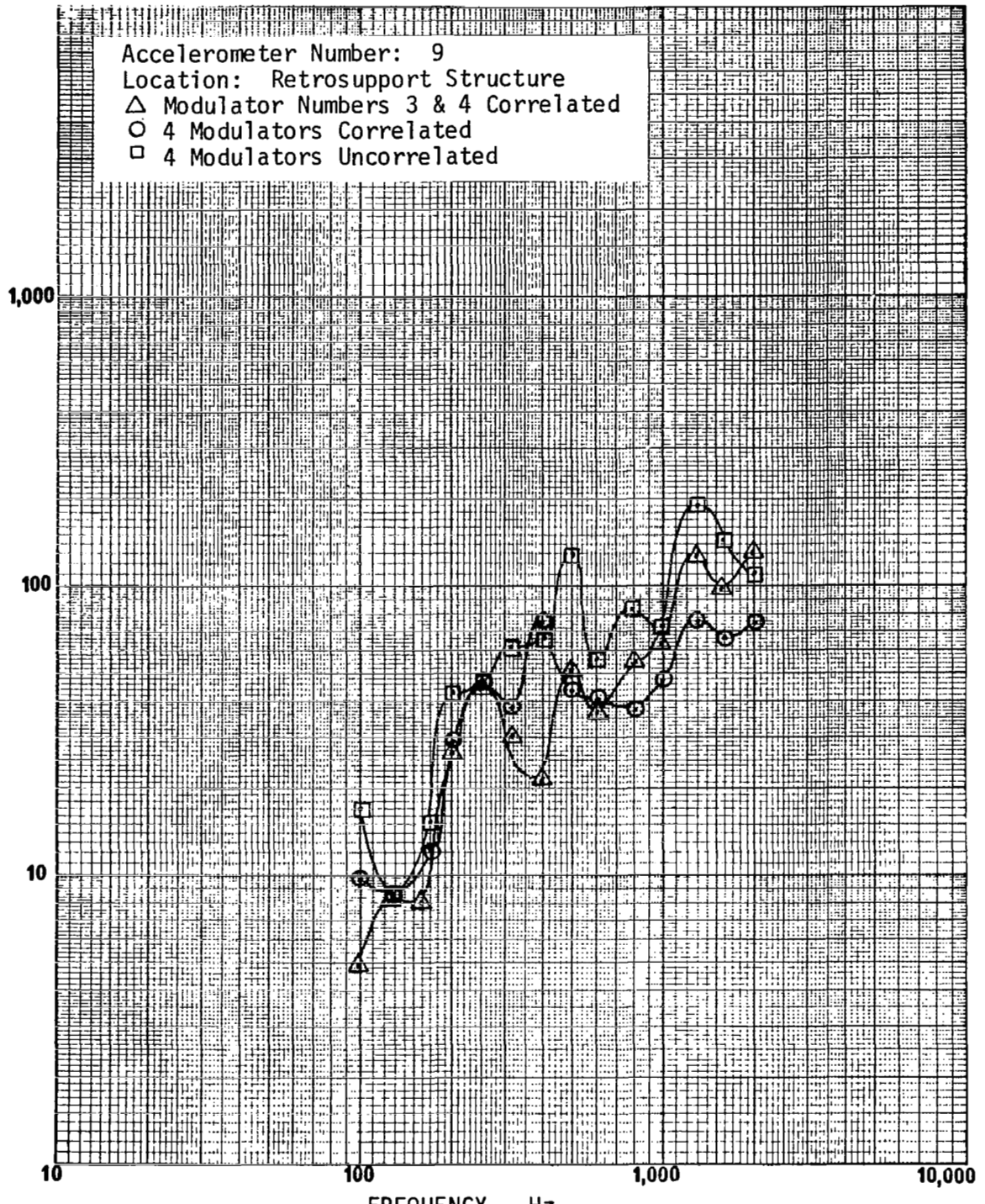

FREQUENCY RESPONSE - EFFECT OF MODULATOR CONFIGURATION

FIGURE 36

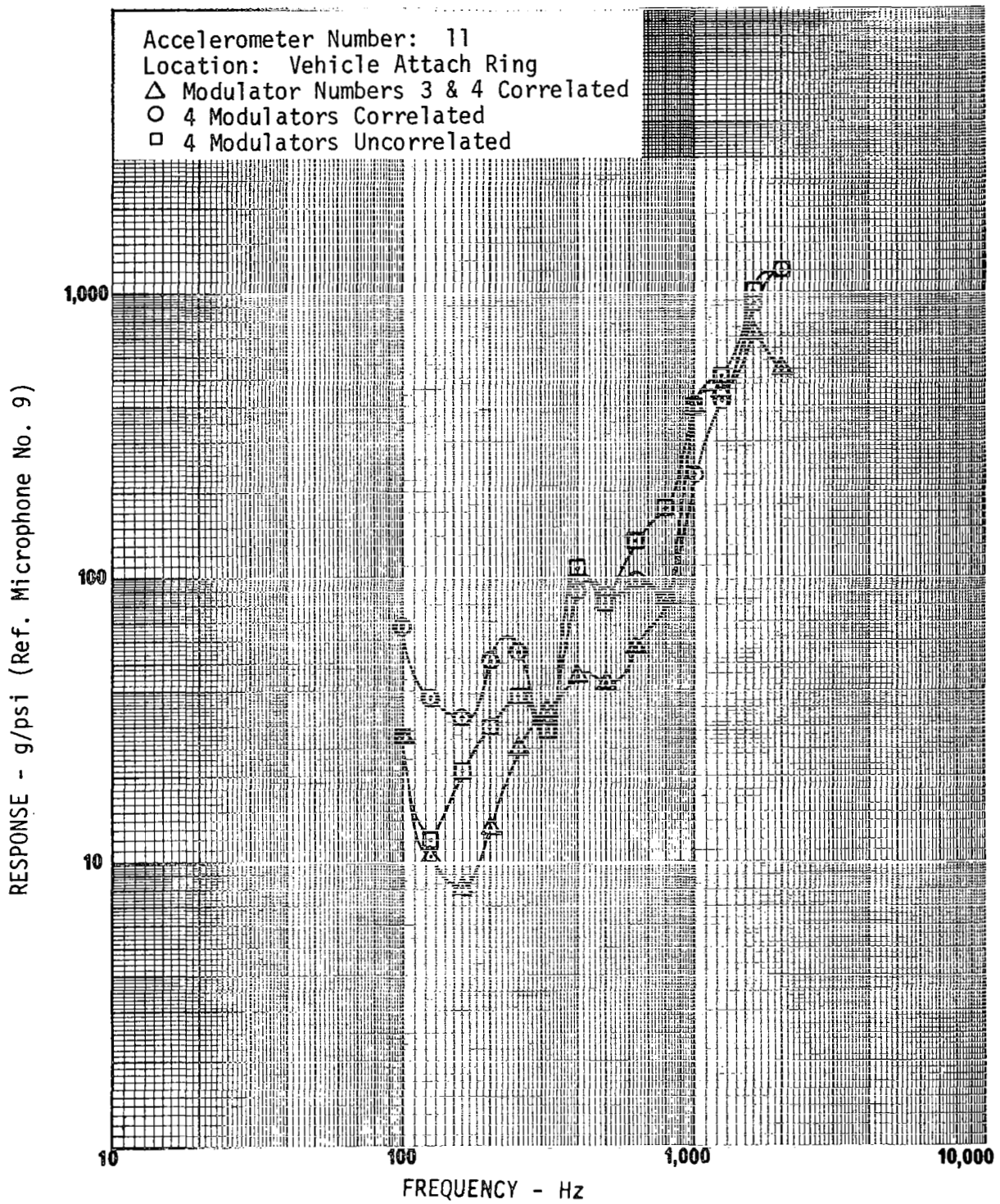

FREQUENCY RESPONSE - EFFECT OF MODULATOR CONFIGURATION

FIGURE 37

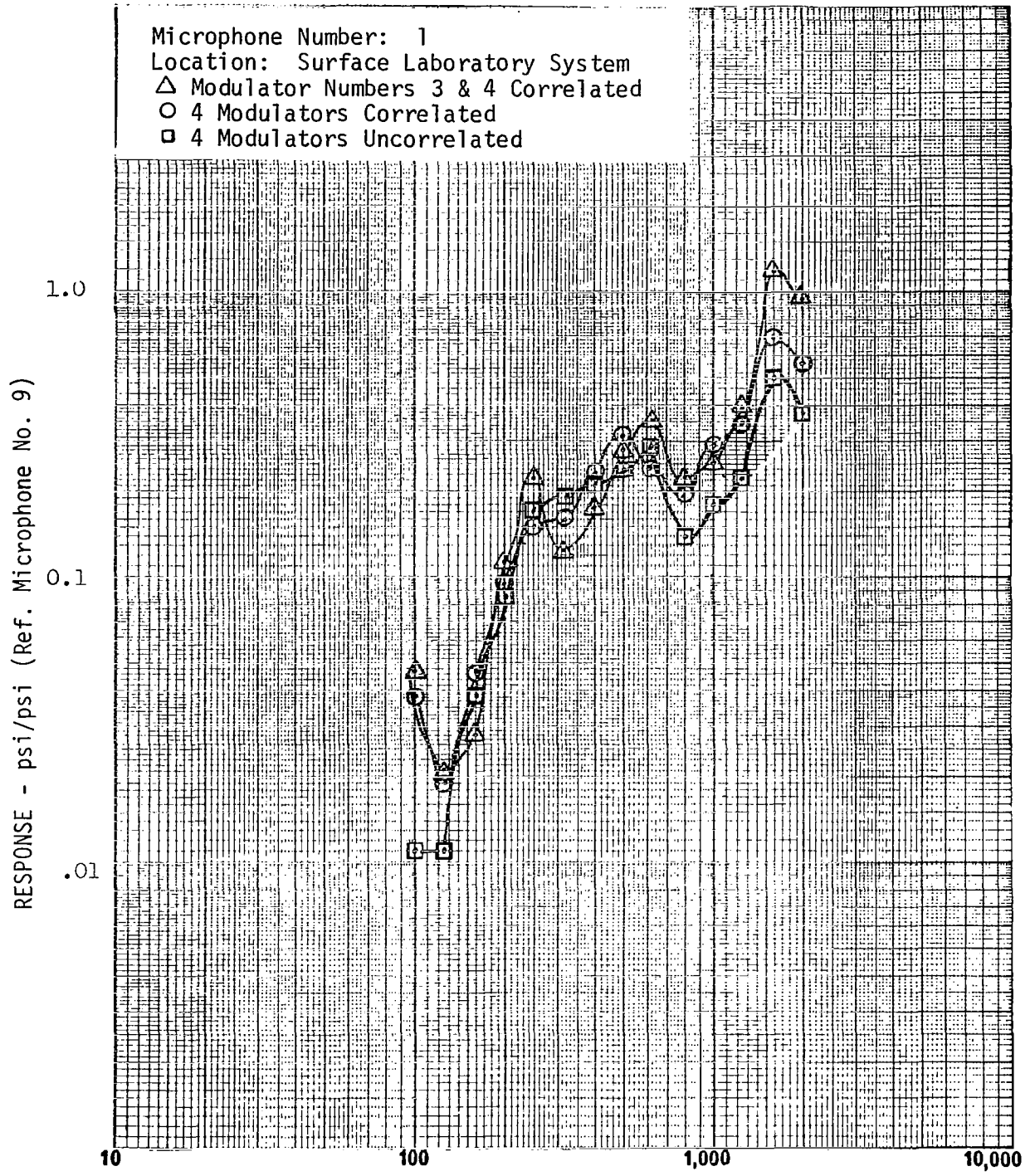

FREQUENCY RESPONSE - EFFECT OF MODULATOR CONFIGURATION

FIGURE 38

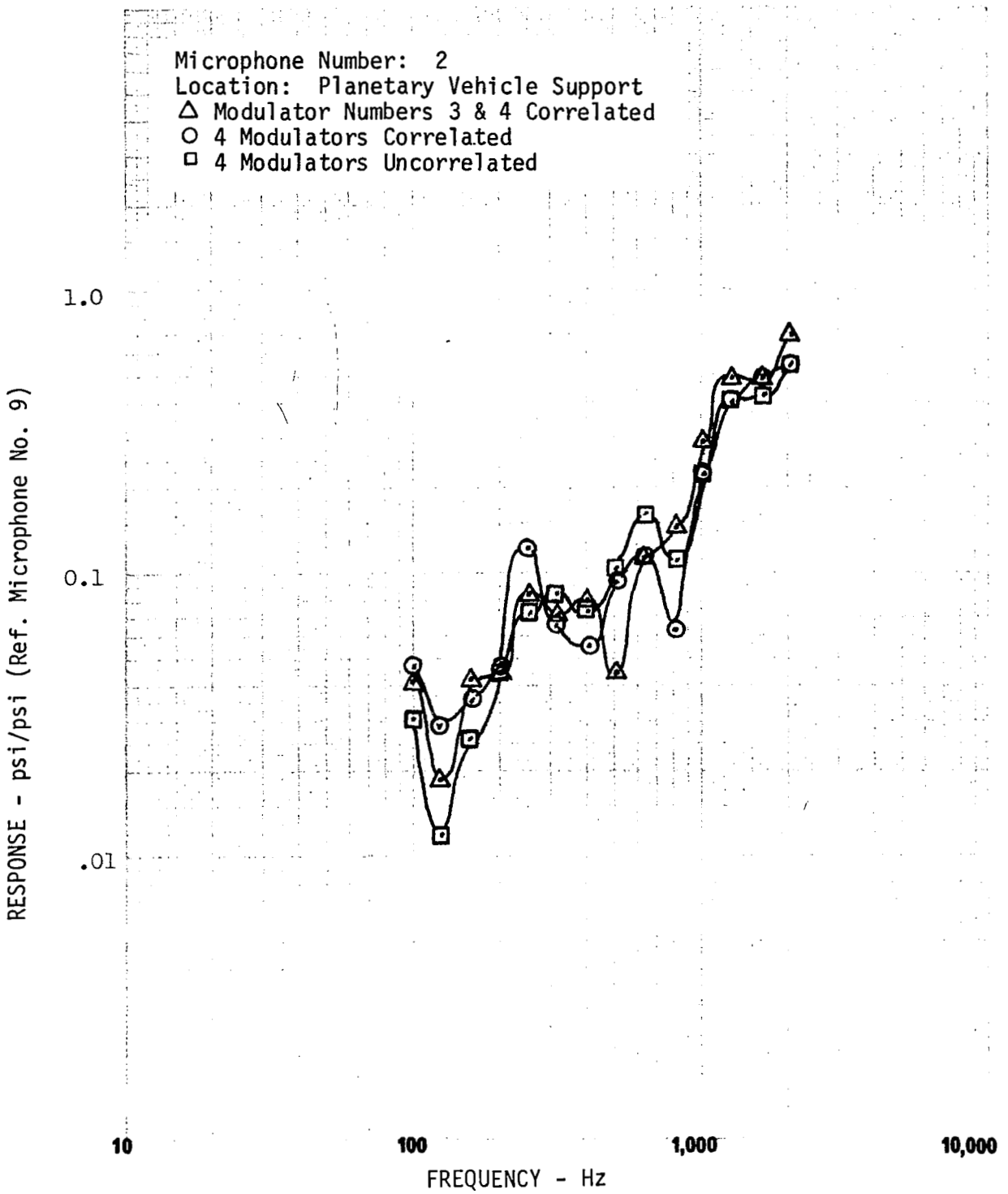

FREQUENCY RESPONSE - EFFECT OF MODULATOR CONFIGURATION

FIGURE 39

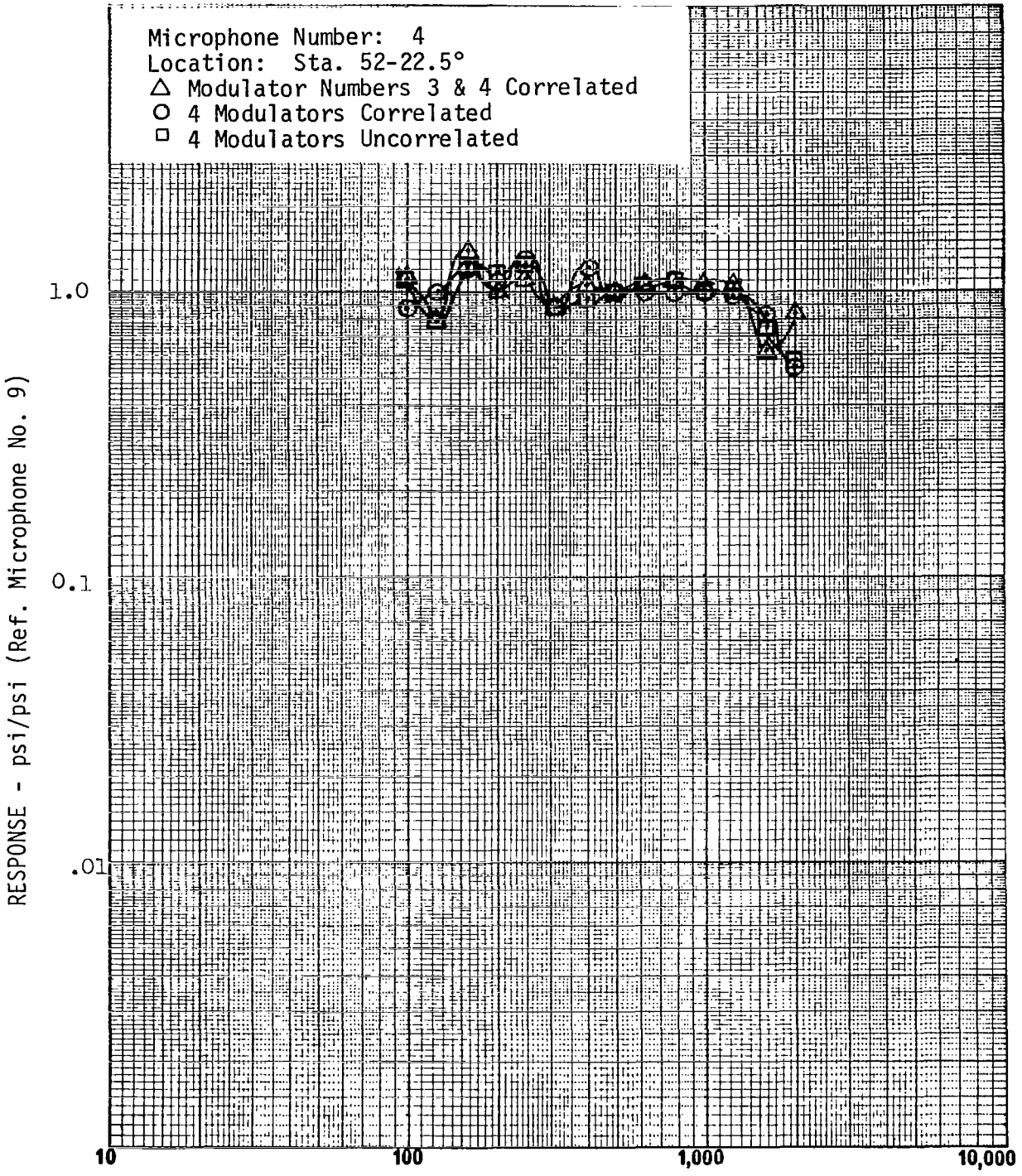

FREQUENCY RESPONSE - EFFECT OF MODULATOR CONFIGURATION

FIGURE 40

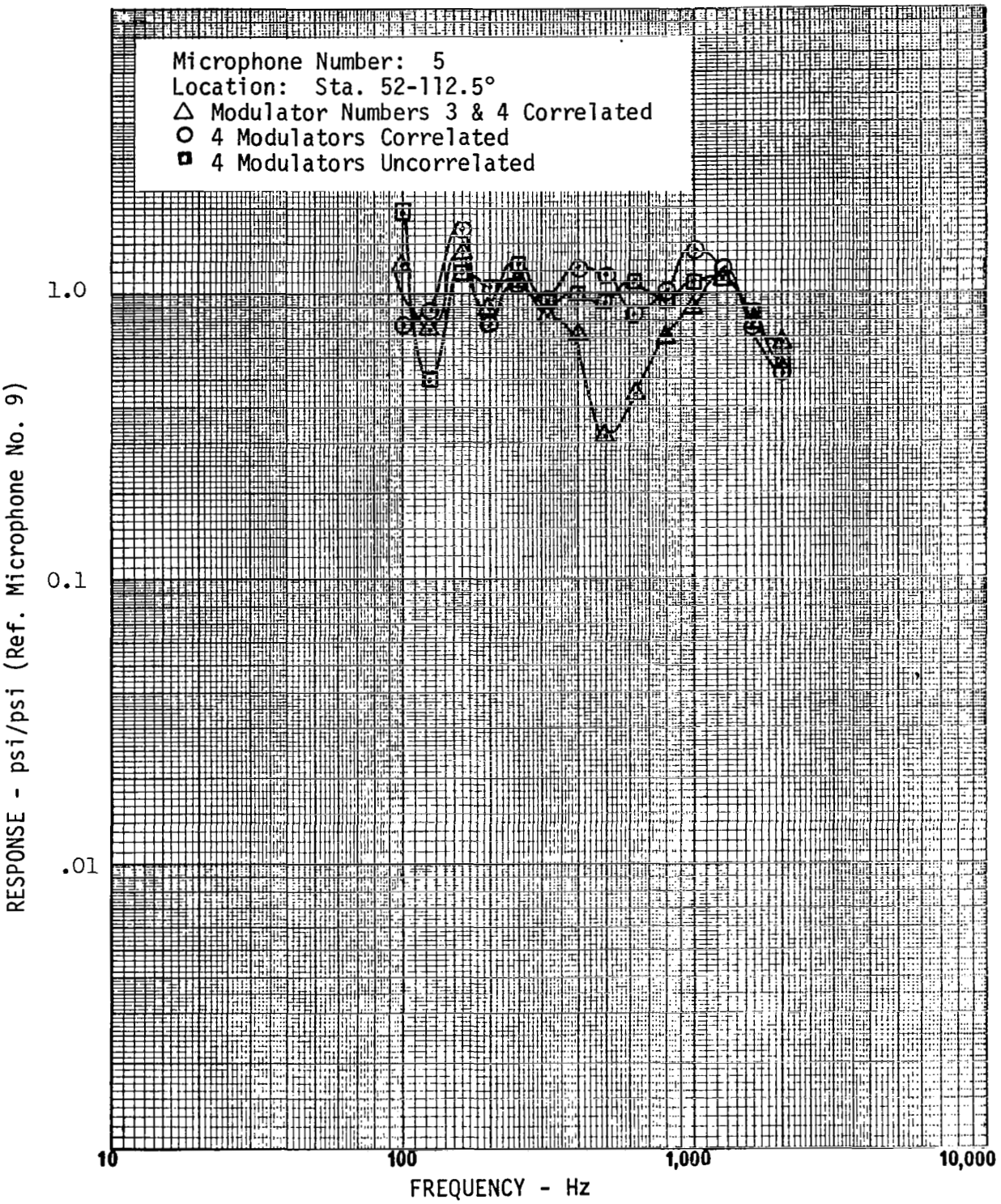

FREQUENCY RESPONSE - EFFECT OF MODULATOR CONFIGURATION

FIGURE 41

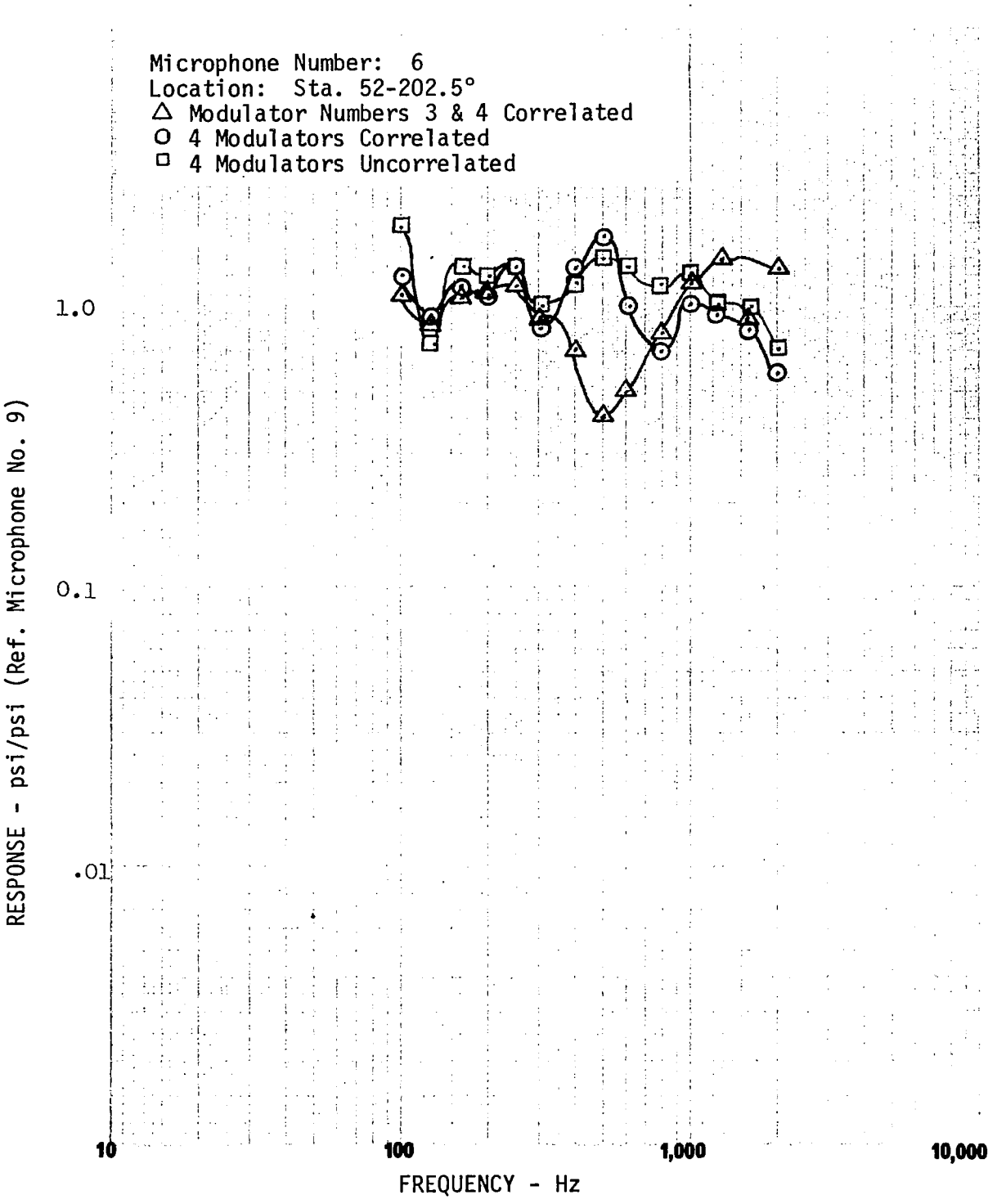

FREQUENCY RESPONSE - EFFECT OF MODULATOR CONFIGURATION

FIGURE 42

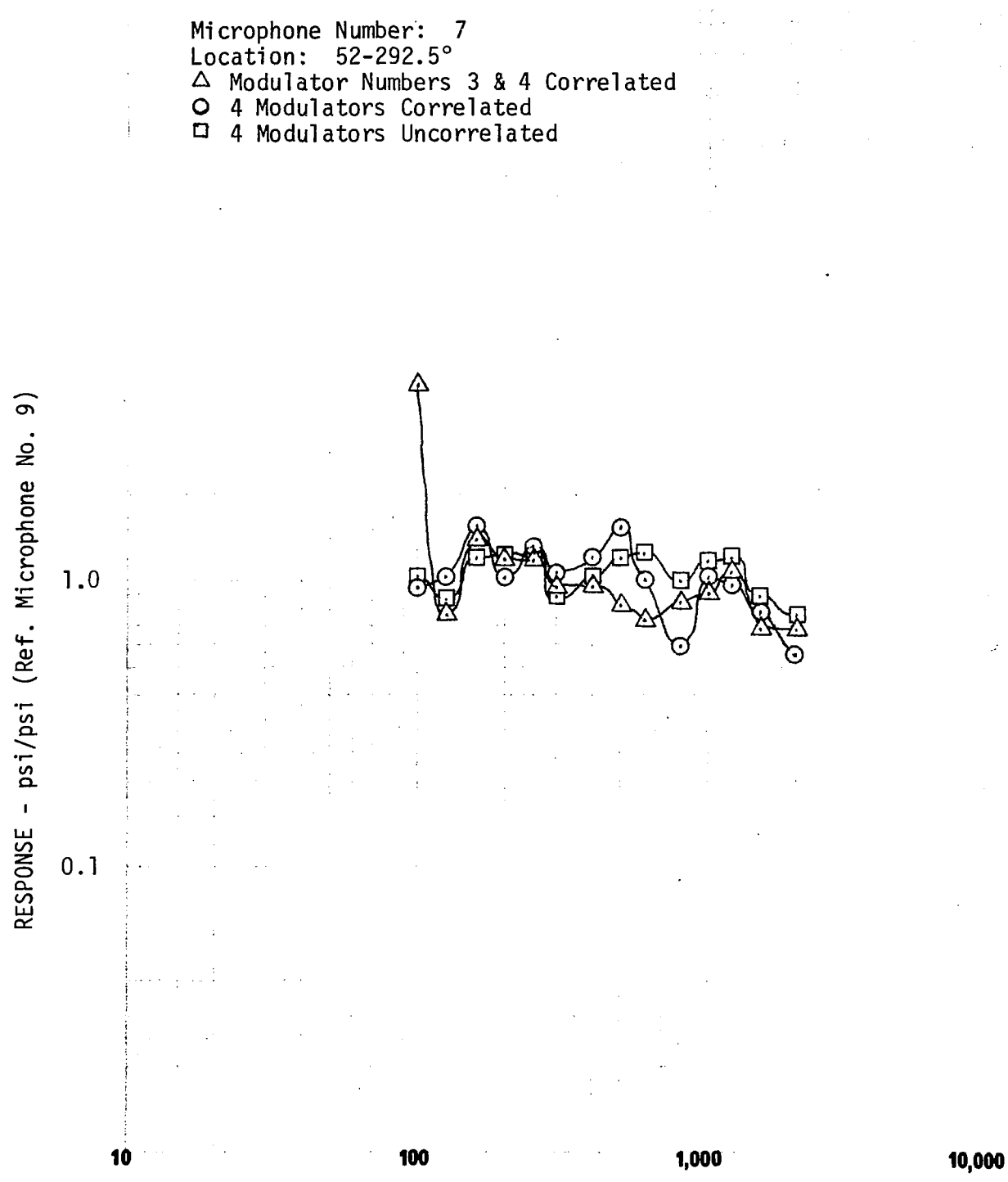

FREQUENCY RESPONSE - EFFECT OF MODULATOR CONFIGURATION

FIGURE 43

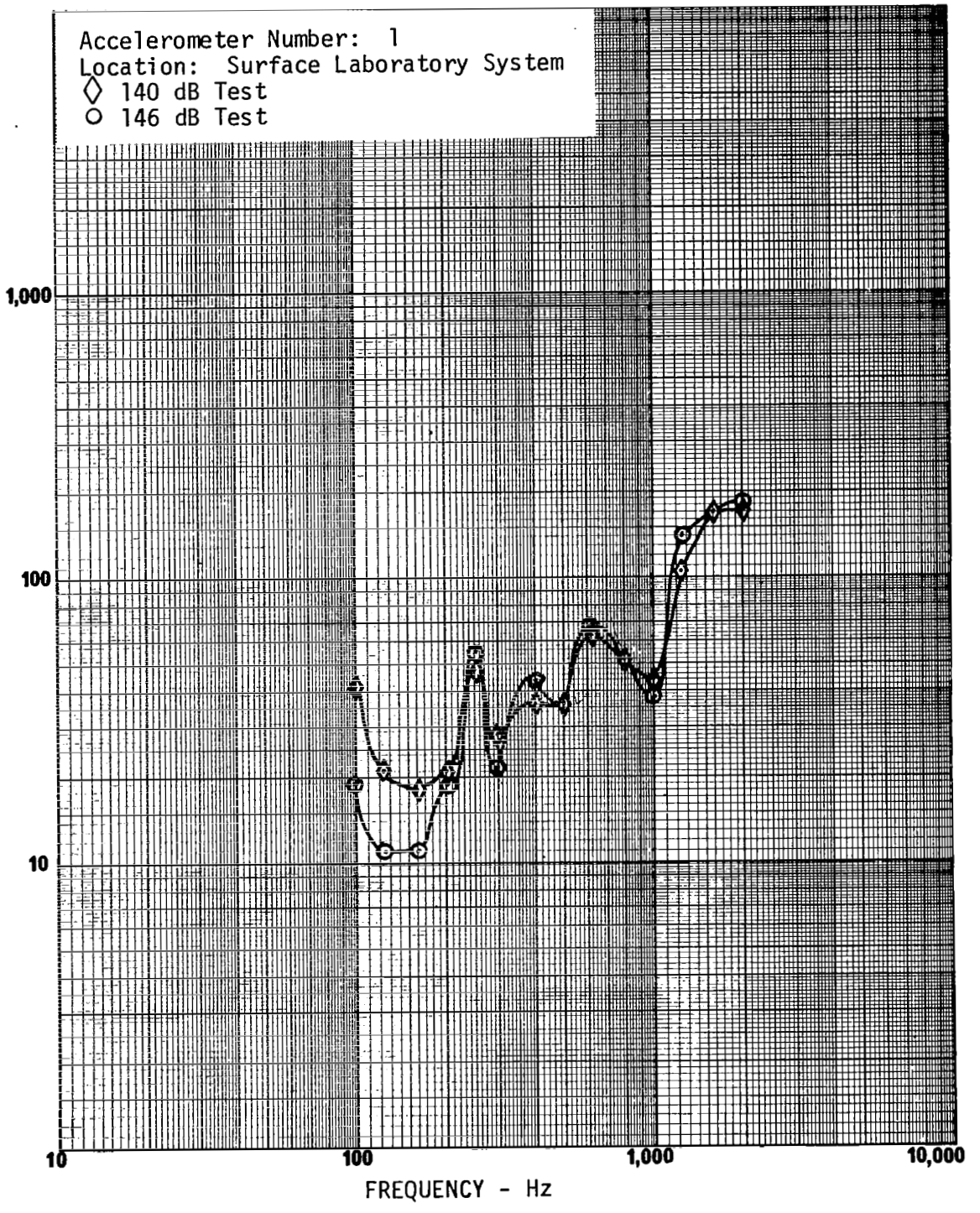

FREQUENCY RESPONSE - LINEARITY INVESTIGATION

FIGURE 44

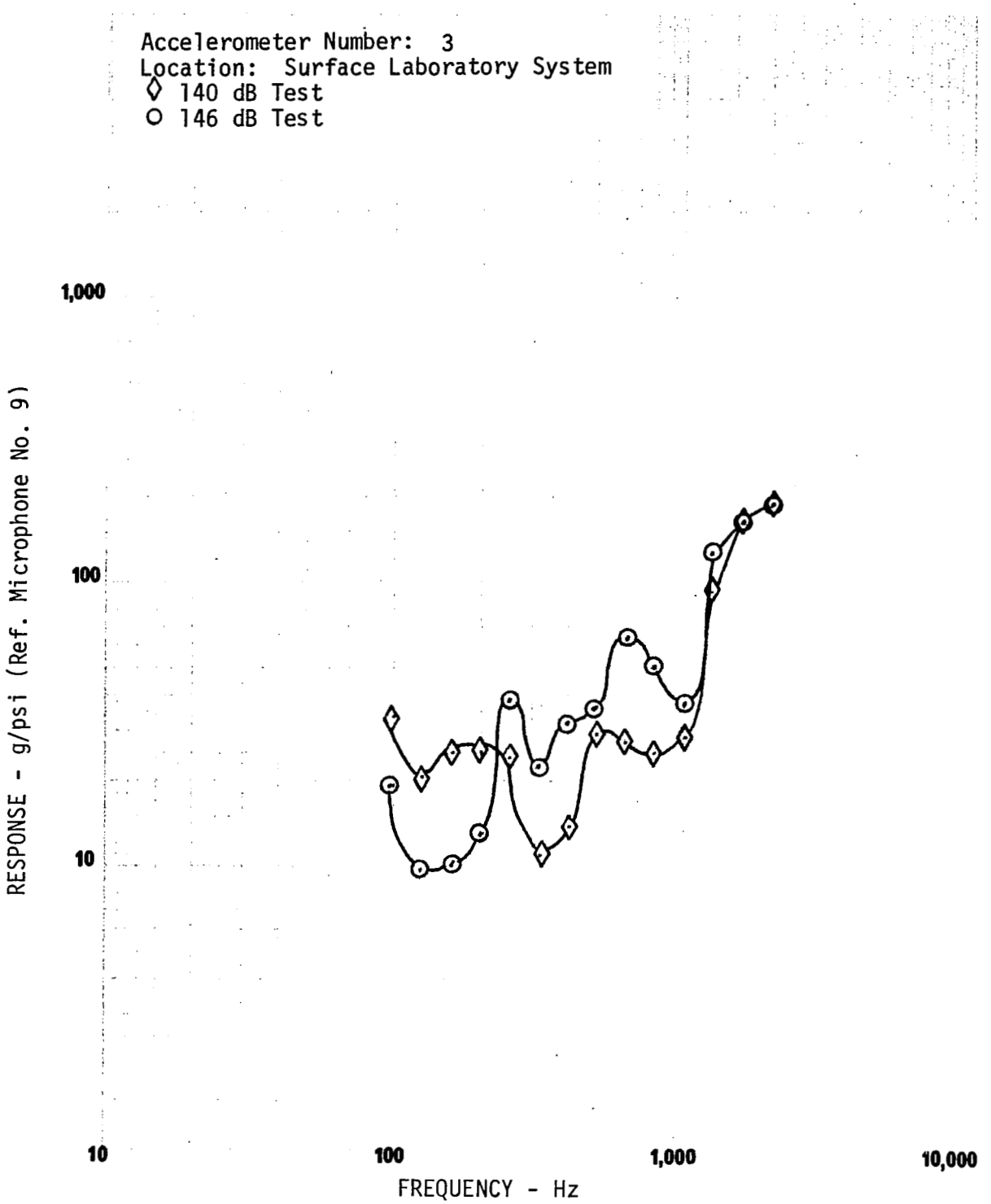

FREQUENCY RESPONSE - LINEARITY INVESTIGATION

FIGURE 45

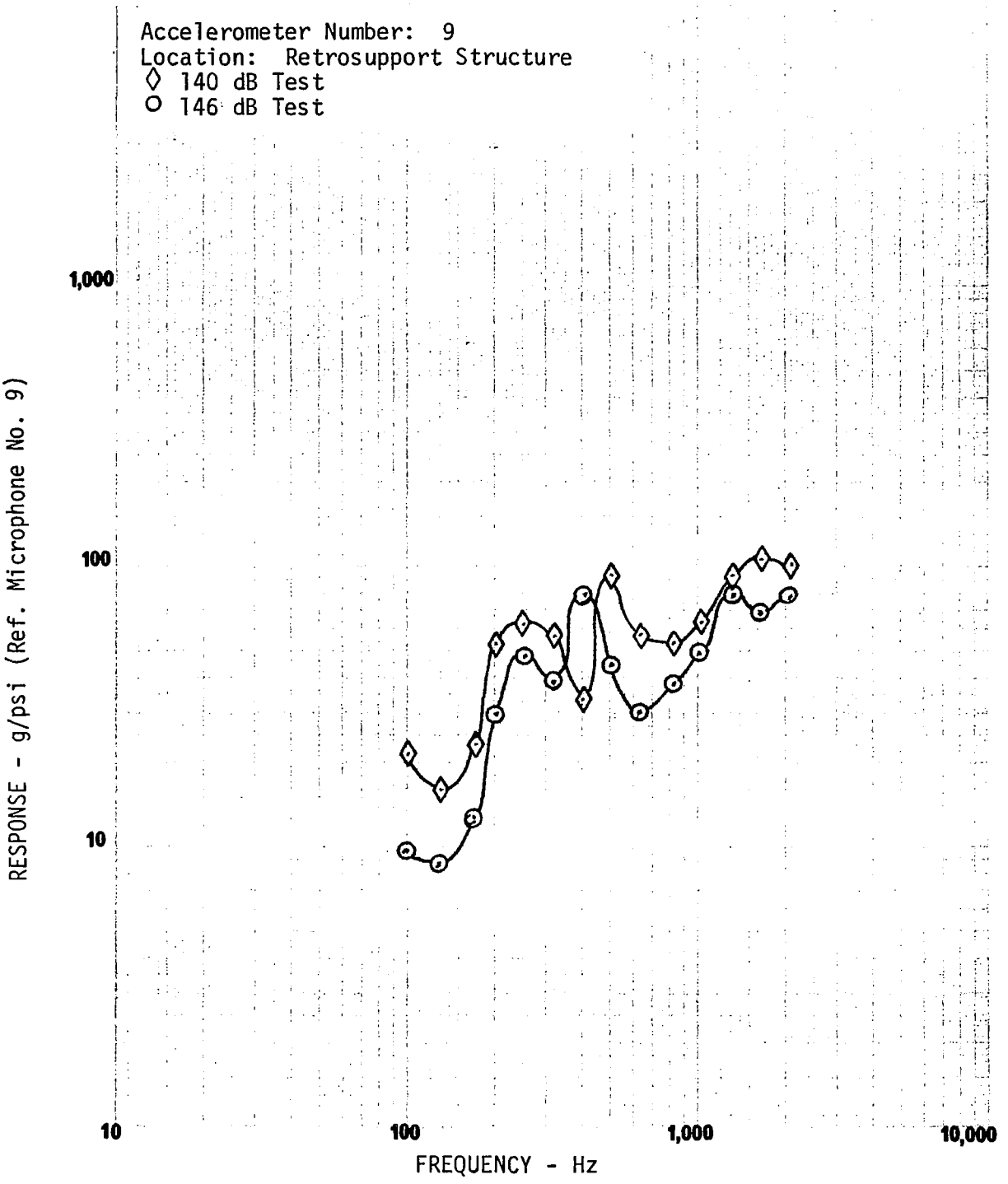

FREQUENCY RESPONSE - LINEARITY INVESTIGATION

FIGURE 46

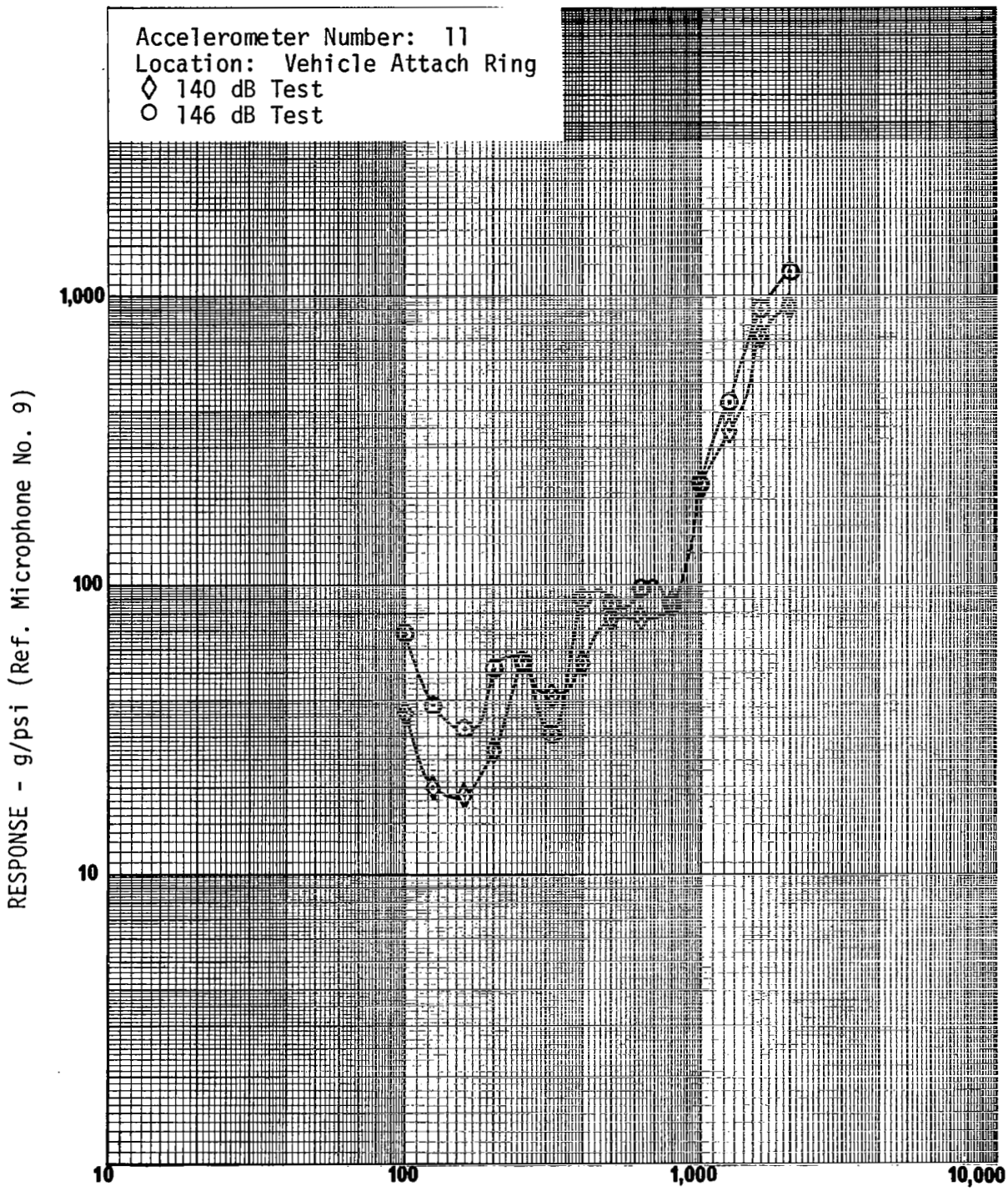

FREQUENCY RESPONSE - LINEARITY INVESTIGATION

FIGURE 47

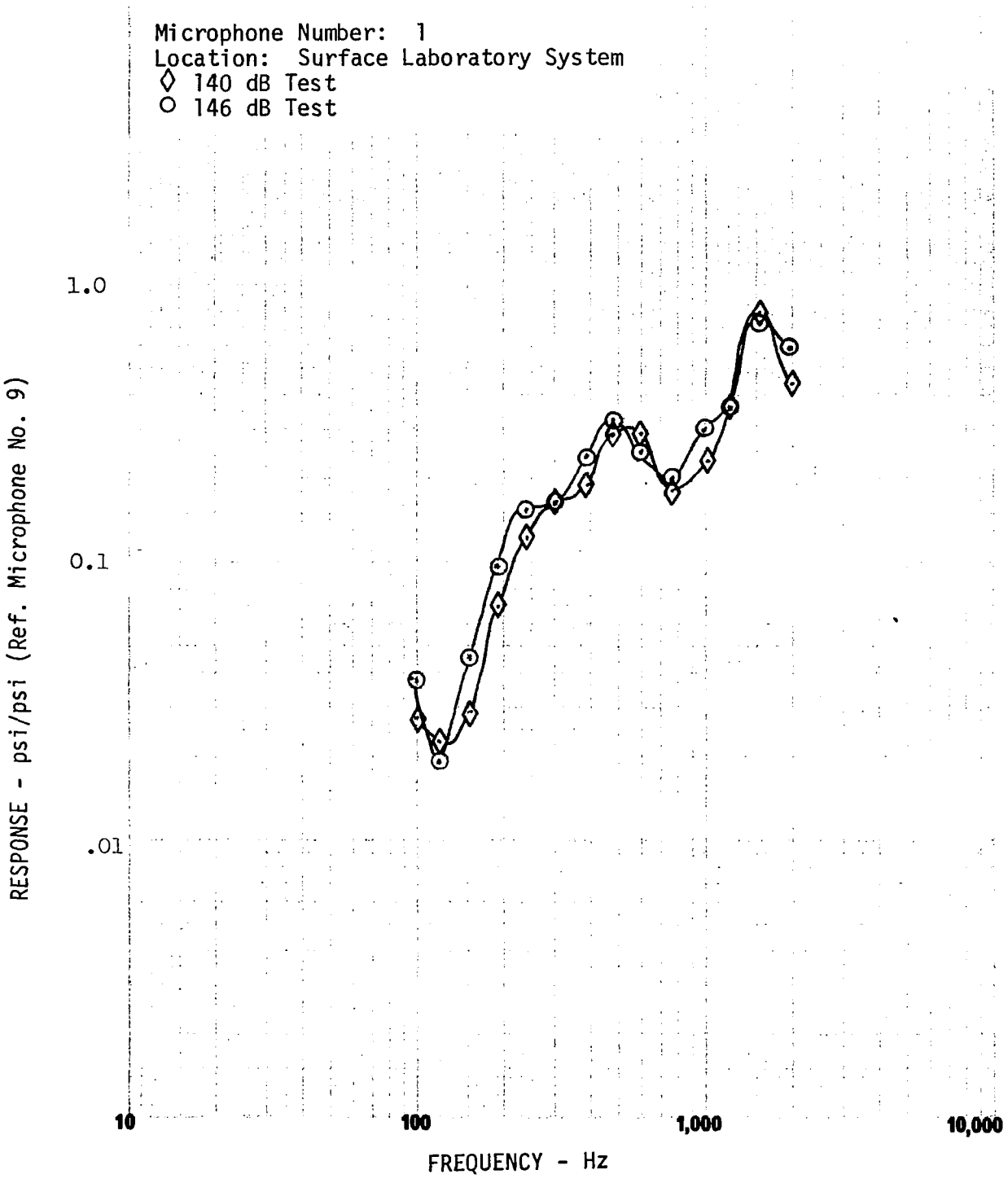

FREQUENCY RESPONSE - LINEARITY INVESTIGATION

FIGURE 48

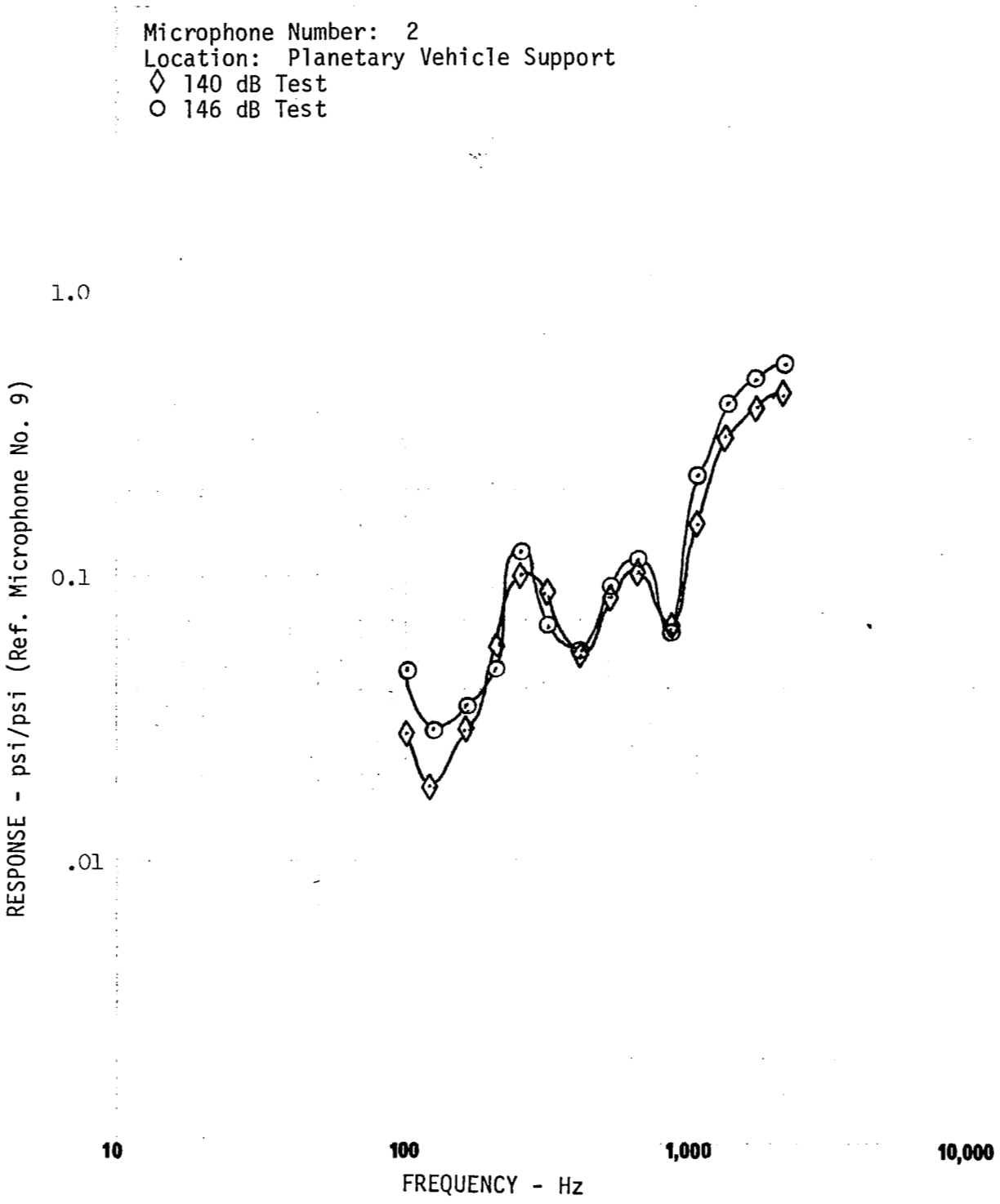

FREQUENCY RESPONSE - LINEARITY INVESTIGATION

FIGURE 49

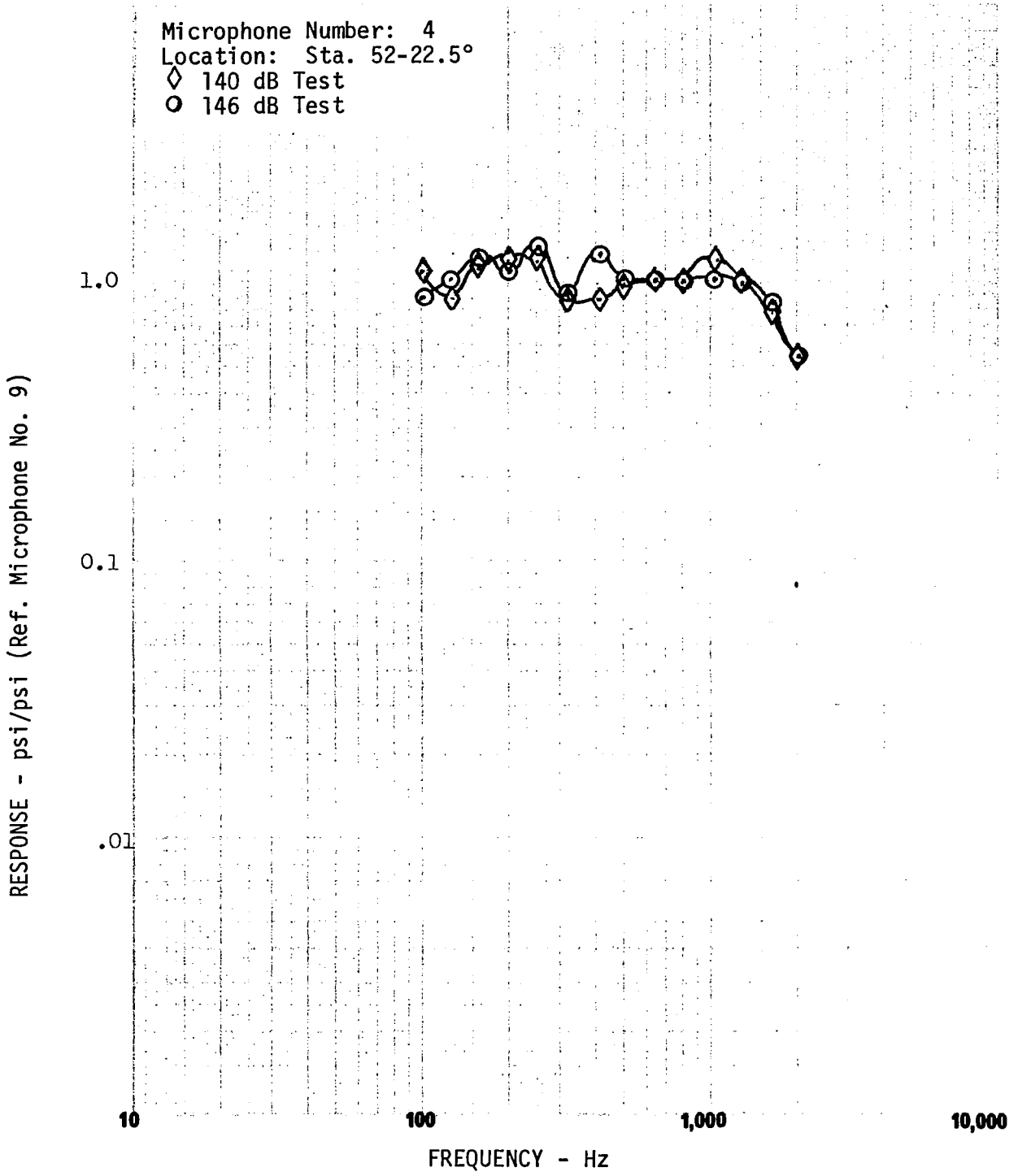

FREQUENCY RESPONSE - LINEARITY INVESTIGATION

FIGURE 50

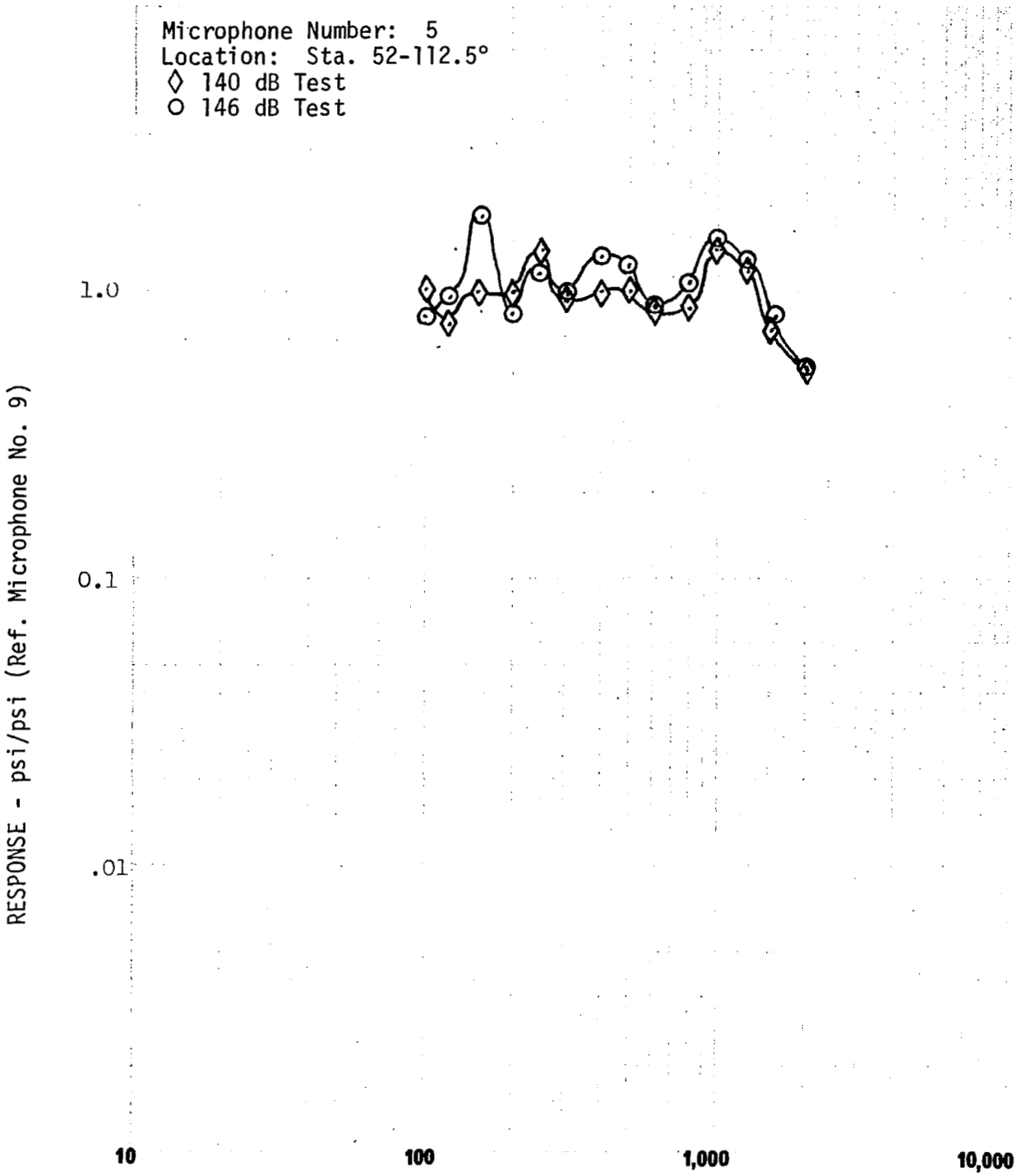

FREQUENCY RESPONSE - LINEARITY INVESTIGATION

FIGURE 51

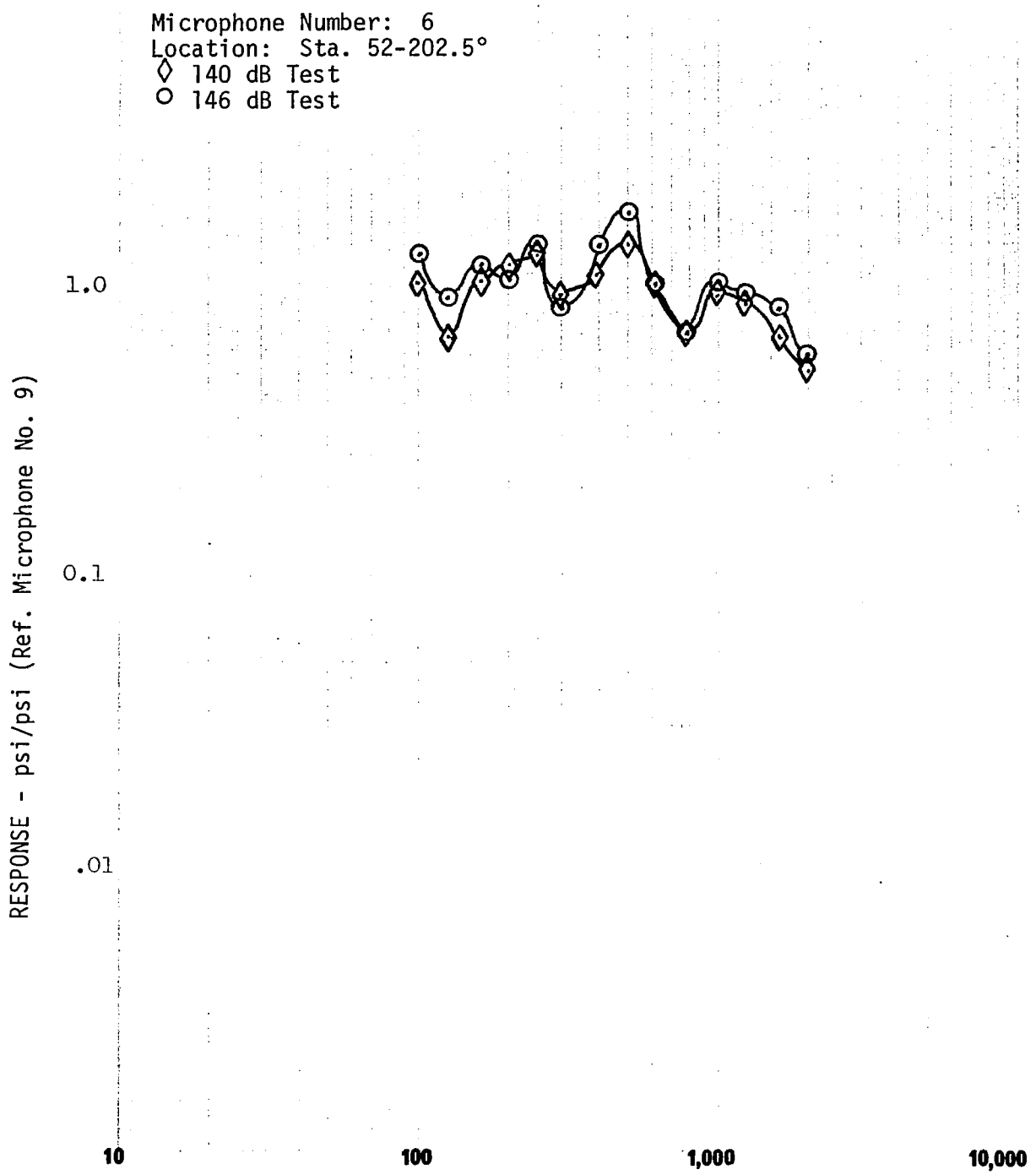

FREQUENCY RESPONSE - LINEARITY INVESTIGATION

FIGURE 52

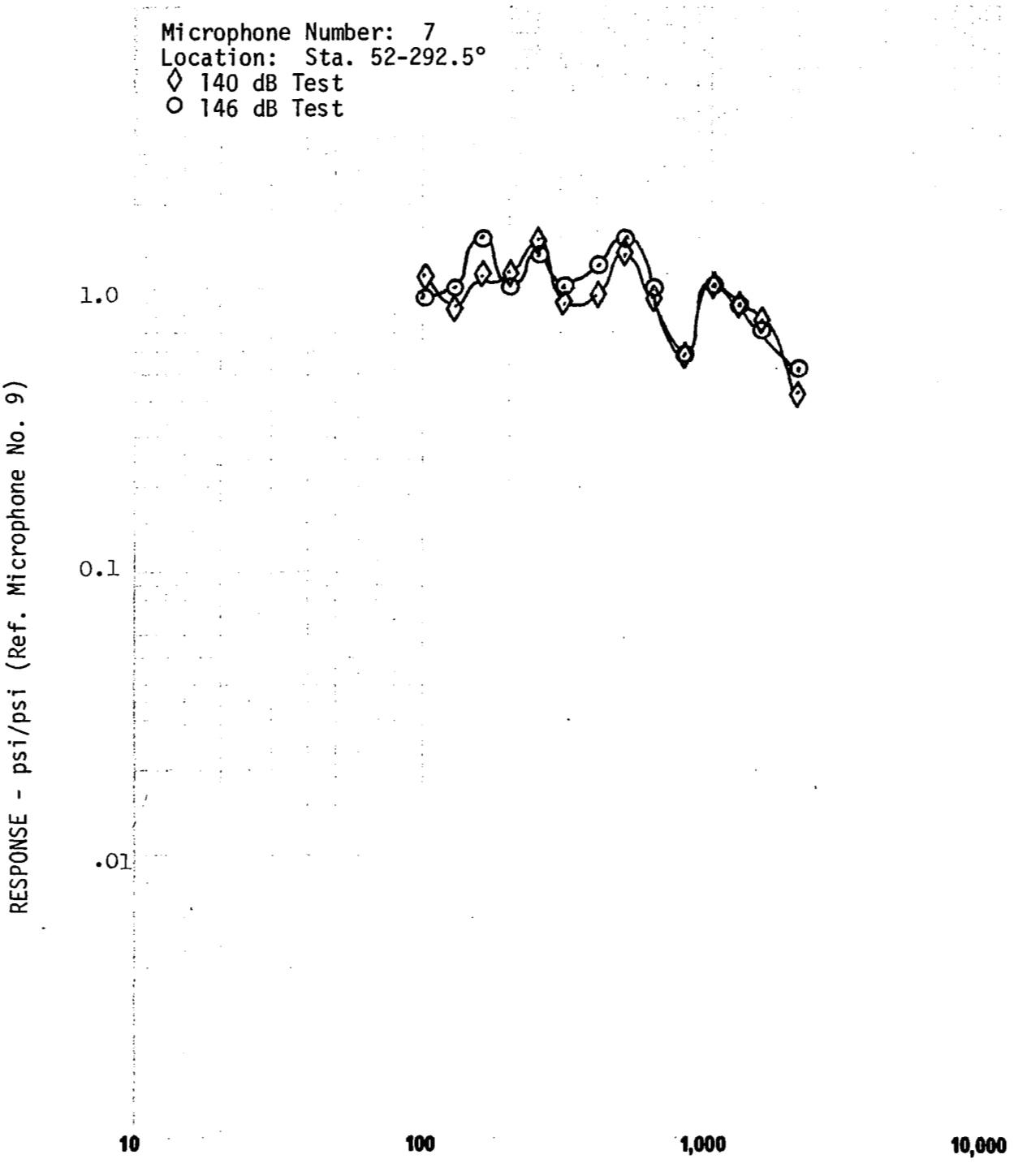

FREQUENCY RESPONSE - LINEARITY INVESTIGATION

FIGURE 53

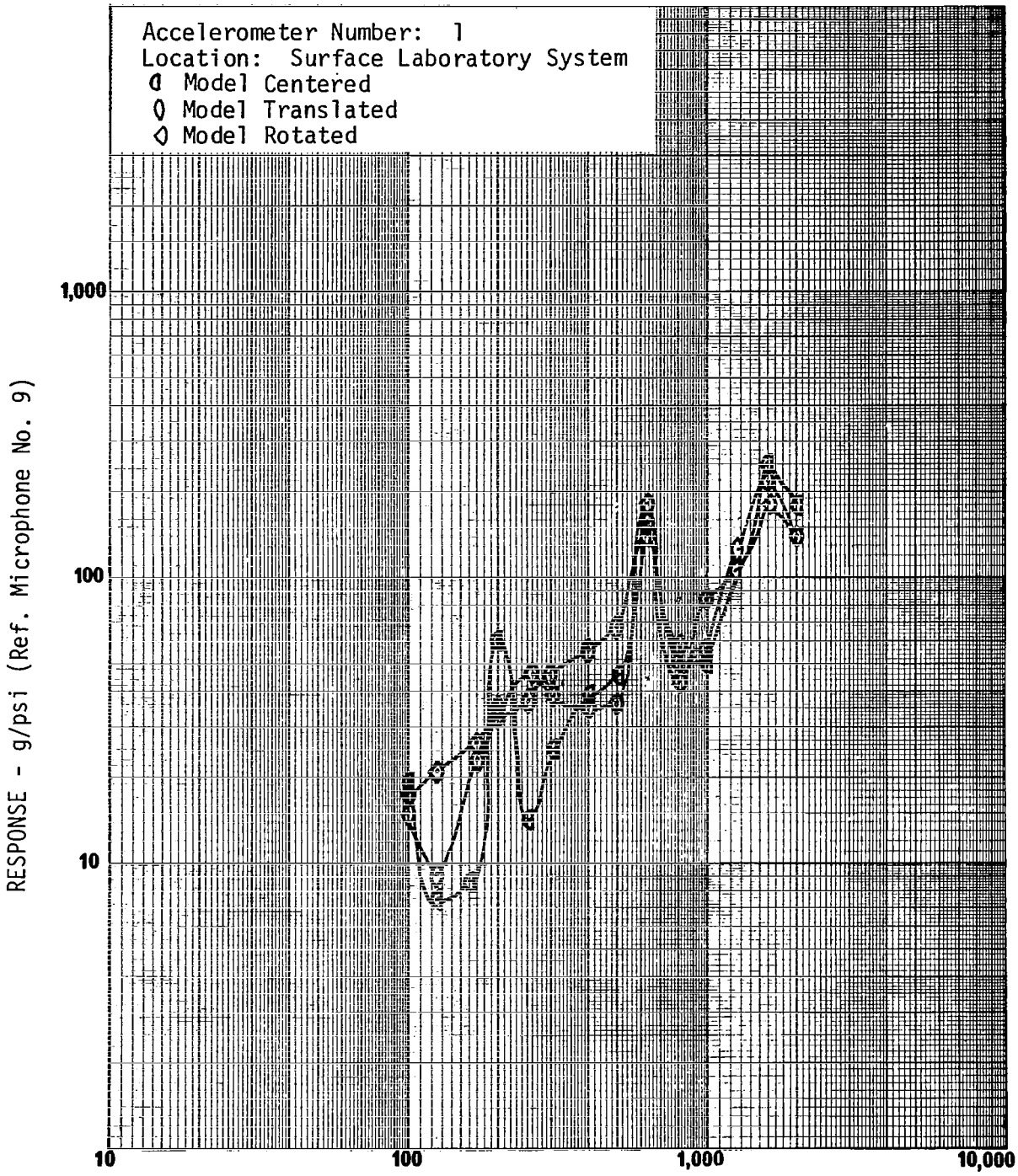

FREQUENCY RESPONSE - EFFECT OF MODEL POSITION

FIGURE 54

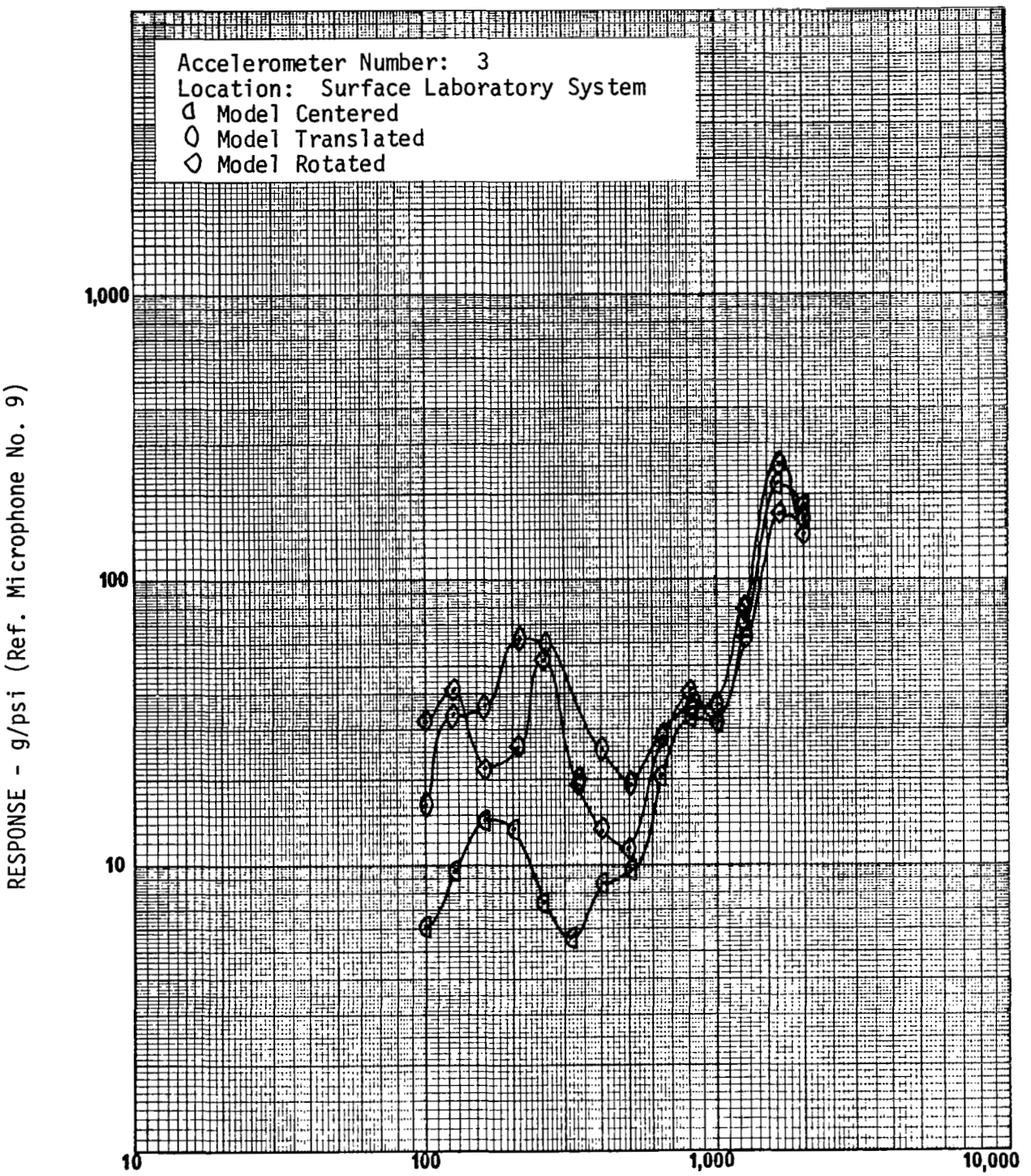

FREQUENCY RESPONSE - EFFECT OF MODEL POSITION

FIGURE 55

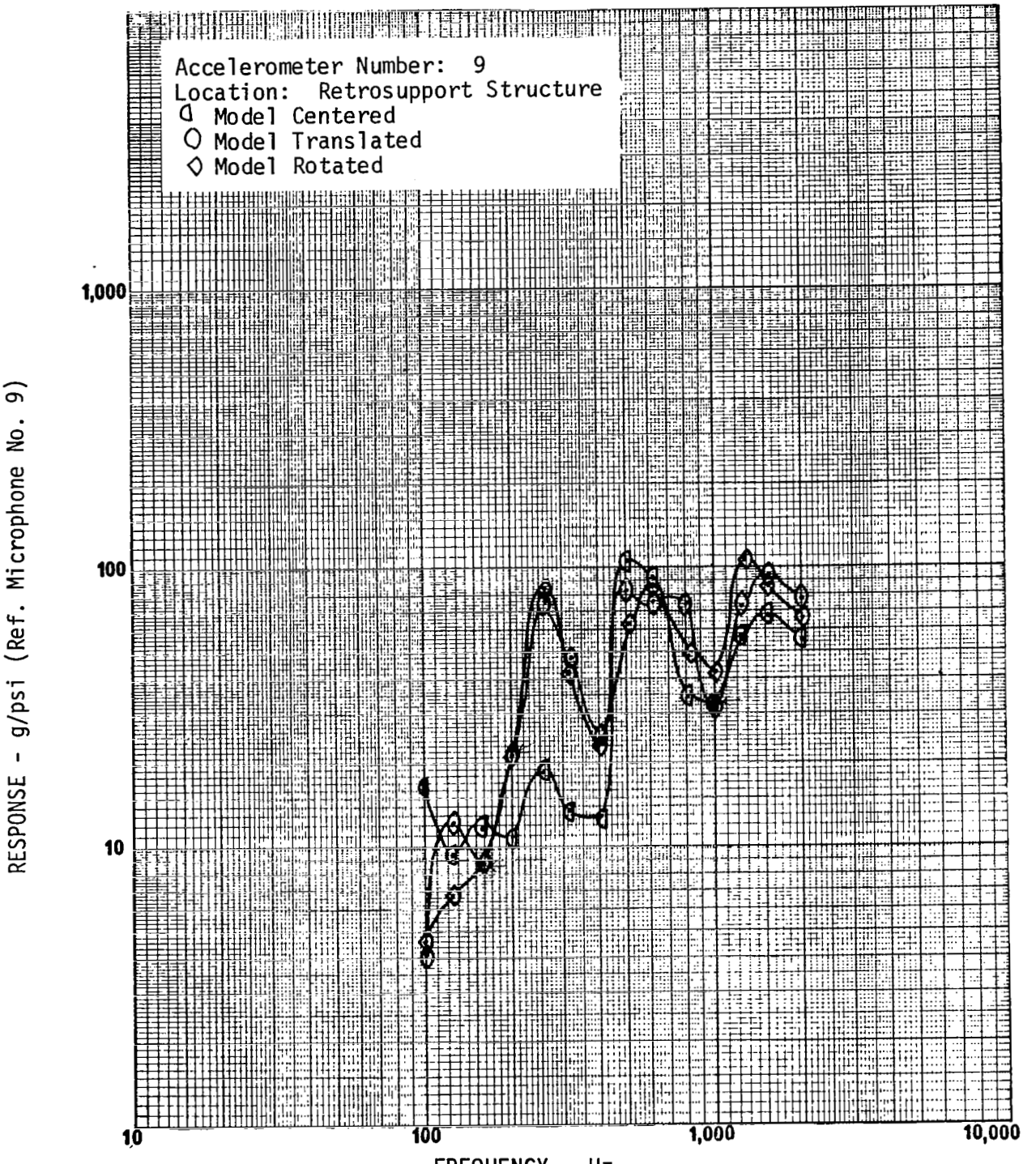

FREQUENCY RESPONSE - EFFECT OF MODEL POSITION

FIGURE 56

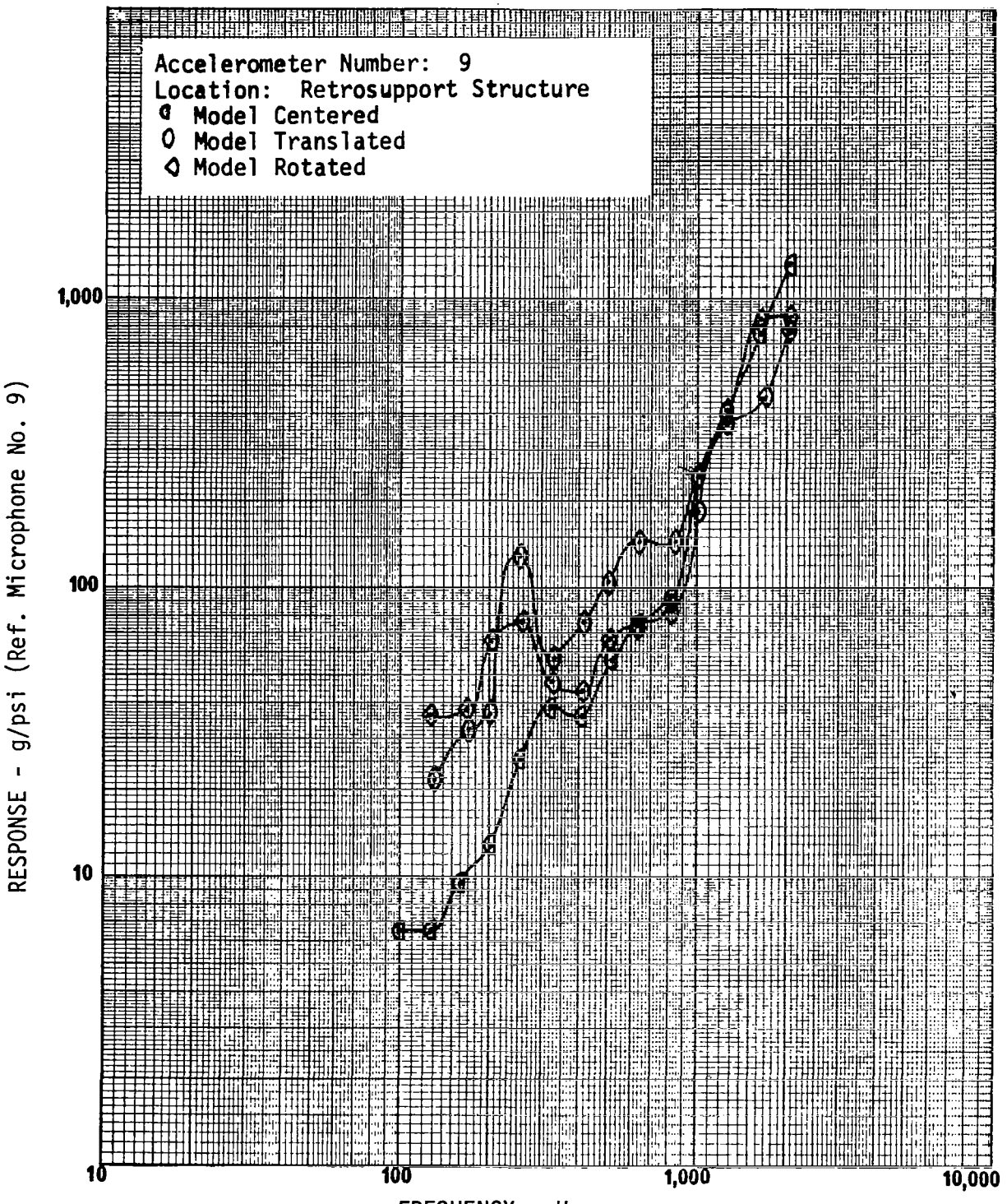

FREQUENCY RESPONSE - EFFECT OF MODEL POSITION

FIGURE 57

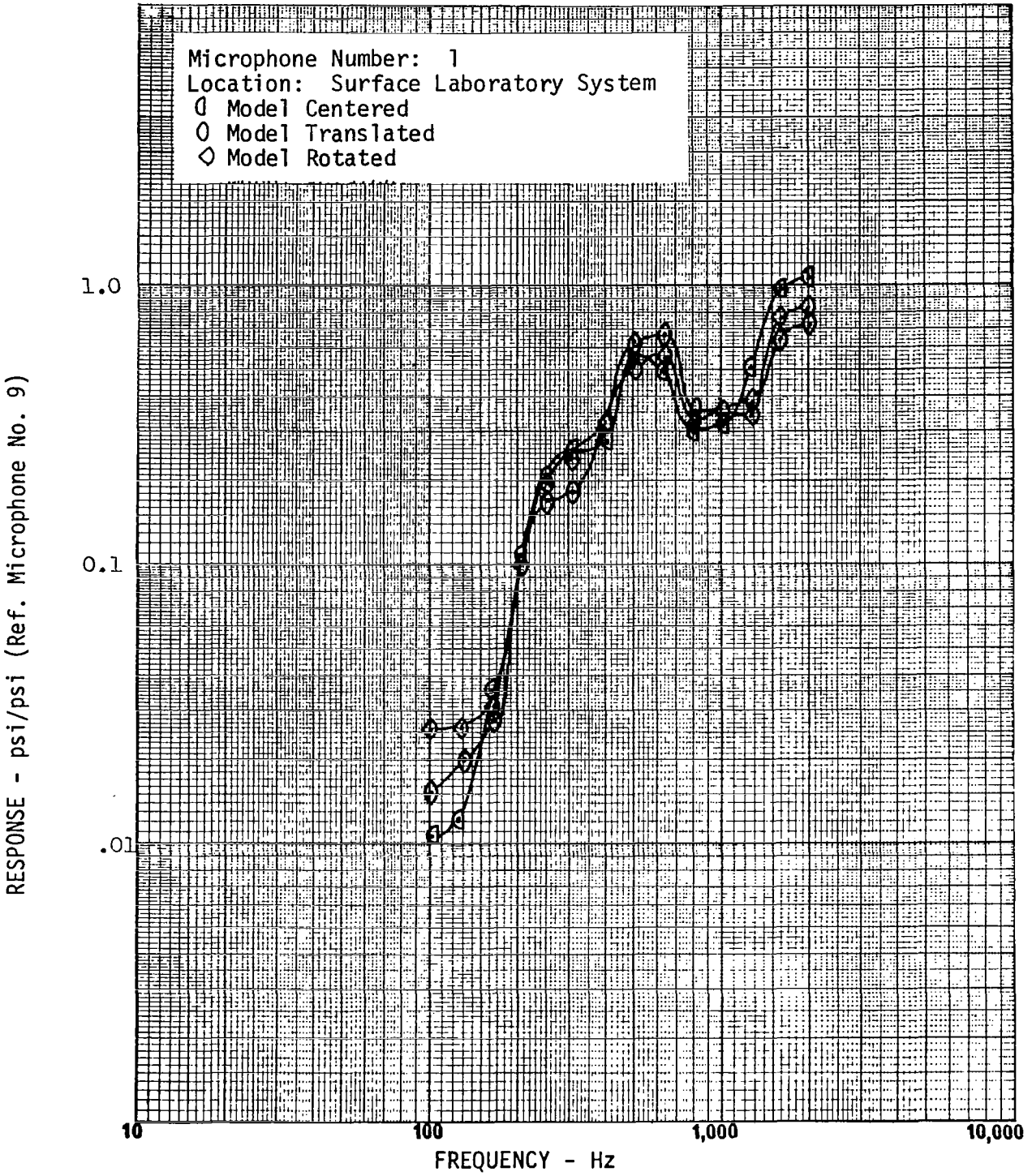

FREQUENCY RESPONSE - EFFECT OF MODEL POSITION

FIGURE 58

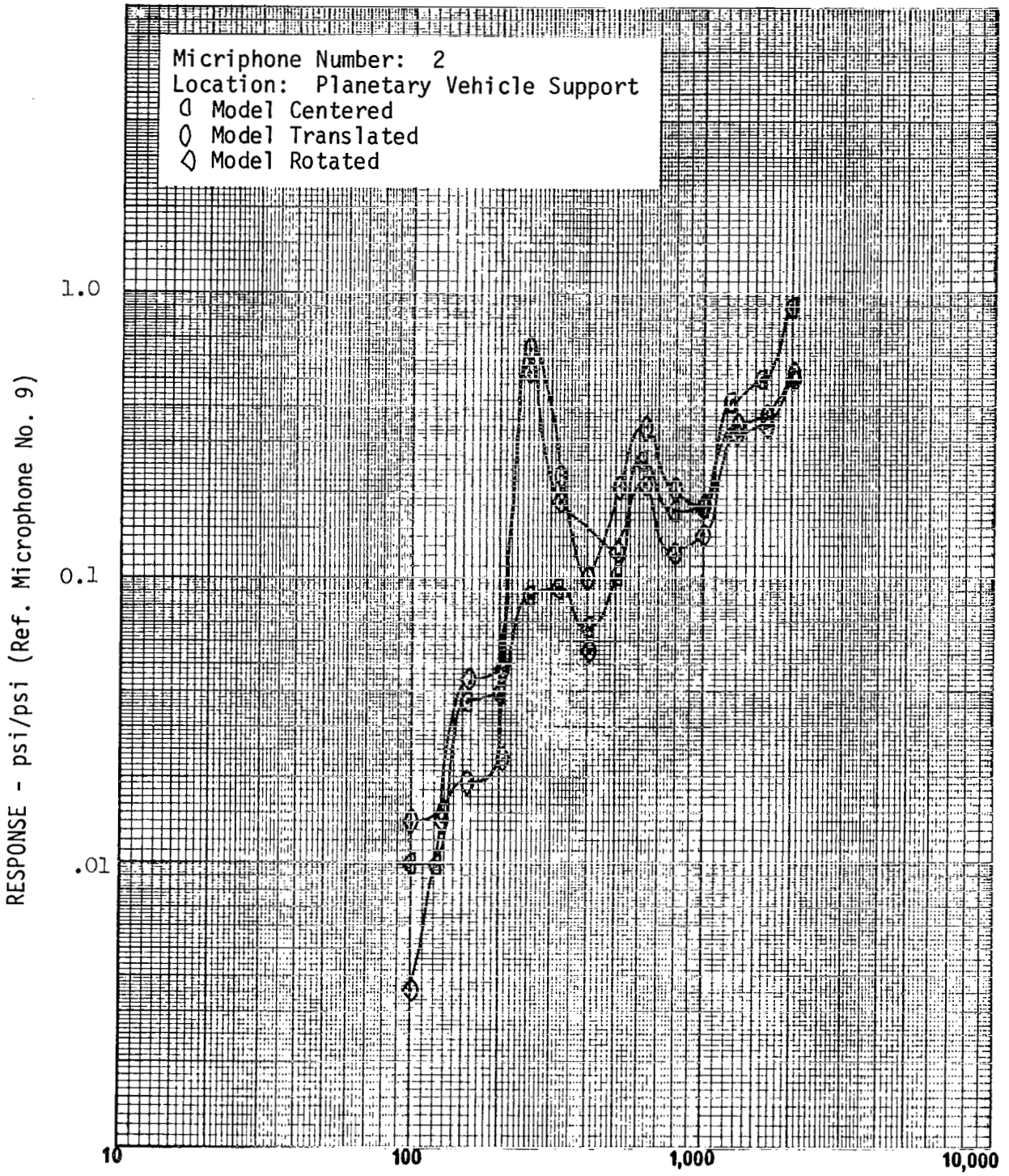

FREQUENCY RESPONSE - EFFECT OF MODEL POSITION

FIGURE 59

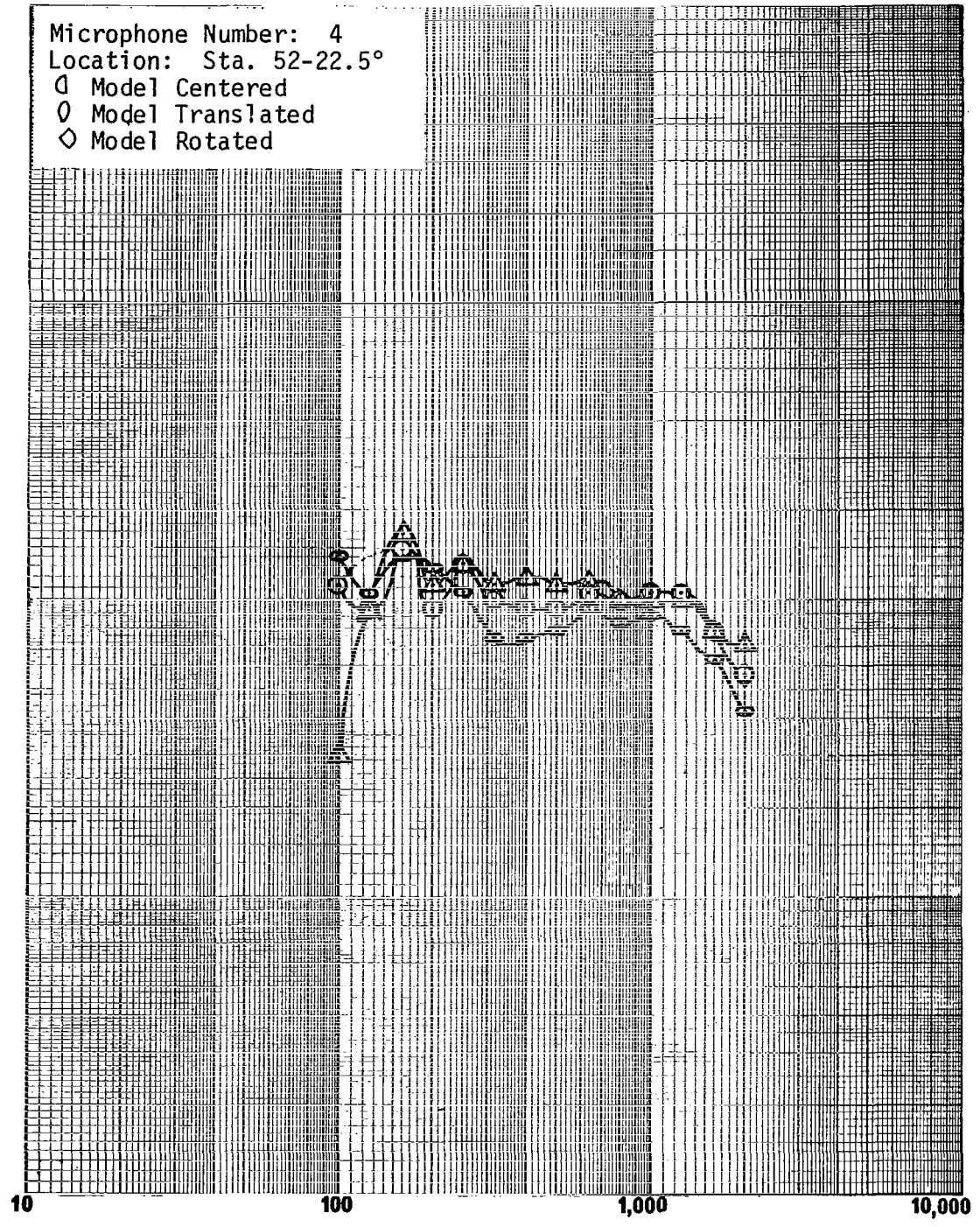

FREQUENCY RESPONSE - EFFECT OF MODEL POSITION

FIGURE 60

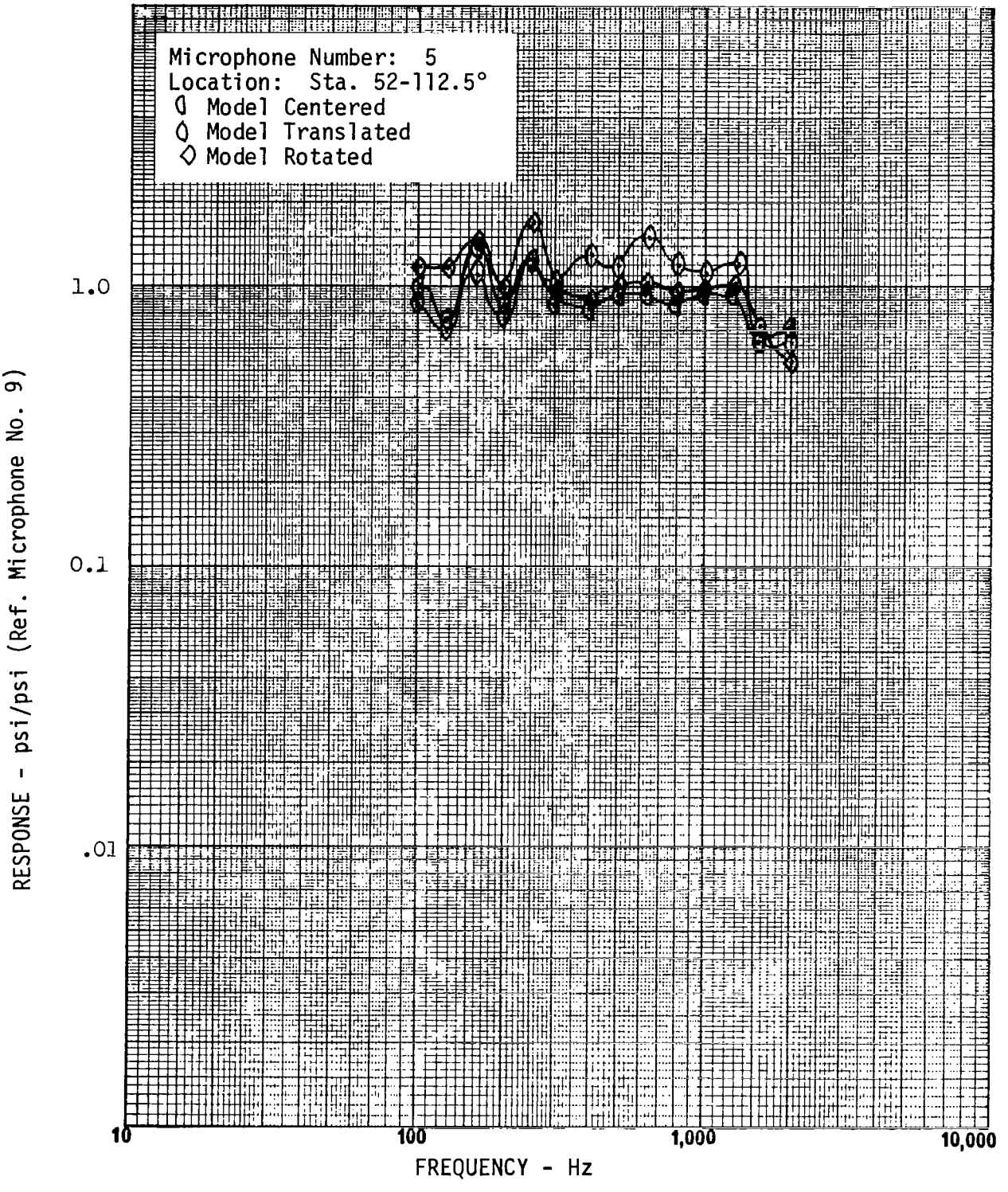

FREQUENCY RESPONSE - EFFECT OF MODEL POSITION

FIGURE 61

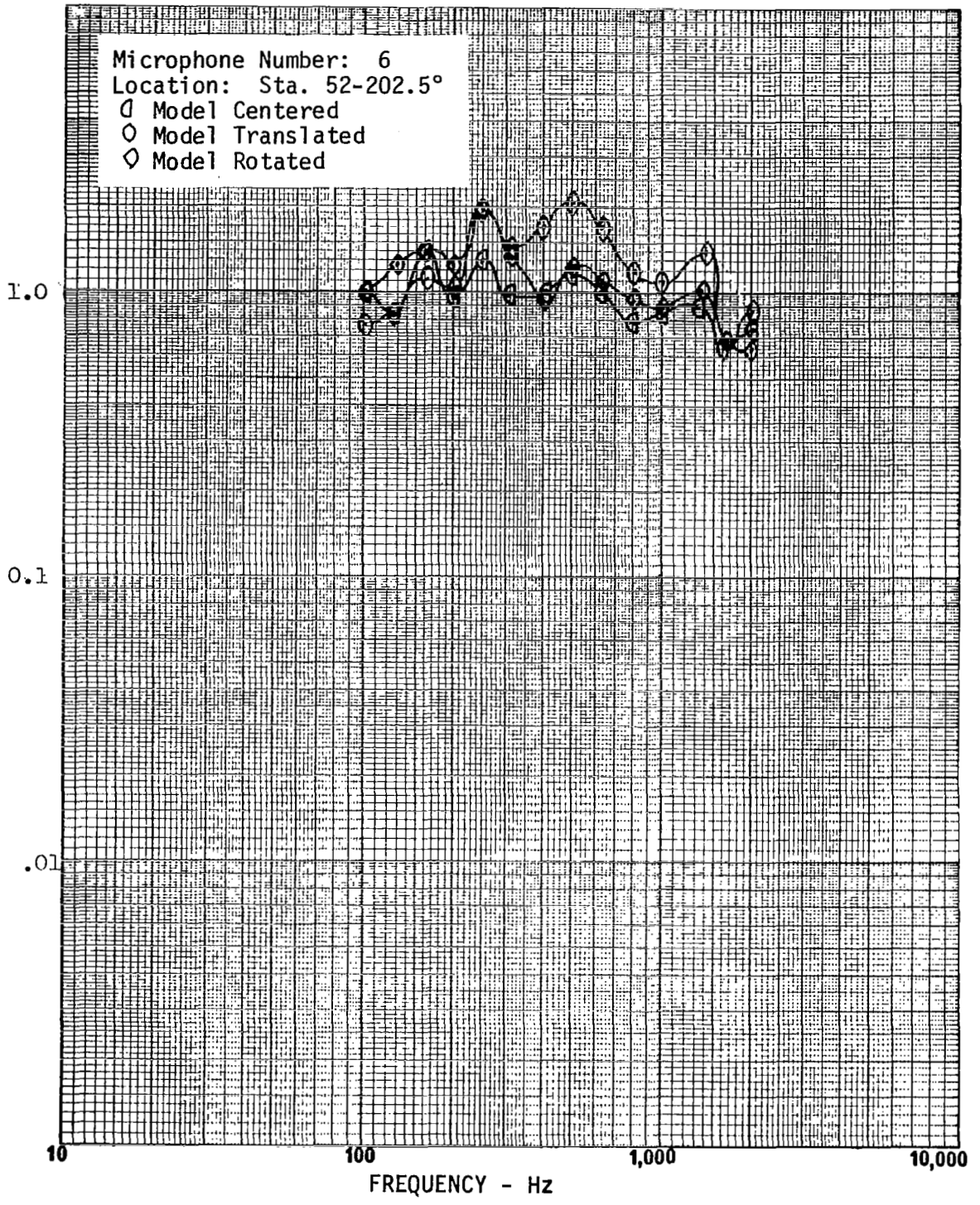

FREQUENCY RESPONSE - EFFECT OF MODEL POSITION

FIGURE 62

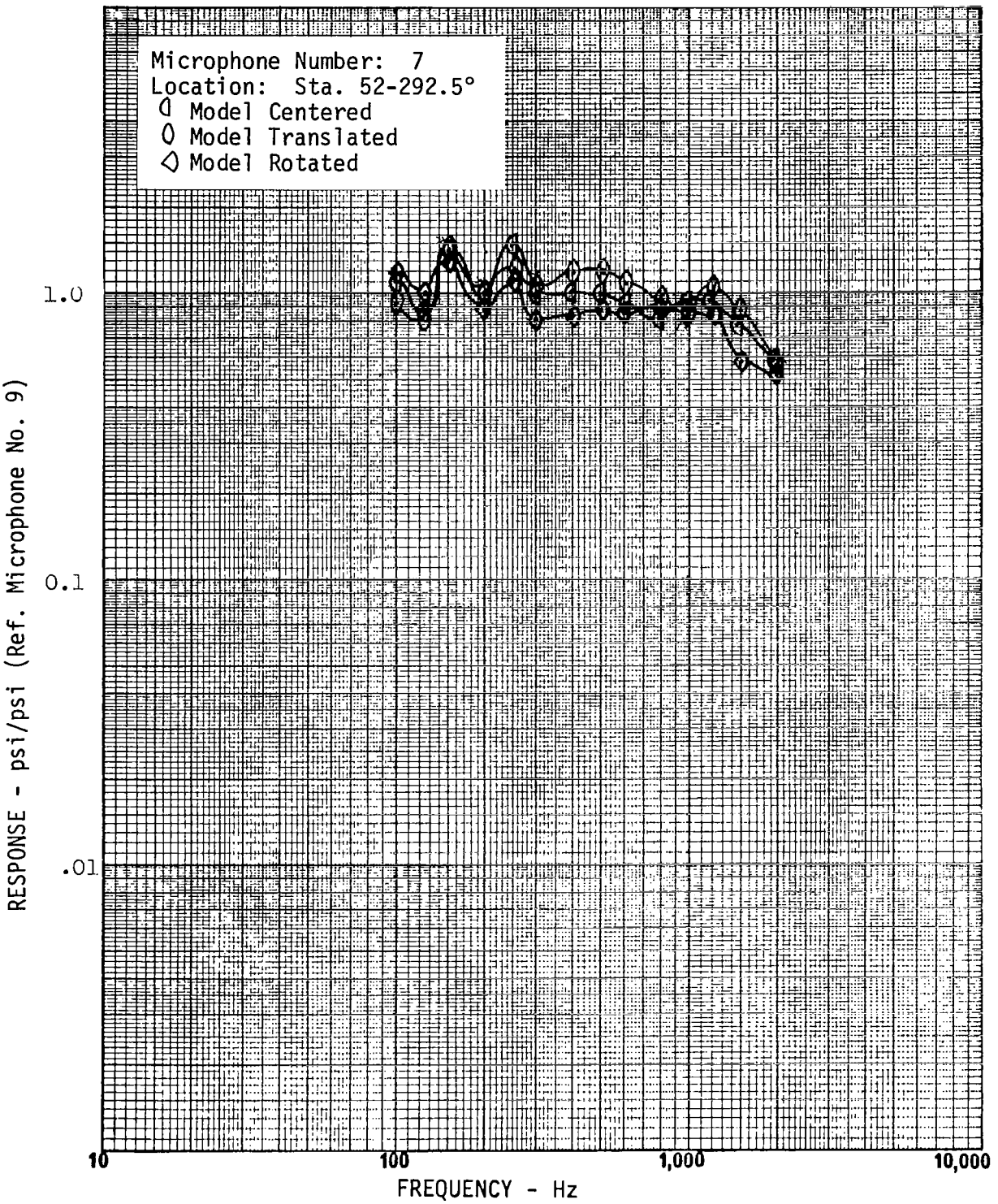

FREQUENCY RESPONSE - EFFECT OF MODEL POSITION

FIGURE 63

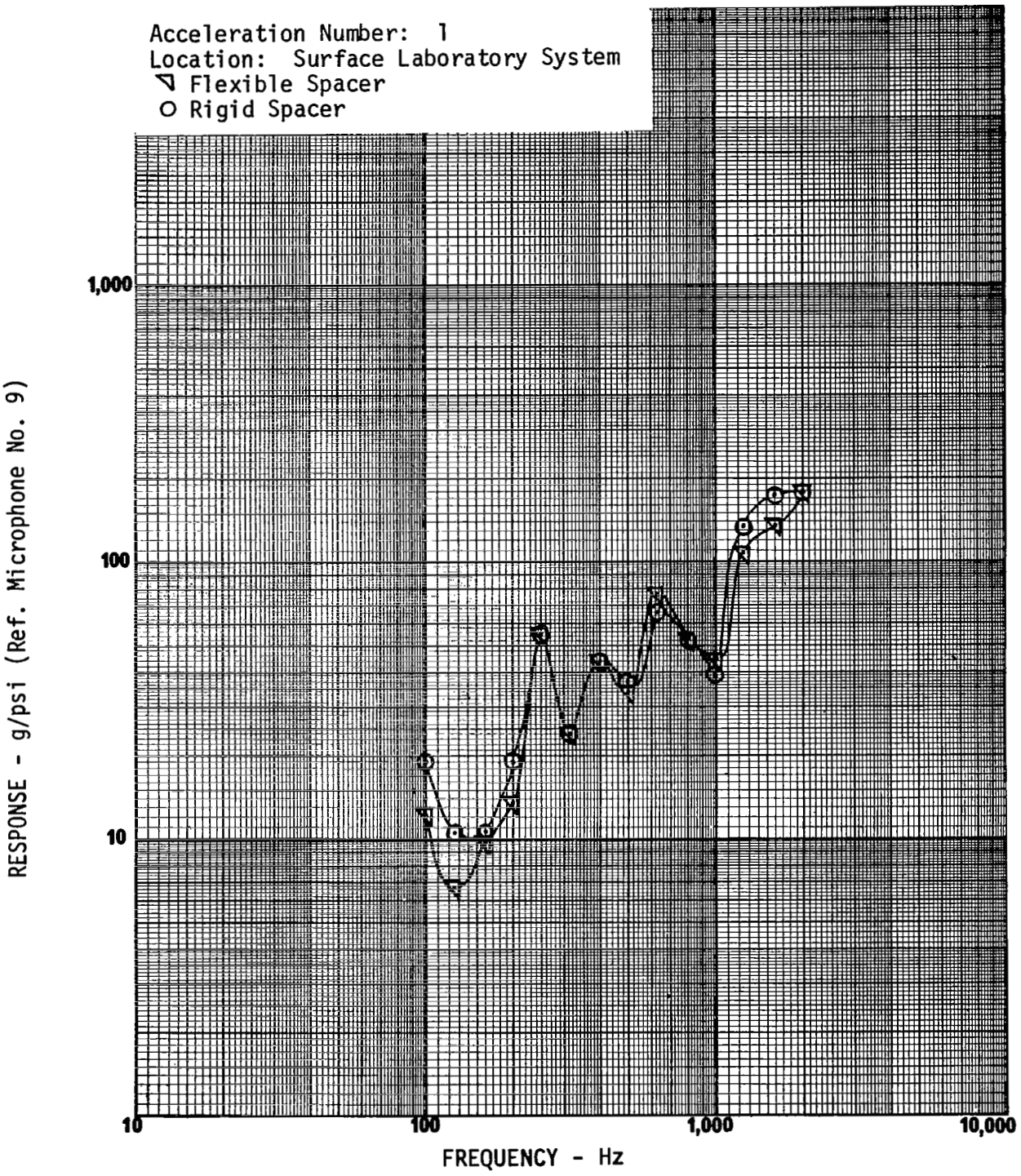

FREQUENCY RESPONSE - EFFECT OF BOUNDARY CONDITION

FIGURE 64

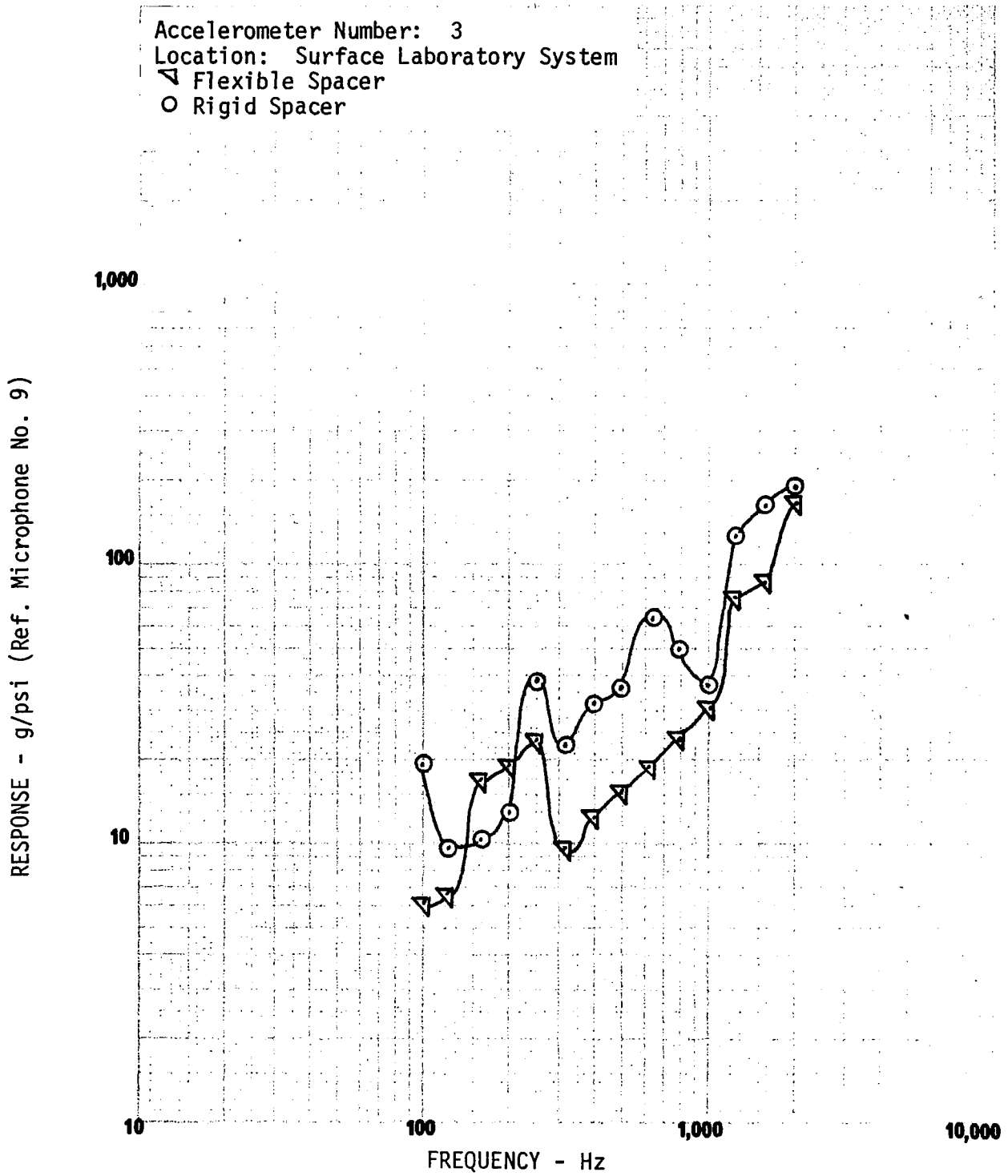

FREQUENCY RESPONSE - EFFECT OF BOUNDARY CONDITION

FIGURE 65

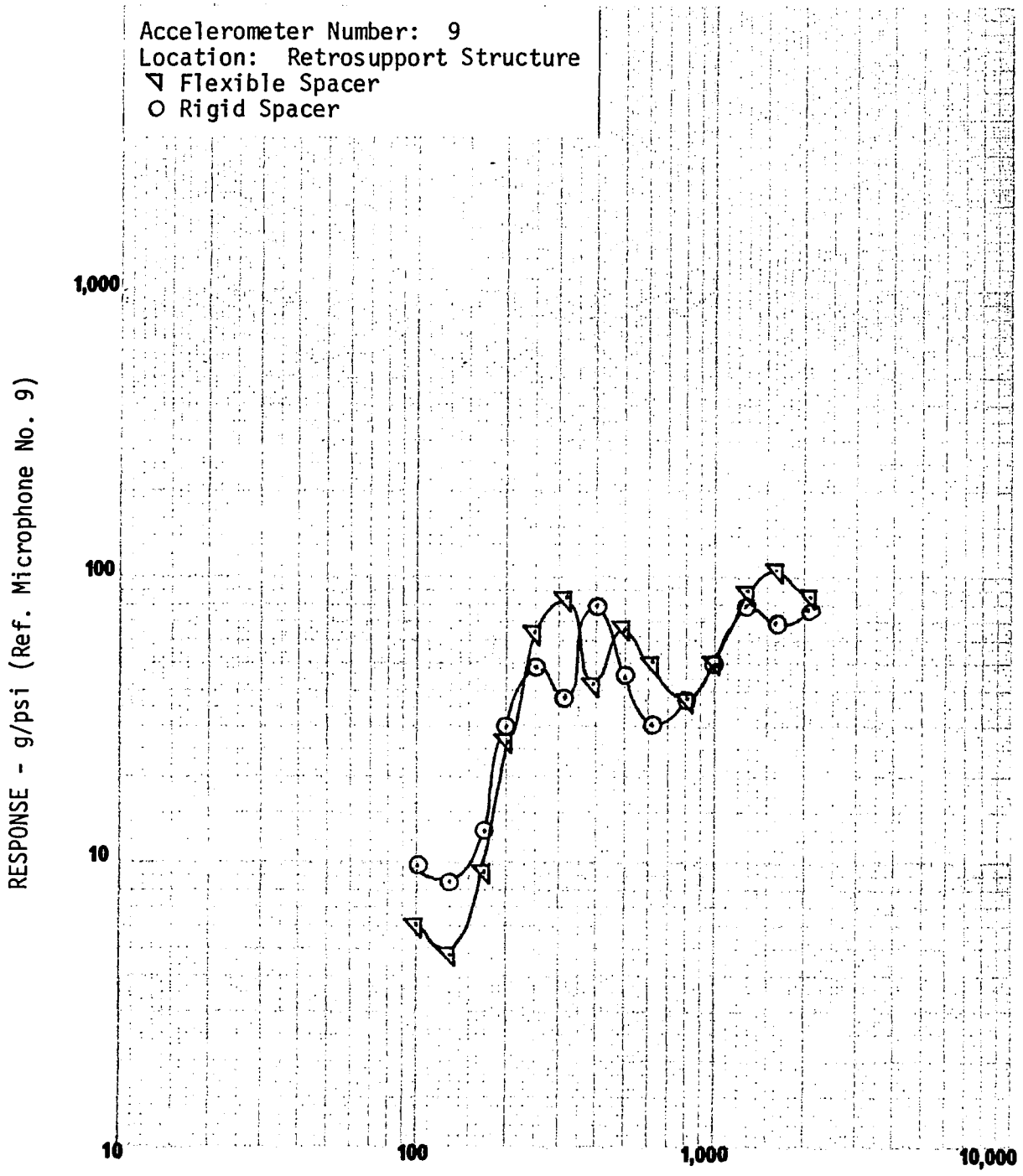

FREQUENCY RESPONSE - EFFECT OF BOUNDARY CONDITION

FIGURE 66

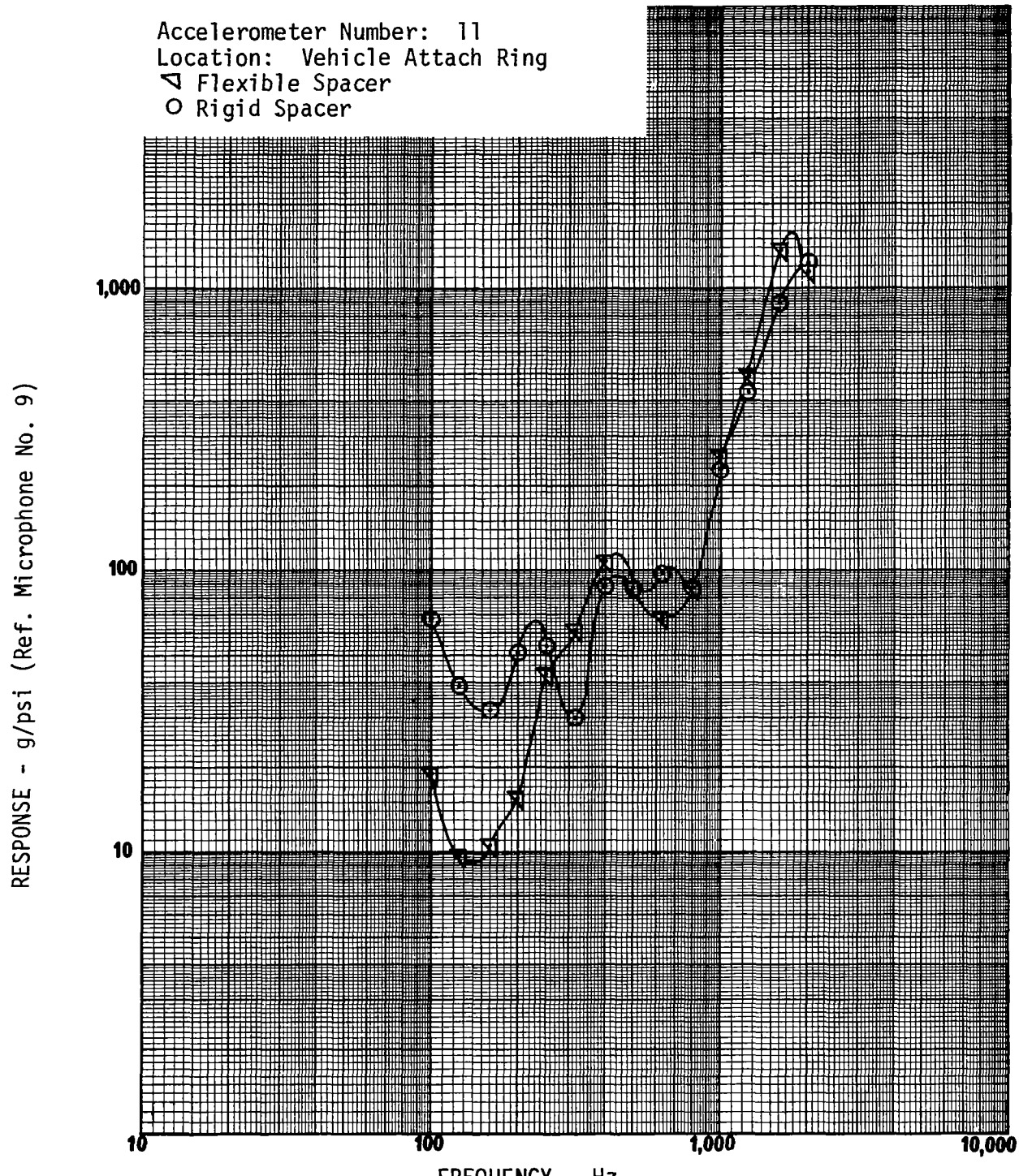

FREQUENCY RESPONSE - EFFECT OF BOUNDARY CONDITION

FIGURE 67

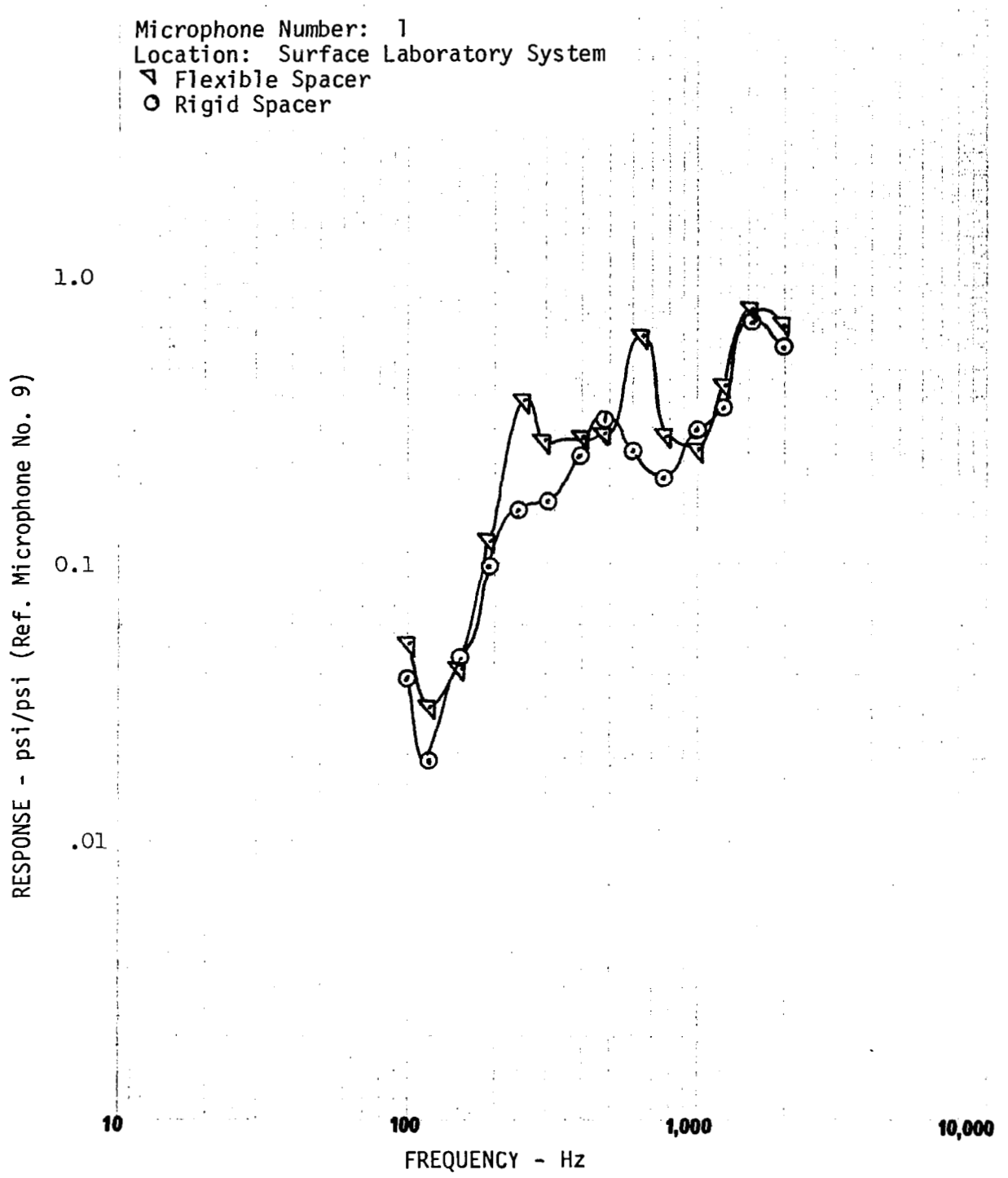

FREQUENCY RESPONSE - EFFECT OF BOUNDARY CONDITION

FIGURE 68

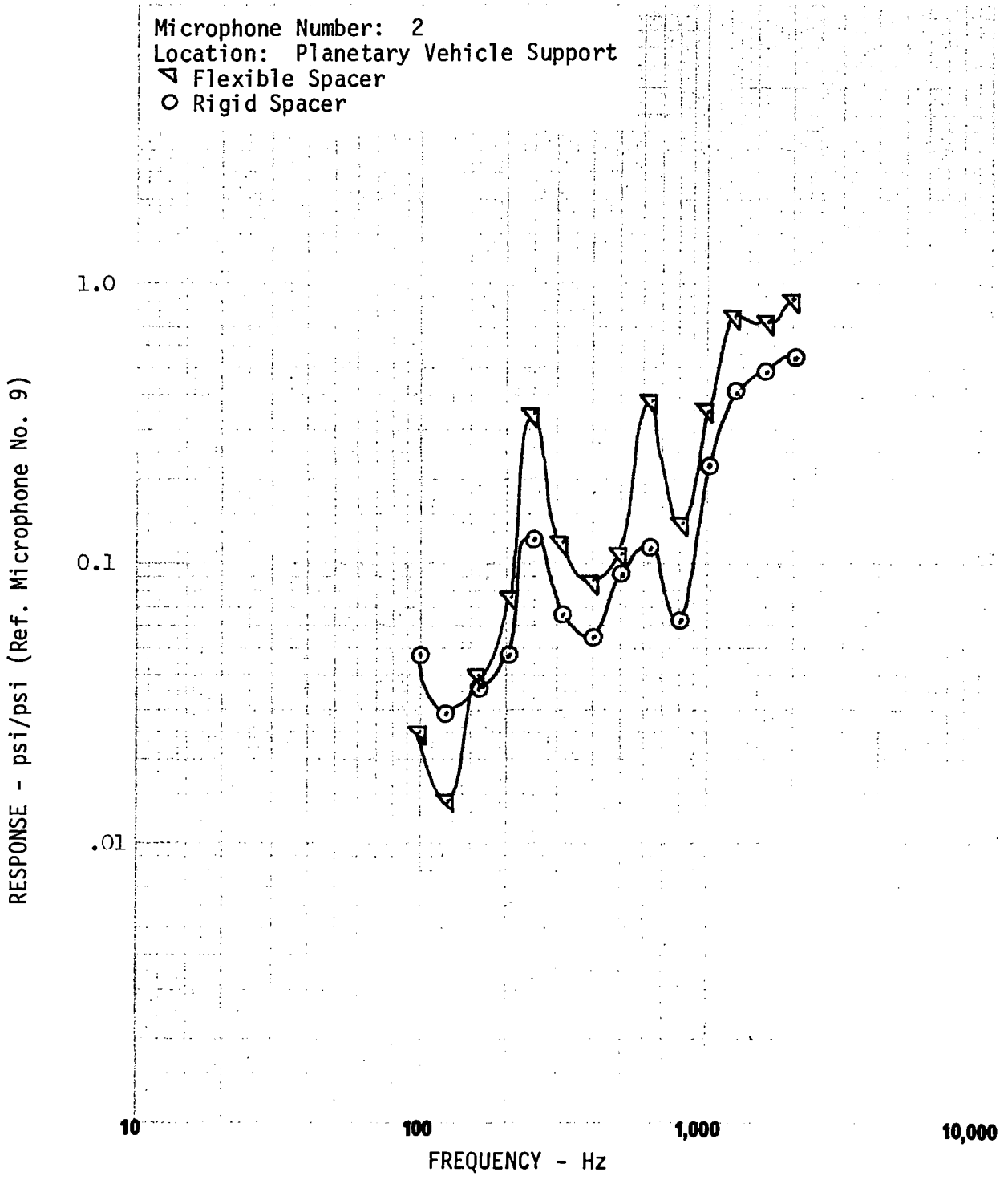

FREQUENCY RESPONSE - EFFECT OF BOUNDARY CONDITION

FIGURE 69

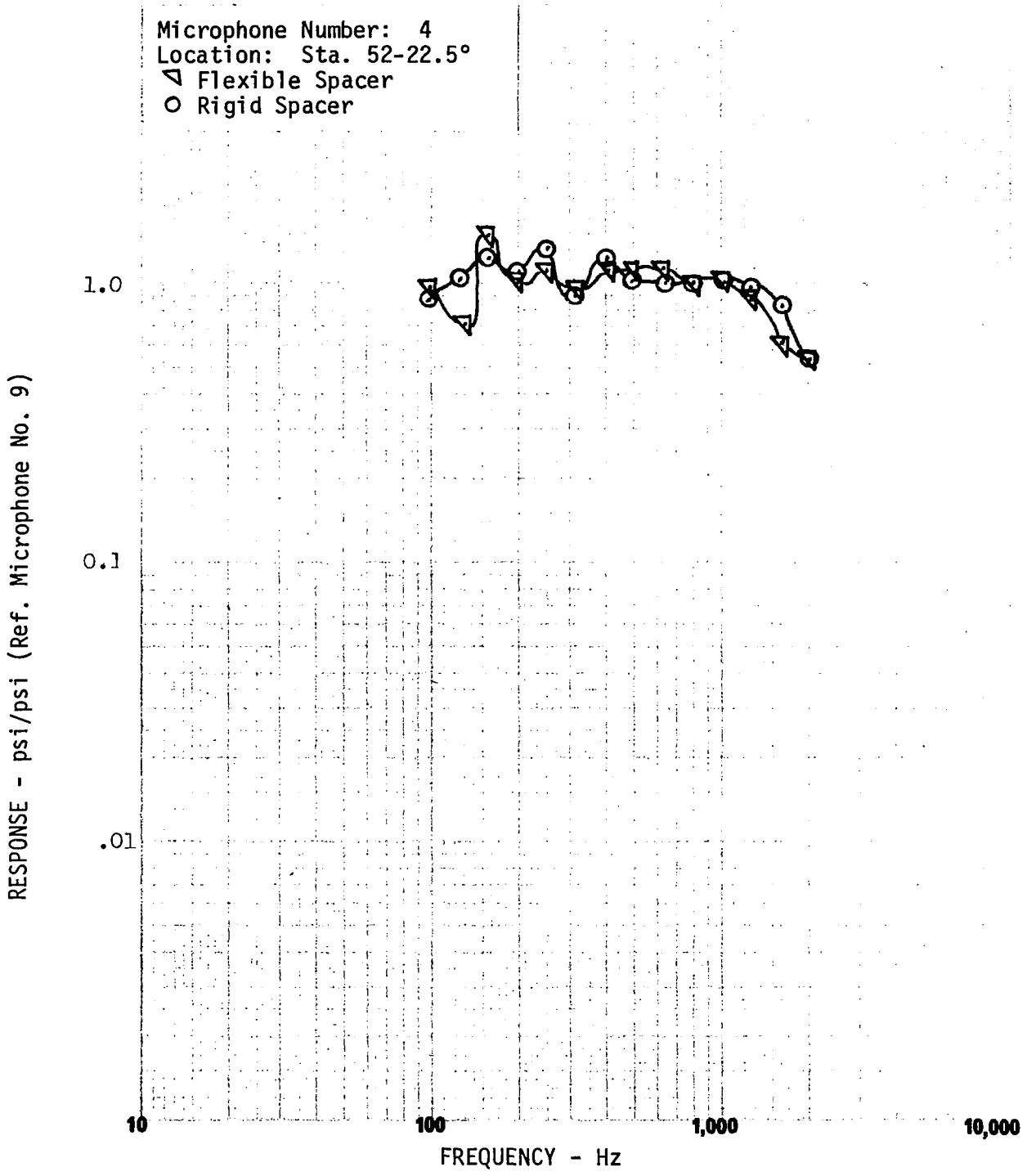

FREQUENCY RESPONSE - EFFECT OF BOUNDARY CONDITION

FIGURE 70

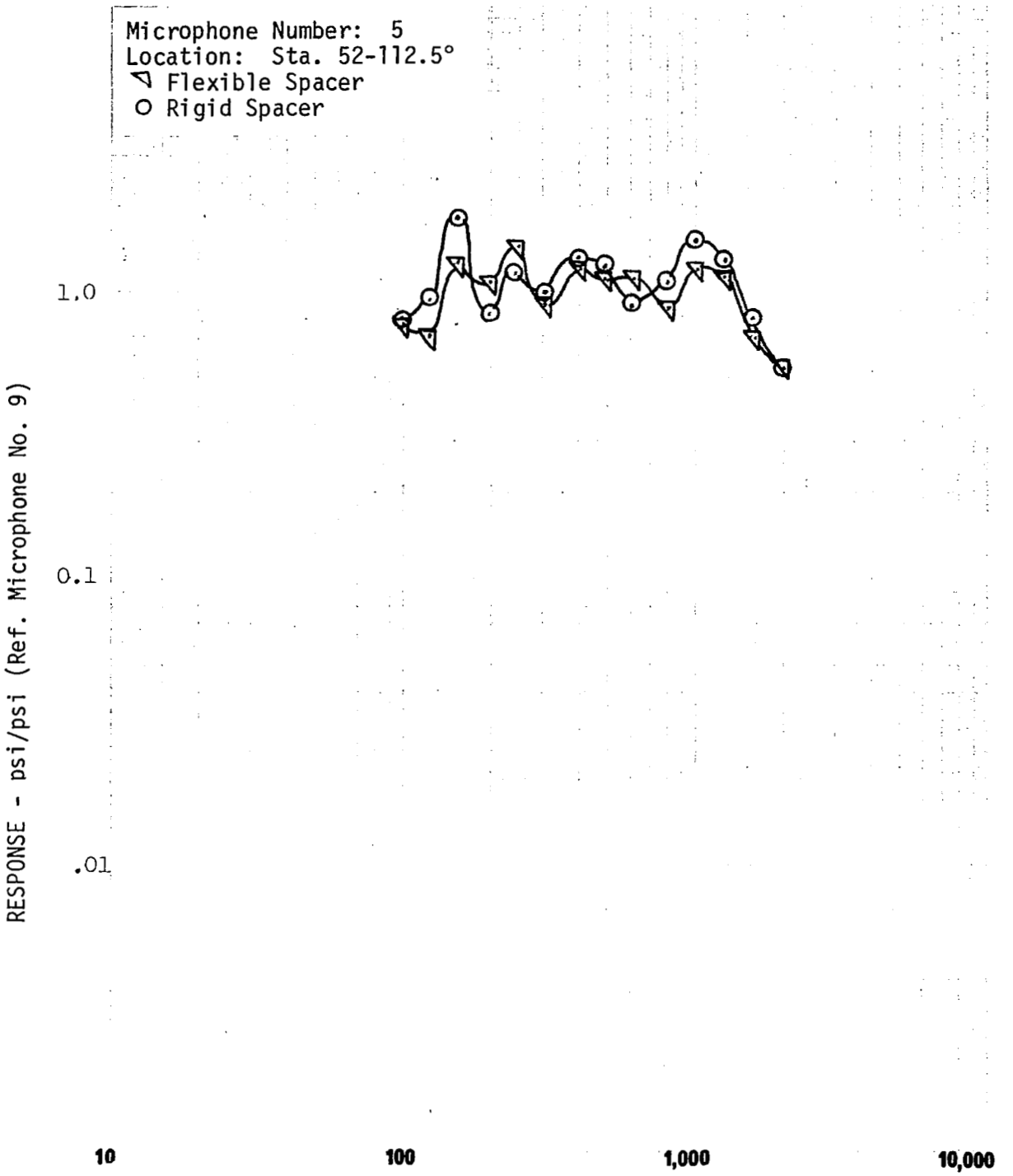

FREQUENCY RESPONSE - EFFECT OF BOUNDARY CONDITION

FIGURE 71

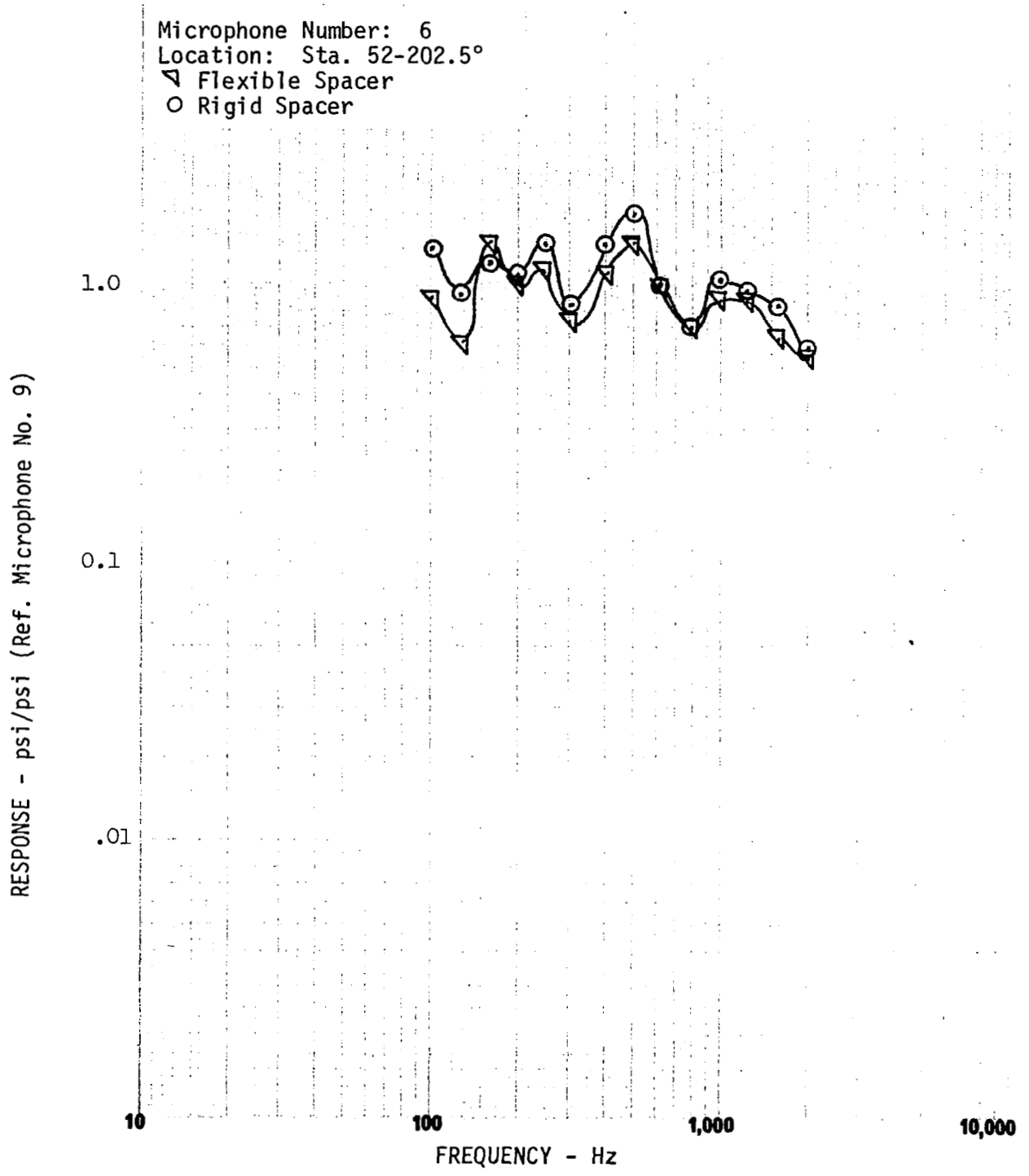

FREQUENCY RESPONSE - EFFECT OF BOUNDARY CONDITION

FIGURE 72

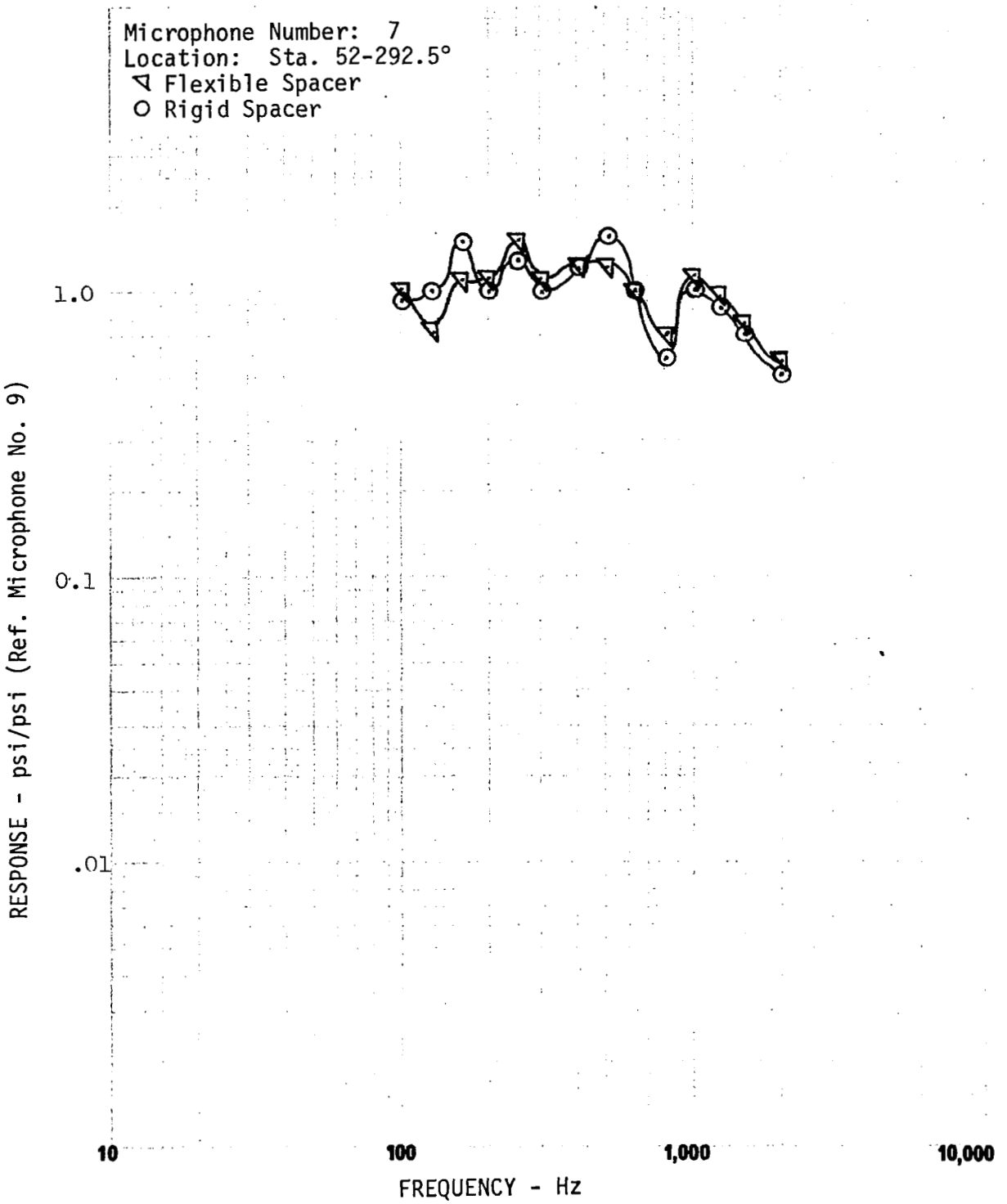

FREQUENCY RESPONSE - EFFECT OF BOUNDARY CONDITION

FIGURE 73

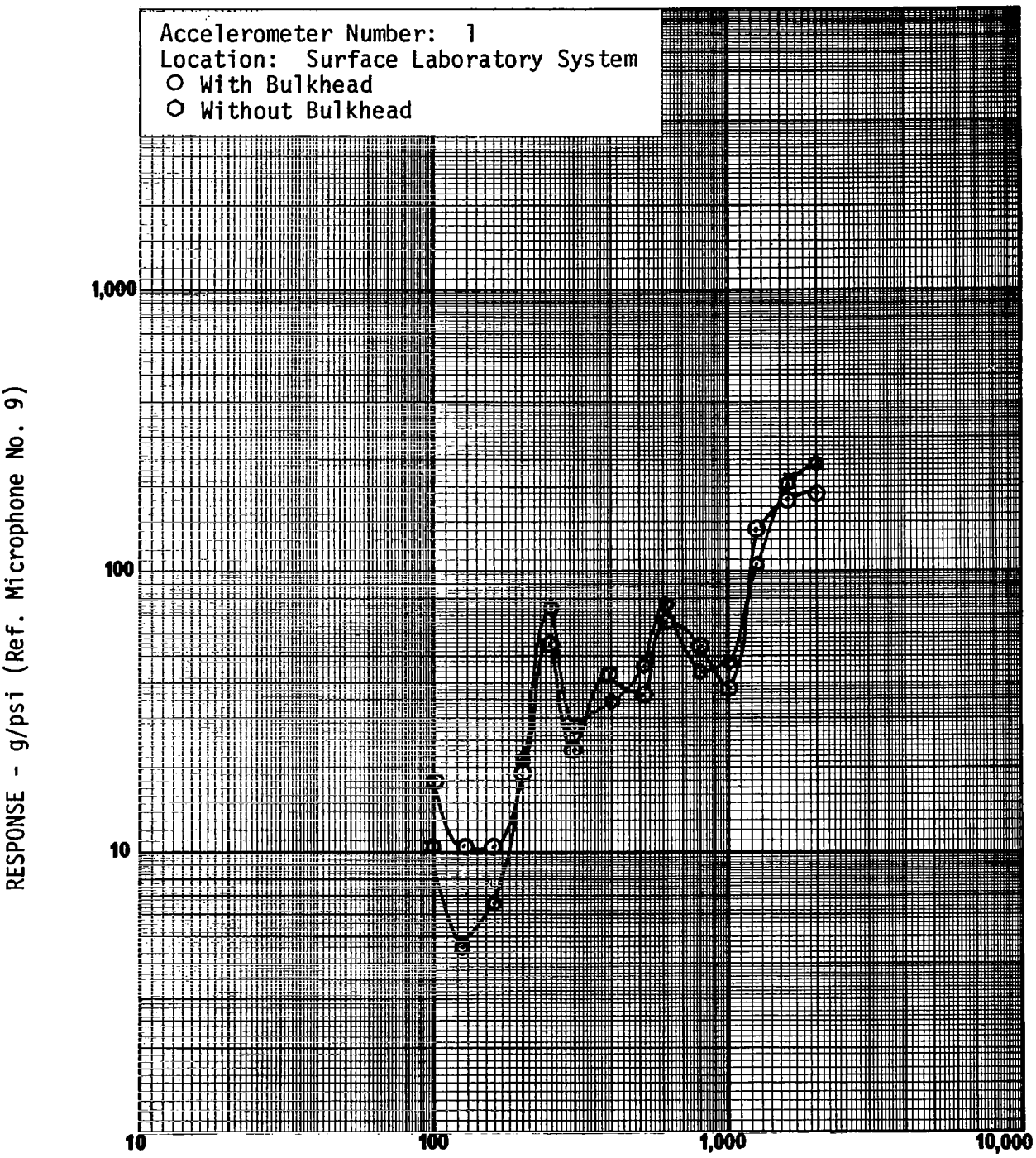

FREQUENCY RESPONSE - EFFECT OF AFT BULKHEAD

FIGURE 74

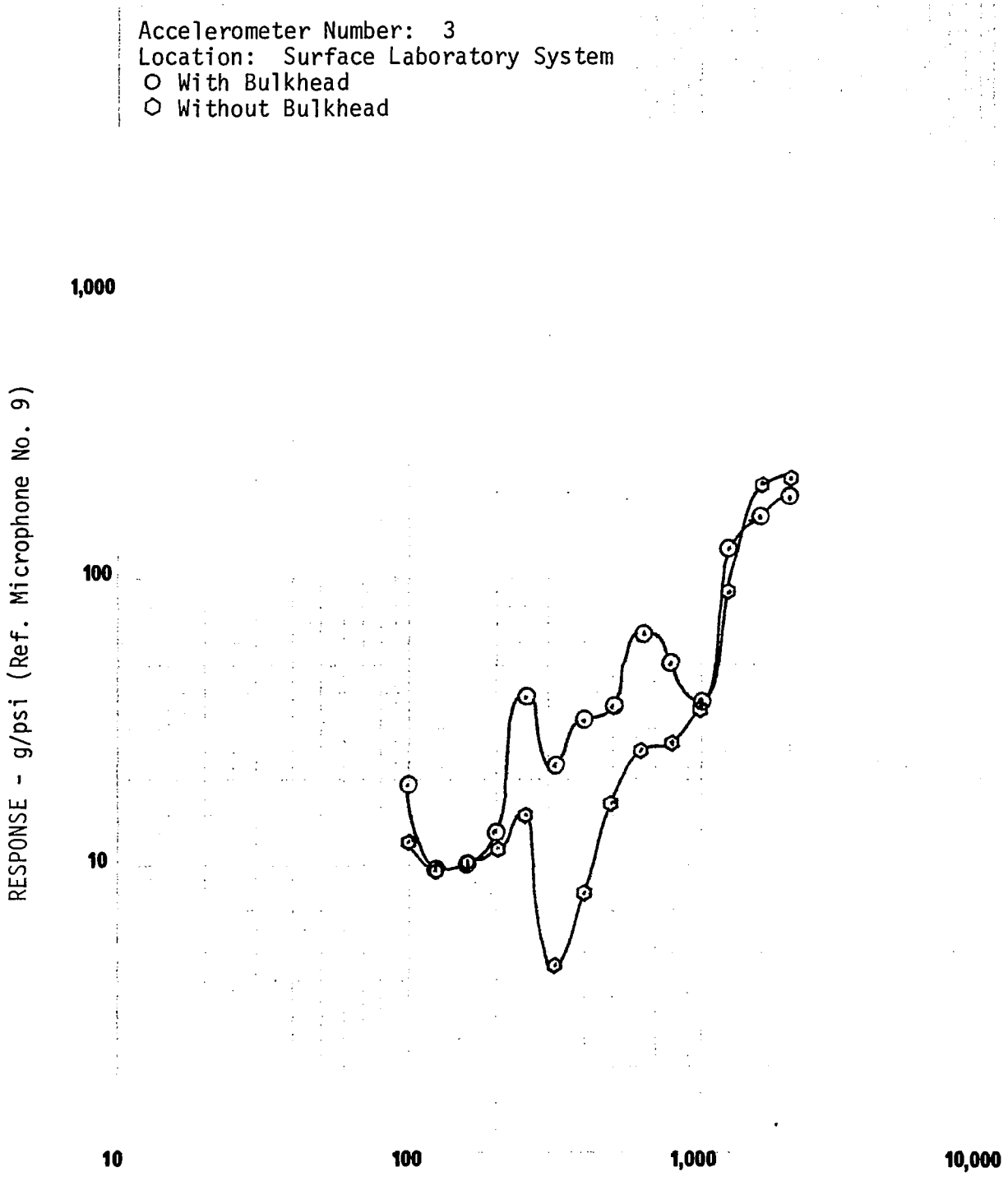

FREQUENCY RESPONSE - EFFECT OF AFT BULKHEAD

FIGURE 75

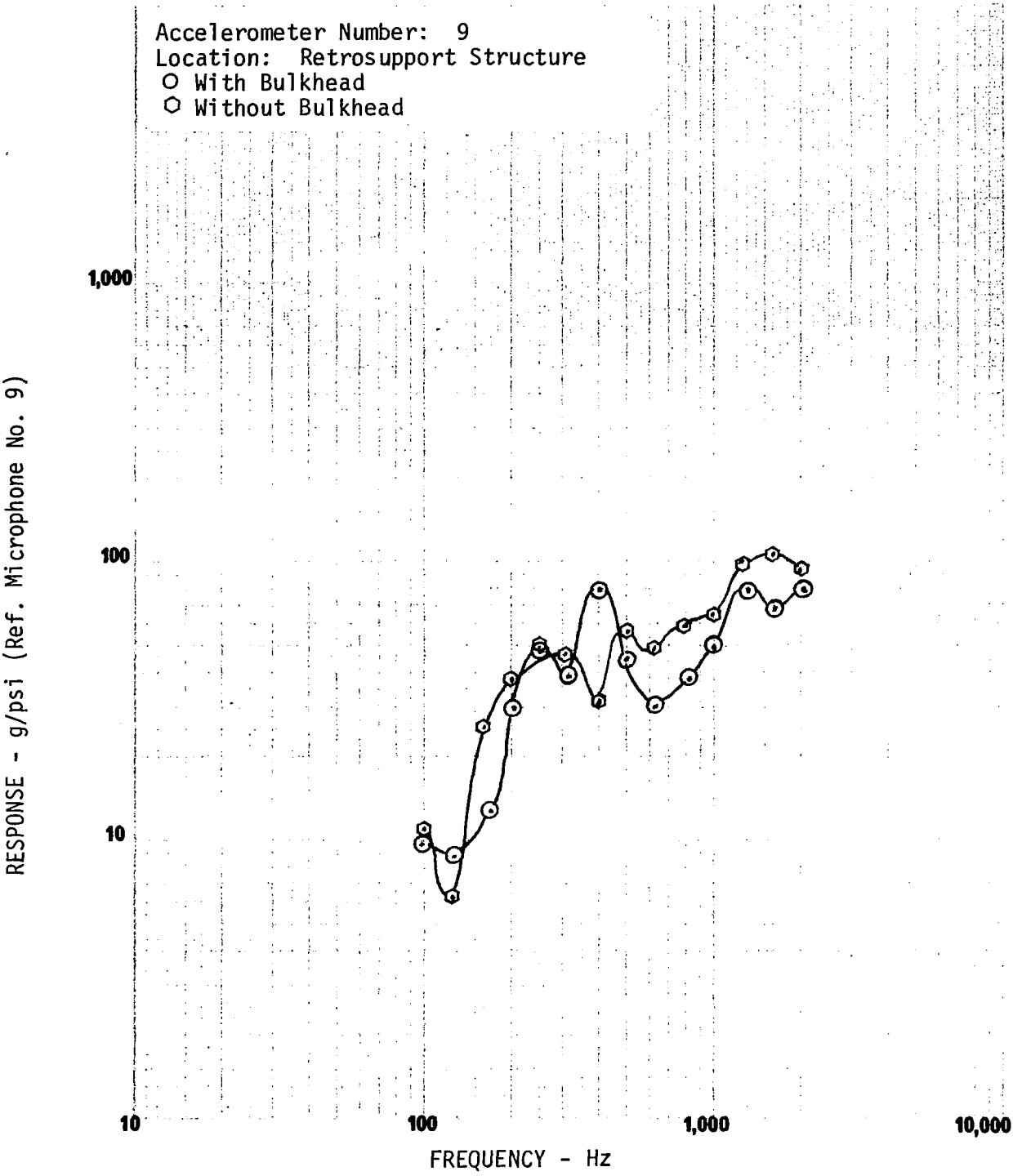

FREQUENCY RESPONSE - EFFECT OF AFT BULKHEAD

FIGURE 76

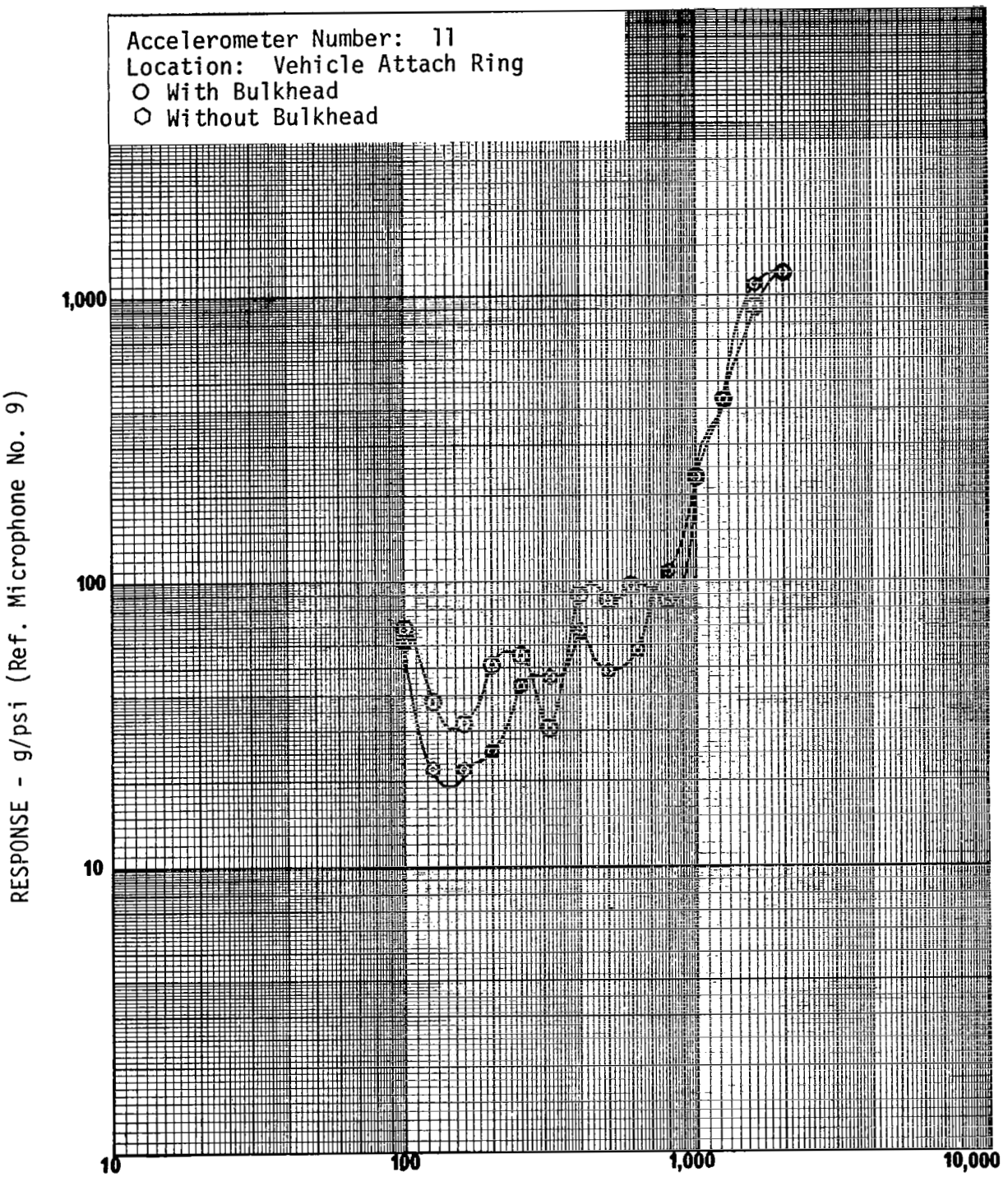

FREQUENCY RESPONSE - EFFECT OF AFT BULKHEAD

FIGURE 77

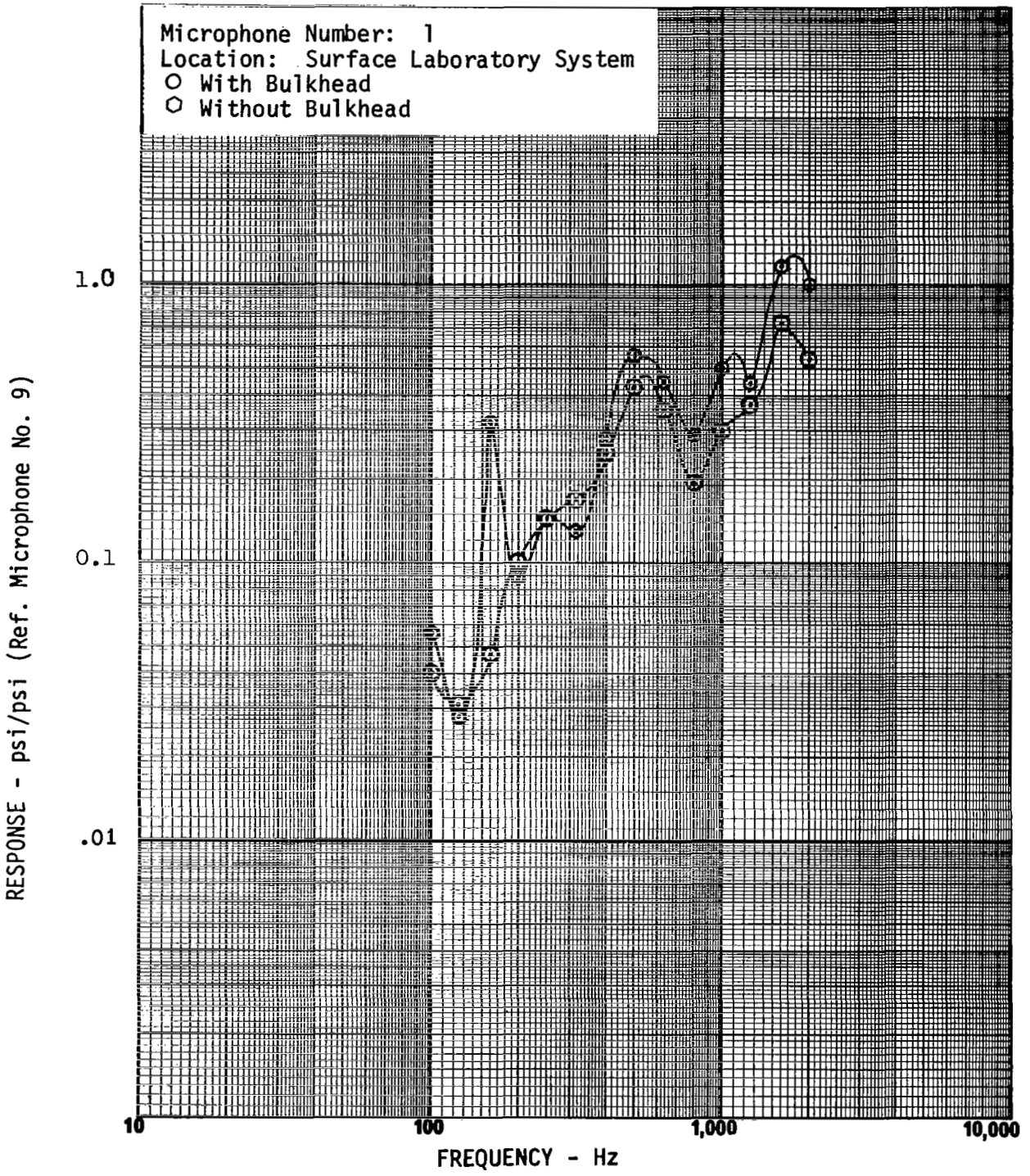

FREQUENCY RESPONSE - EFFECT OF AFT BULKHEAD

FIGURE 78

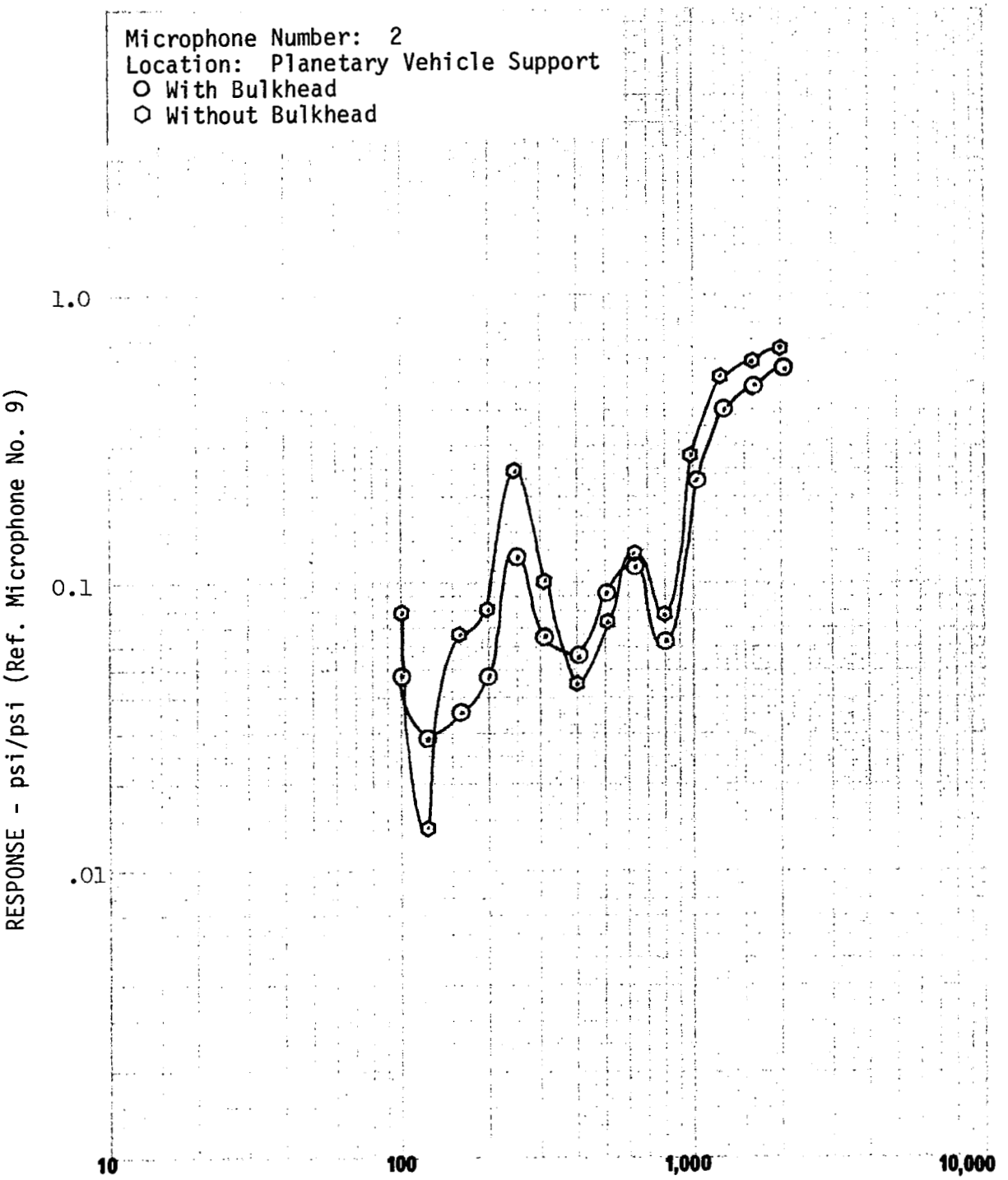

FREQUENCY RESPONSE - EFFECT OF AFT BULKHEAD

FIGURE 79

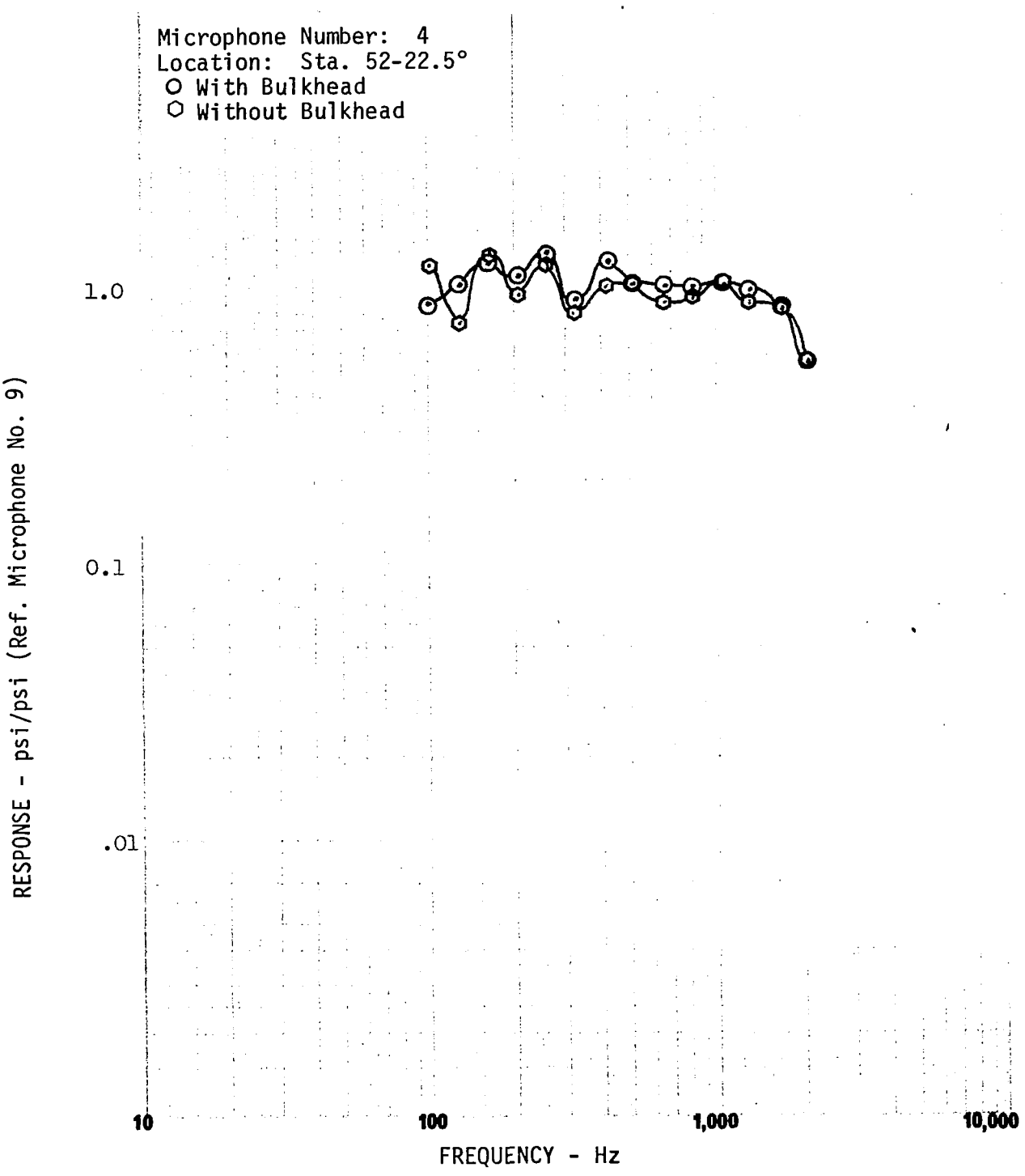

FREQUENCY RESPONSE - EFFECT OF AFT BULKHEAD

FIGURE 80

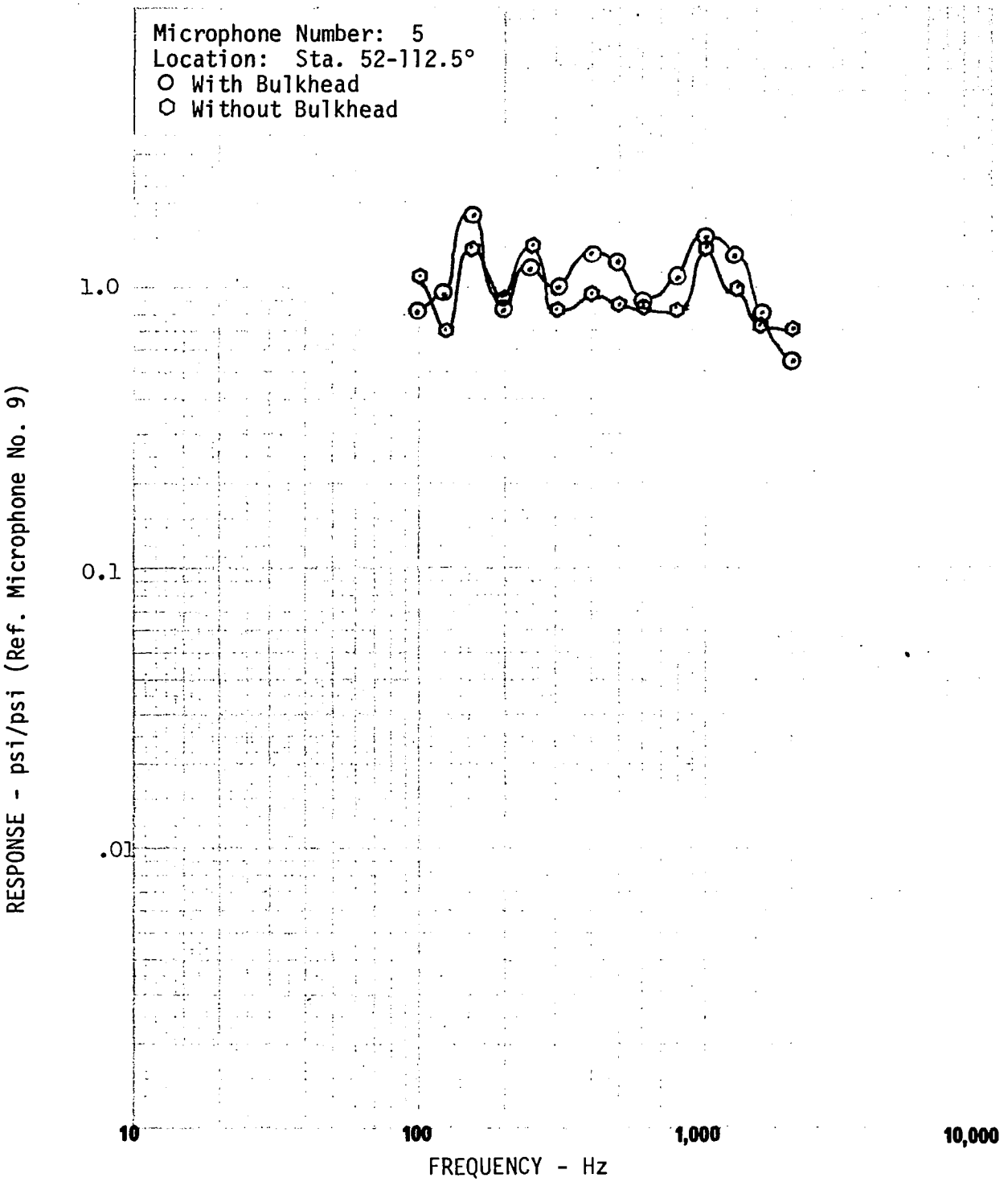

FREQUENCY RESPONSE - EFFECT OF AFT BULKHEAD

FIGURE 81

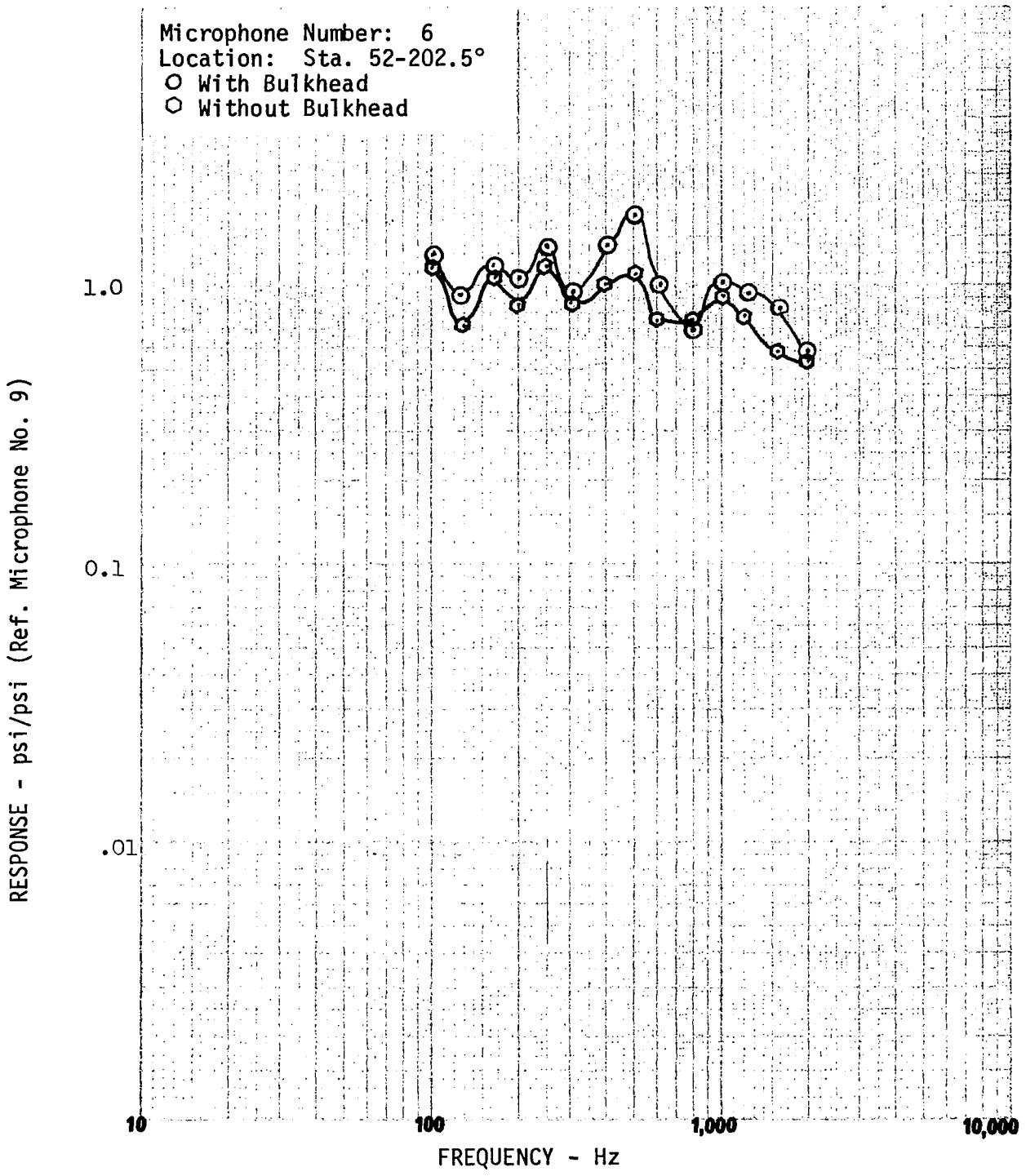

FREQUENCY RESPONSE - EFFECT OF AFT BULKHEAD

FIGURE 82

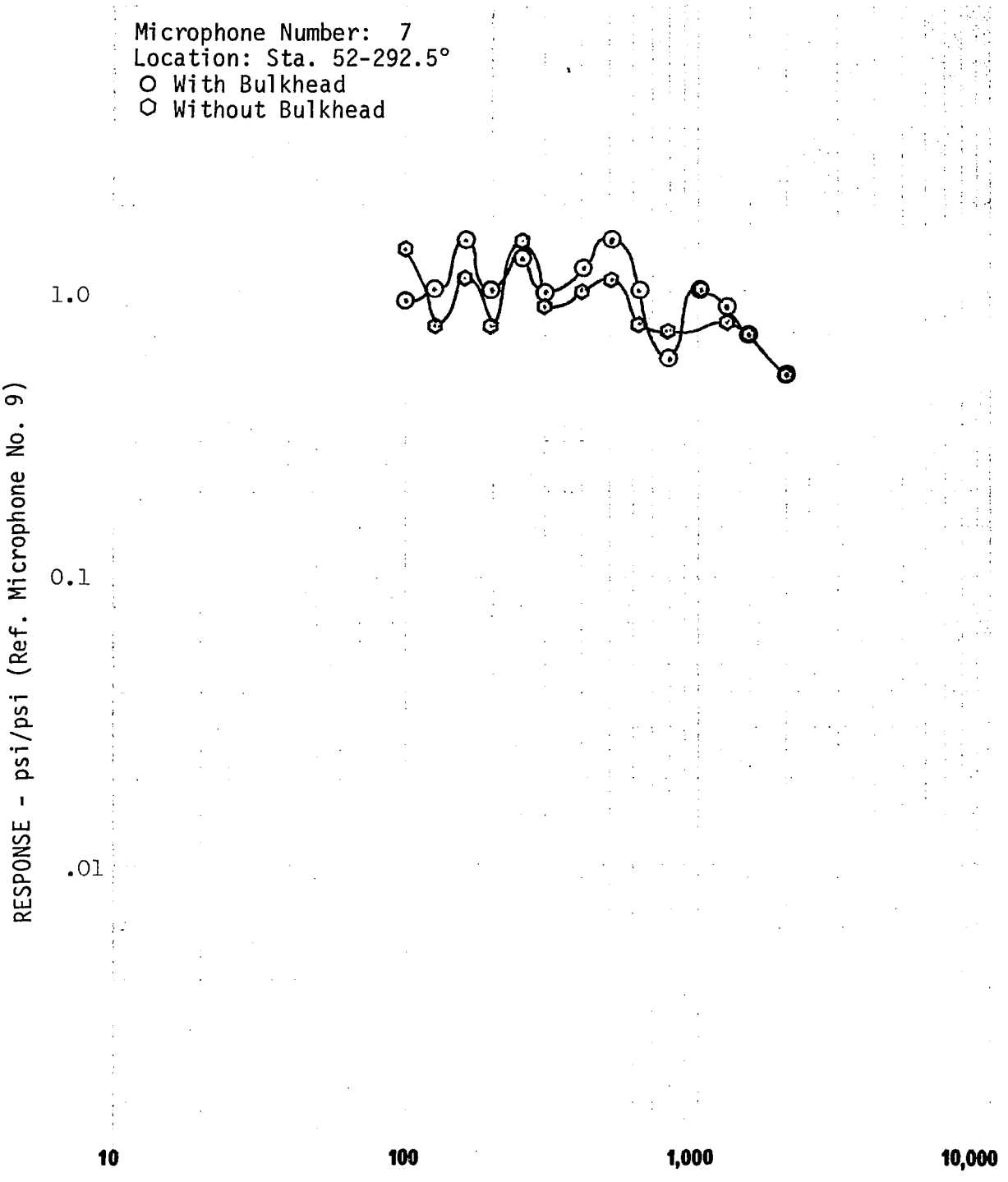

FREQUENCY RESPONSE - EFFECT OF AFT BULKHEAD

FIGURE 83

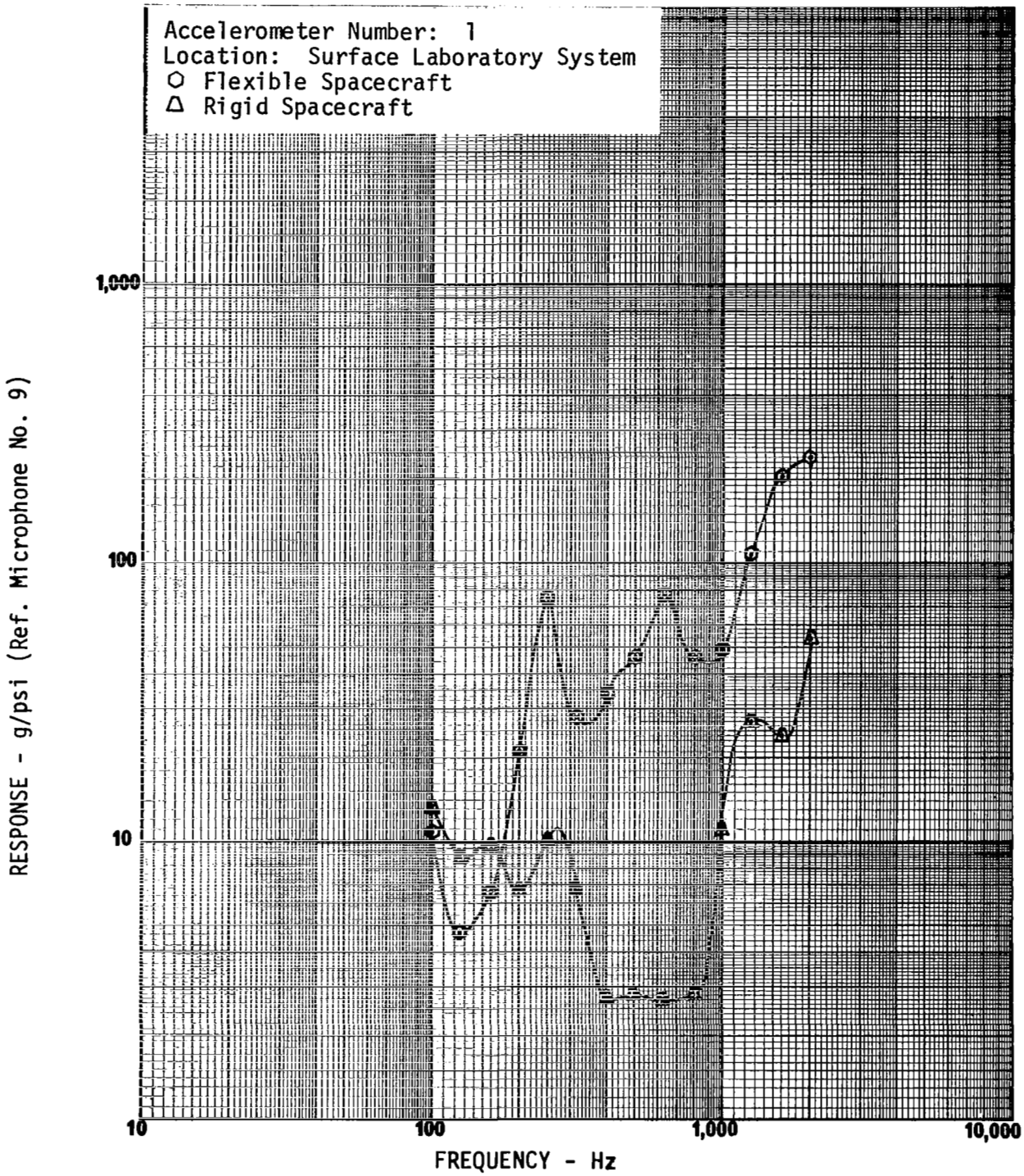

FREQUENCY RESPONSE - EFFECT OF RIGID SPACECRAFT

FIGURE 84

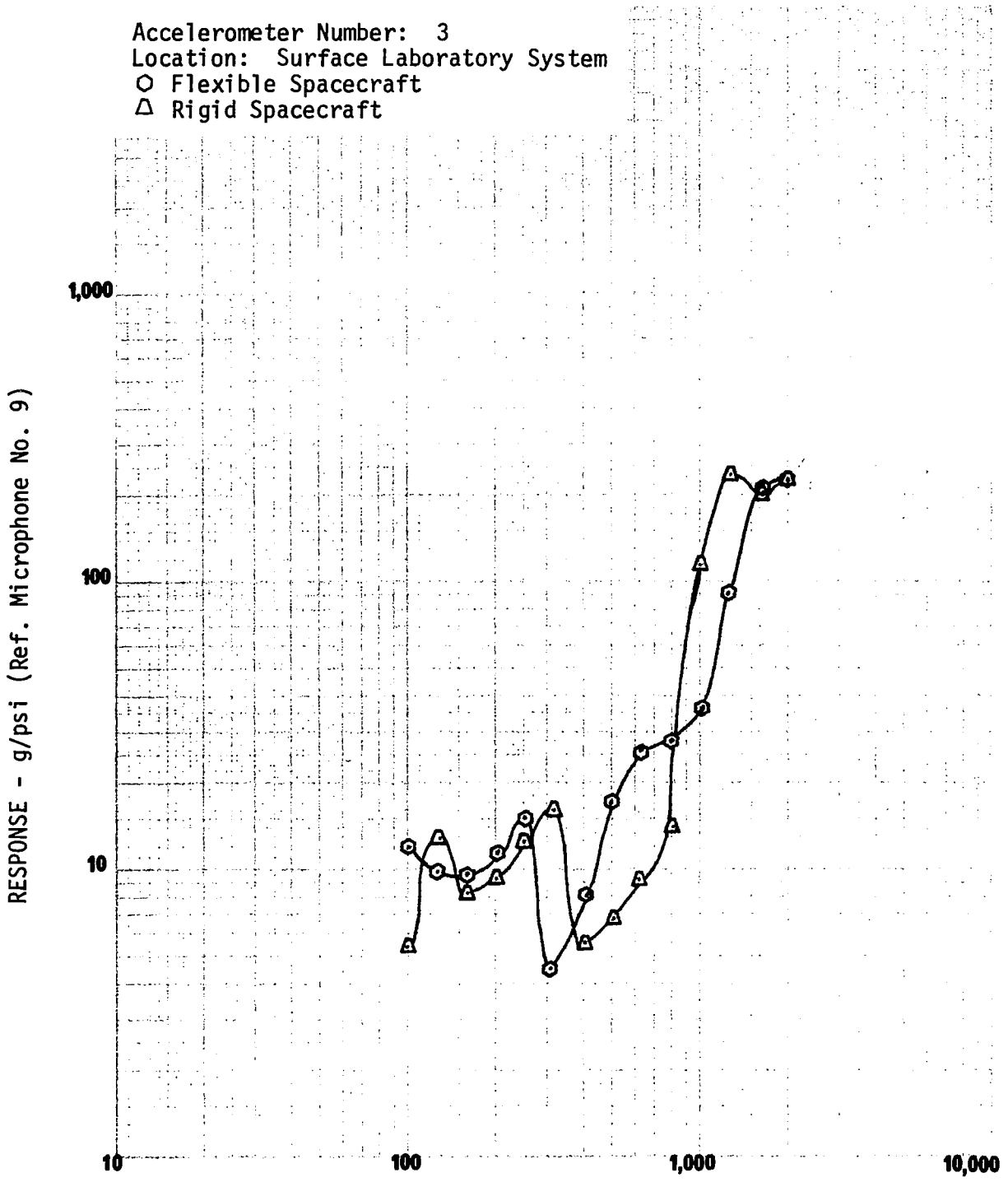

FREQUENCY RESPONSE - EFFECT OF RIGID SPACECRAFT

FIGURE 85

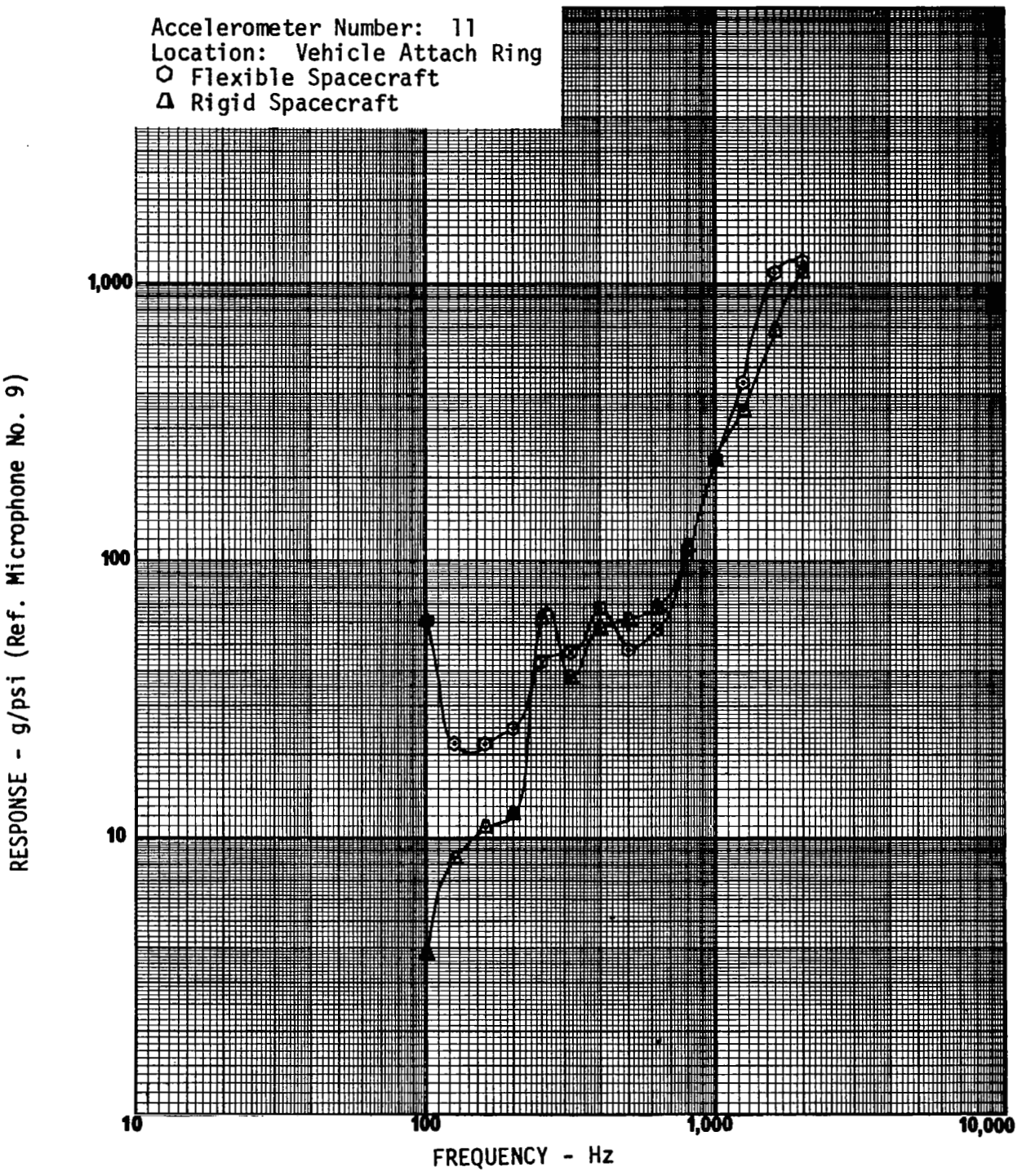

FREQUENCY RESPONSE - EFFECT OF RIGID SPACECRAFT

FIGURE 86

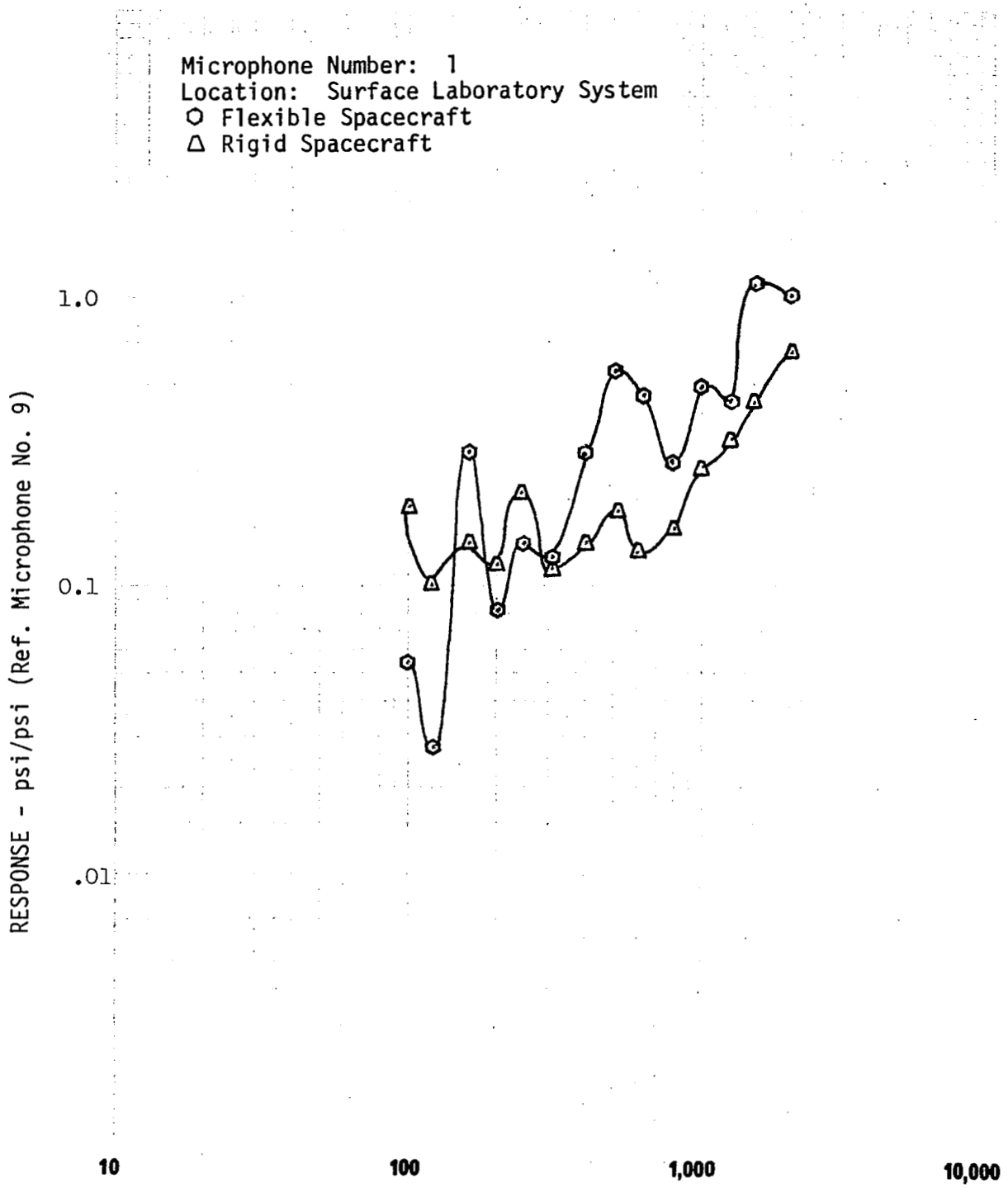

FREQUENCY RESPONSE - EFFECT OF RIGID SPACECRAFT

FIGURE 87

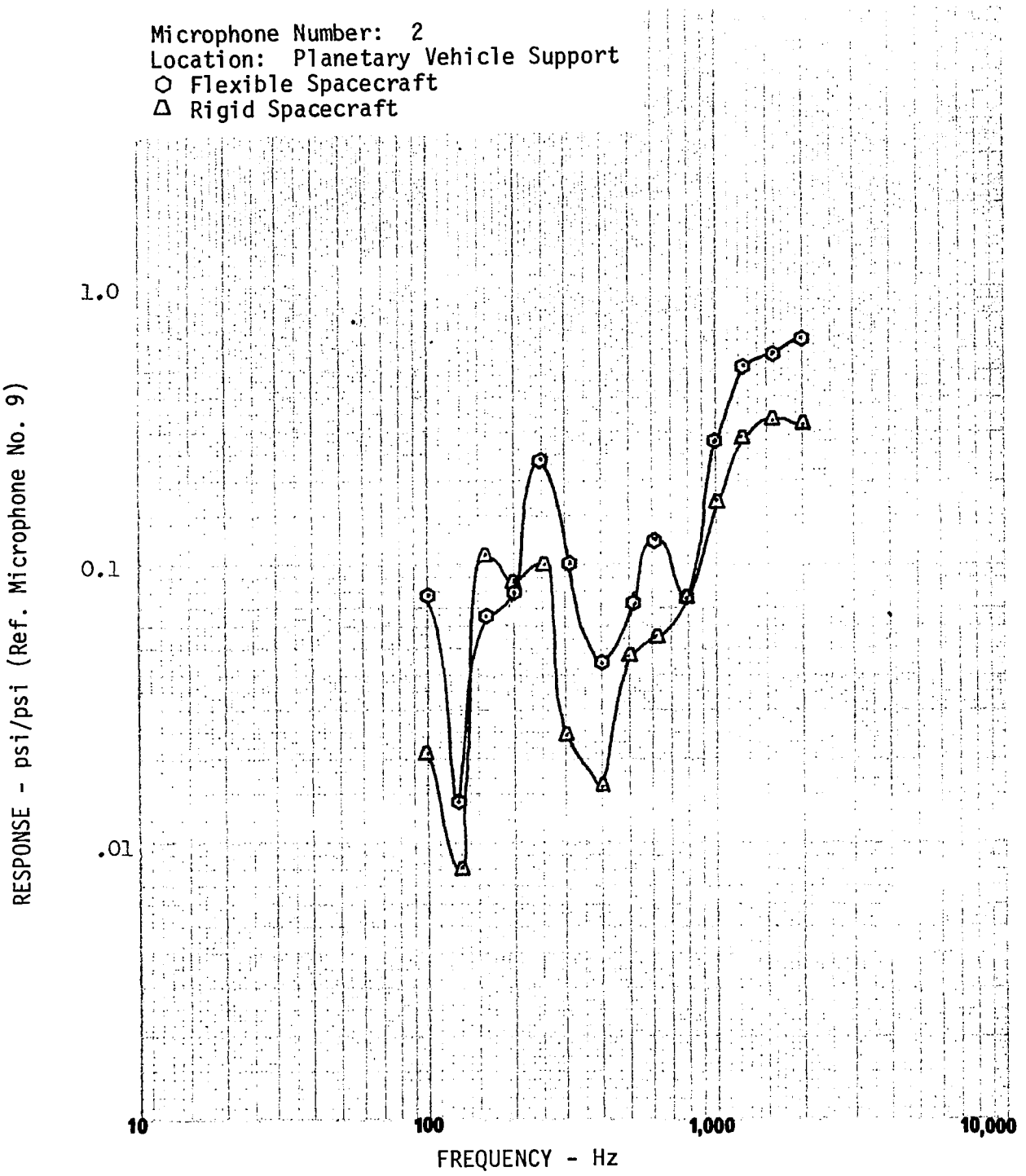

FREQUENCY RESPONSE - EFFECT OF RIGID SPACECRAFT

FIGURE 88

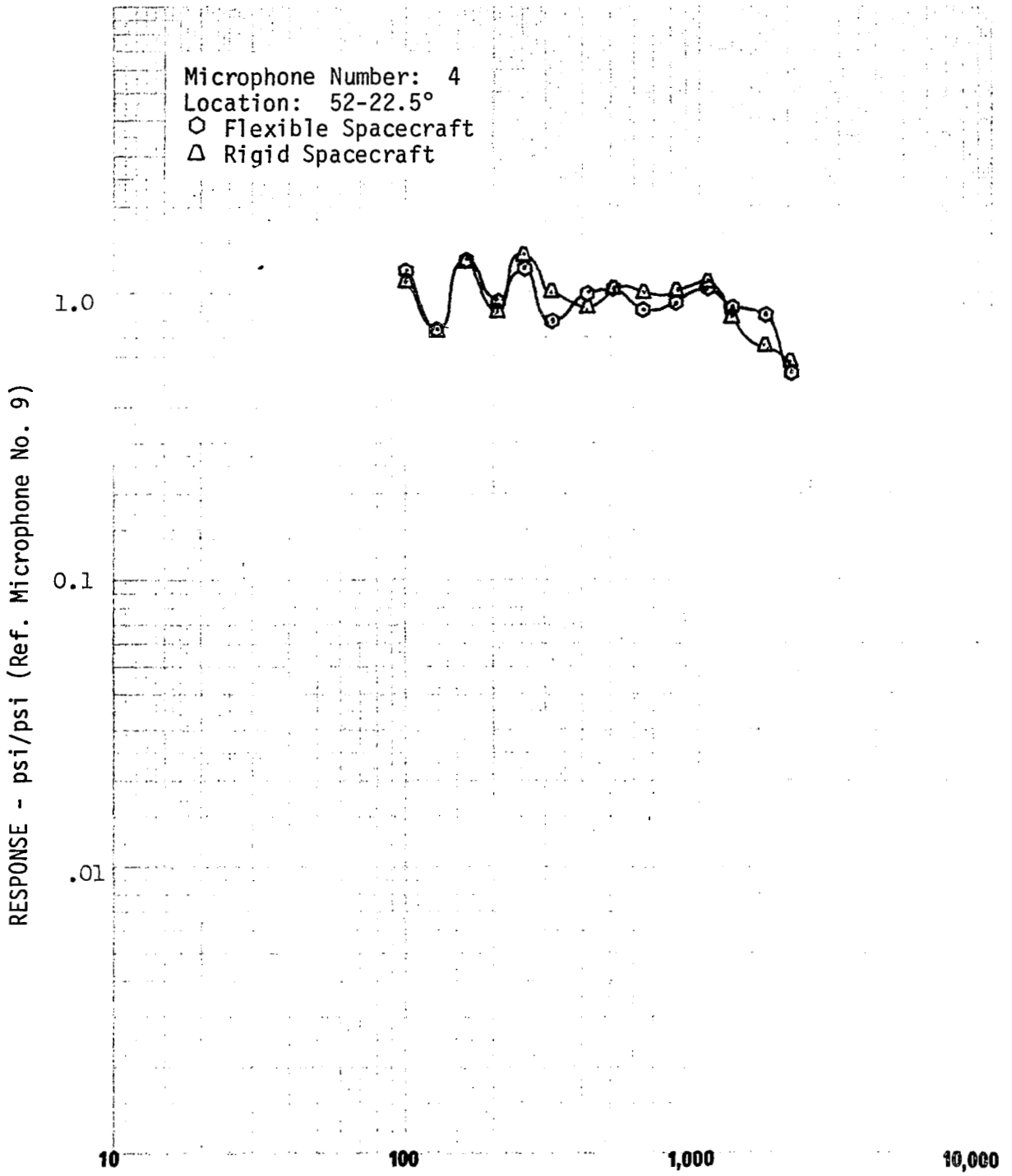

FREQUENCY RESPONSE - EFFECT OF RIGID SPACECRAFT

FIGURE 89

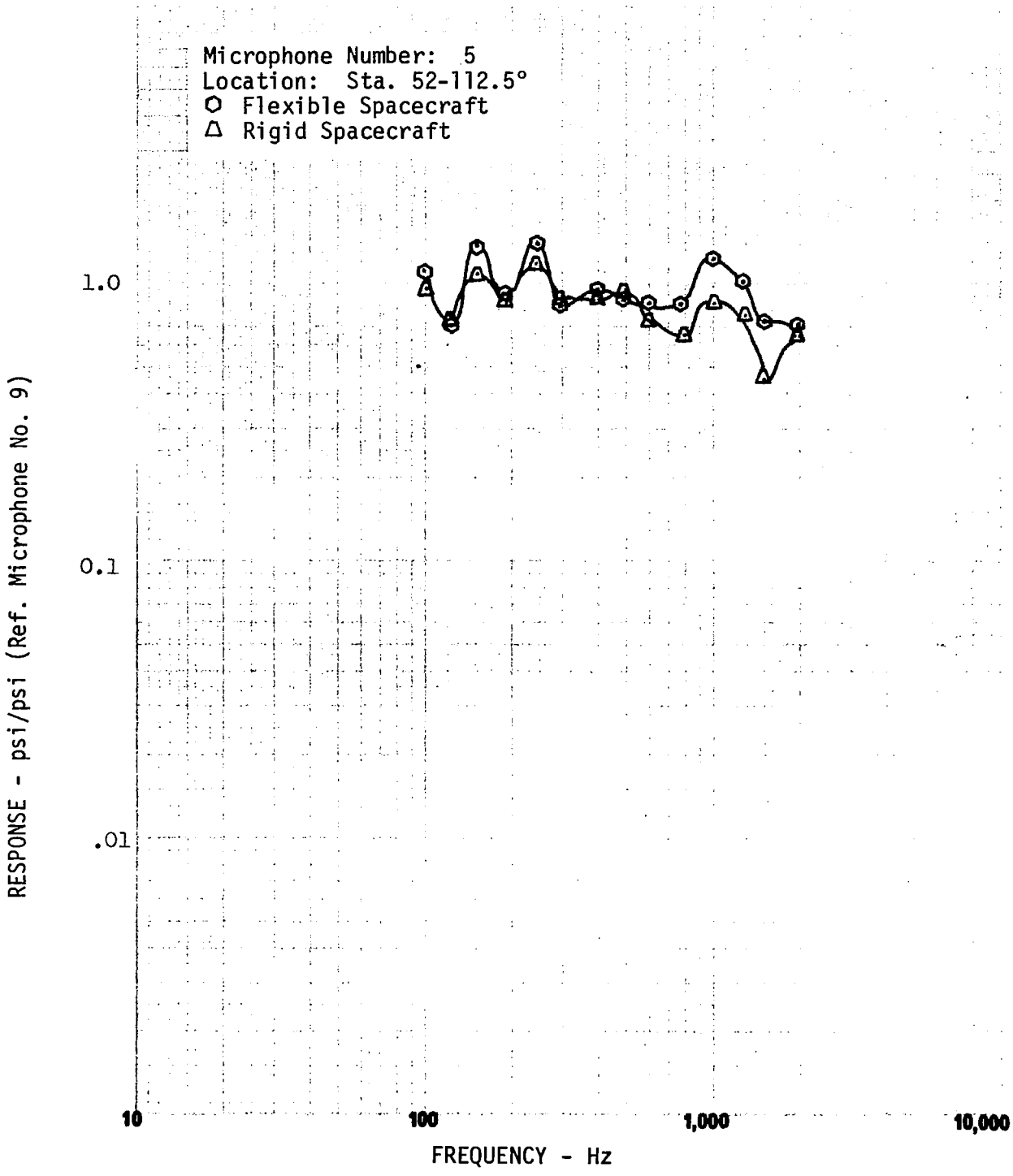

FREQUENCY RESPONSE - EFFECT OF RIGID SPACECRAFT

FIGURE 90

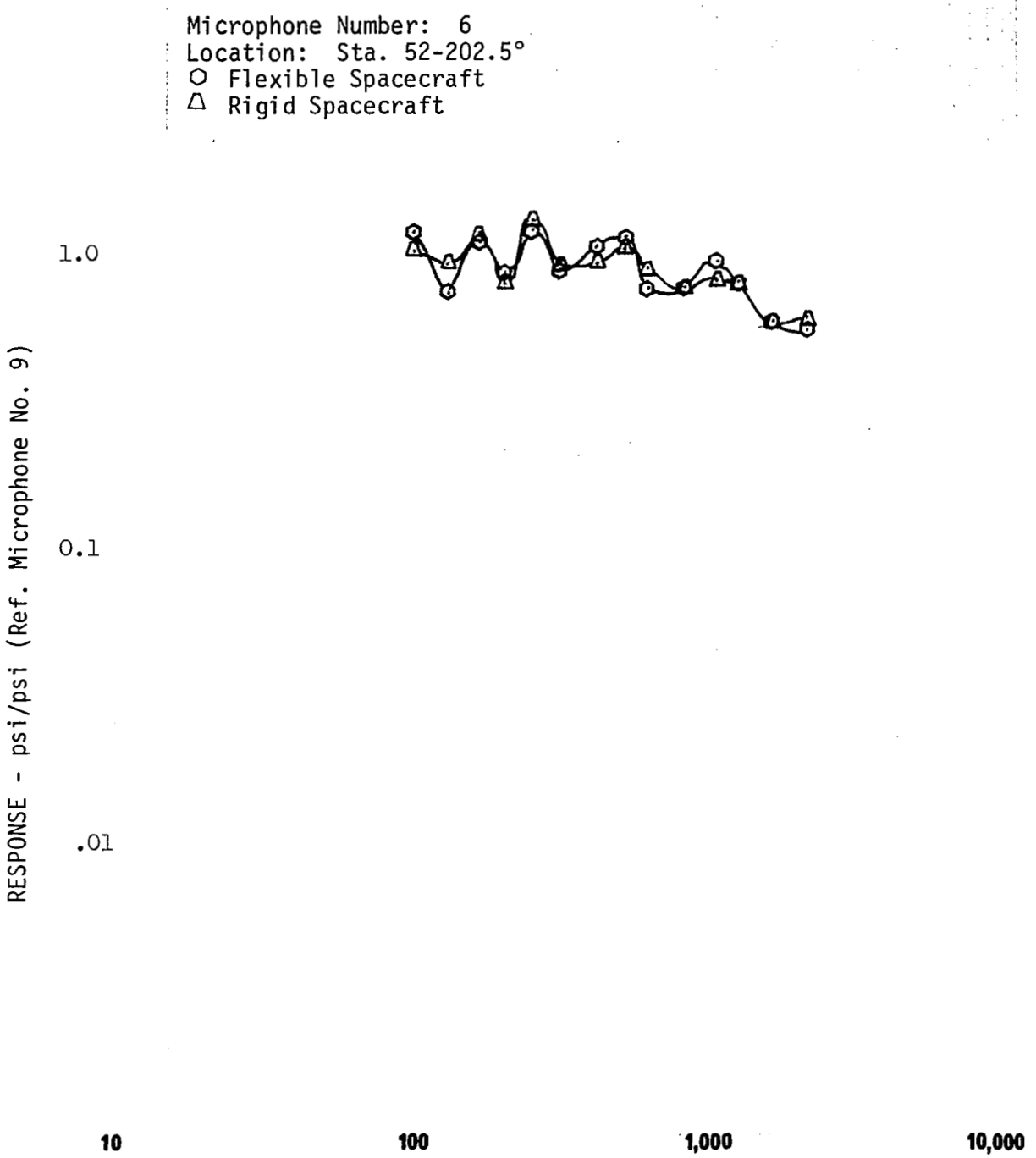

FREQUENCY RESPONSE - EFFECT OF RIGID SPACECRAFT

FIGURE 91

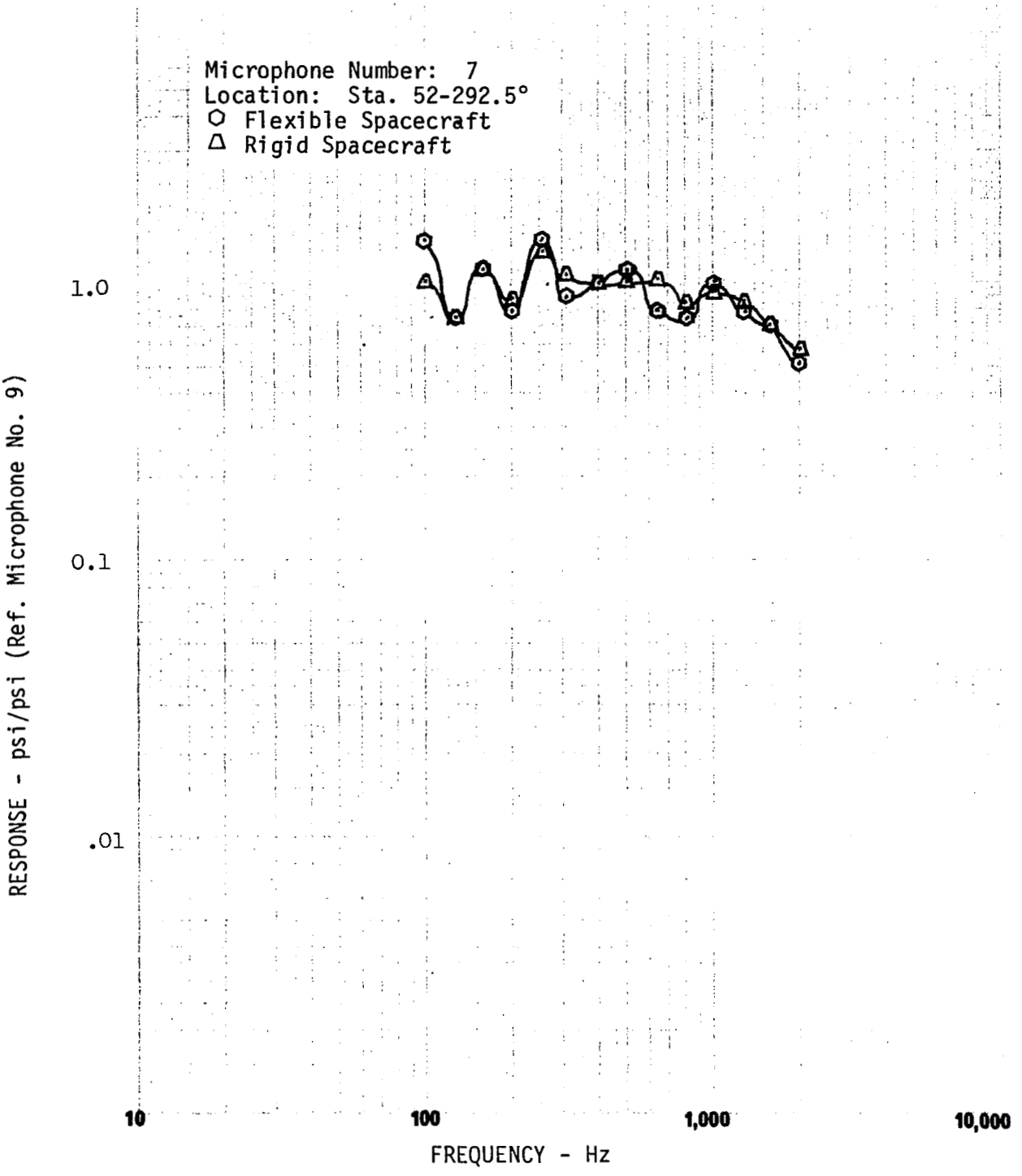

FREQUENCY RESPONSE - EFFECT OF RIGID SPACECRAFT

FIGURE 92